Variable Magnetization Pattern Permanent Magnet Synchronous Machines

by

Ryoko Imamura

A dissertation submitted in partial fulfillment of

the requirements for the degree of

Doctor of Philosophy

(Mechanical Engineering)

at the

UNIVERSITY OF WISCONSIN – MADISON

2019

Date of final oral examination: 2/27/2019

The examination is approved by the following members of the Final Oral Committee:
Lorenz, Robert D., Professor, Mechanical Engineering
Zinn, Michael, Professor, Mechanical Engineering
Jahns, Thomas M., Professor, Electrical and Computer Engineering
Ludois, Daniel C., Assistant Professor, Electrical and Computer Engineering
Severson, Eric L., Assistant Professor, Electrical and Computer Engineering

Abstract

This thesis proposes a new design approach for surface permanent magnet machines (SPMSMs) to have a dynamically modifiable spatial attribute utilizing de/re-magnetizing property of the permanent magnets. The proposed machine design approach enables to have an additional degree of freedom in motor drive systems in terms of the effective pole arc, adding more flexibility in torque and loss control.

This work can be categorized as an attempt to take material properties into real-time control parameters. It also can be referred to as an approach to have real-time controllability of spatial harmonic components. This thesis shows that these approaches are not only technically feasible but also have potential benefits that can not be achieved by conventional machines.

In this work, a simplified modeling method to capture spatial de/re-magnetization is built using an extended version of the conventional magnetic equivalent circuit model. A methodology to change the spatial magnetization distribution in permanent magnets in machines is developed based on the constructed model. Inherent limitations of the methodology are investigated using multiple machine topologies including distributed and concentrated windings.

In addition, a design procedure and control sequence for machines to implement the proposed spatial magnetization distribution change method are developed. Theoretical design space boundaries for these machines in terms of slot-pole combination and material types are suggested based on analytical calculation. Potential issues in a drive system that affect magnetization patterns shaping capabilities, such as magnetizing current pulse width, torque ripple during magnetization change and the reaction field due to the eddy current in magnets, are investigated. Experiment results to verify the concept is provided using a fabricated prototype 400W servo machine.

Aknowledgement

First, and foremost, I thank my advisor, Prof. Lorenz for opportunities and guidance he gave to me throughout my graduate studies in Wisconsin Electric Machines and Power Electronics Consortium (WEMPEC). His passion and belief in engineering and education had kept me motivated and will keep me inspired from now on too. I thank my Ph.D. committee members, Prof. Jahns, Prof. Ludois, Prof. Severson, and Prof. Zinn. Their suggestions were invaluable to my work. I also would like to thank Prof. Ghandhi and Jim Sember for their arrangement to make my final defense happen. My sincere gratitude goes to Prof. Reigosa, Prof. Akatsu and Prof. Sakai, who had been giving me insightful comments more than two years long through monthly Variable Flux Meeting. Without advice from Lab Manager Kyle Hanson, I could not finish all the experiments in Lab. Also, my life in Lab could not be so joyful without amazing work done by Helene Demont and Kathy Young to maintain this great community.

I appreciate JMAG team in JSOL Corp for giving me an opportunity to pursue my degree in UW-Madison. Arrangements by Dr. Takashi Yamada and skills I got from my first supervisor Dr. Kazuki Semba made this possible. Thanks to the courtesy of Arnold Magnetic Technologies and an arrangement by Dave Farnia, a rotor of the experiment machine for this research was fabricated. His continuous support starting from admission is something I can never thank enough.

I'd like to thank all my colleagues, visiting scholars and people I could luckily get to know through this grad school life. Discussion, suggestions, and support from them made this research so successful and made my life so pleasant.

Lastly, I would like to tell my warmest thank to all of my family for their support and encouragement.

Table of Contents

List of Figures

List of Tables

Nomenclature

Symbol	Description
M	Magnetization [A/m]
J	Magnetic polarization [T]
B	Magnetic flux density [T]
n	Normal vector
r	Distance vector
B_{op}	Magnetic flux density at an operating point [T]
H_{op}	Magnetic field strength at an operating point [A/m]
H_{cJ}	Coercivity [A/m]
B_r	Remanence [T]
A_m	Surface area of permanent magnet [m^2]
A_g	Area of the airgap corresponding to the magnet [m^2]
l_g	Airgap effective length [m]
l_m	Magnet thickness [m]
H_{ext}	External magnetic field strength [A/m]
μ_0	Vacuum permeability $4\pi*10^{-7}$ [1/H]
μ_r	Relative permeability
I_m	Magnitude of the stator winding current [A]
ω_e	Excitation angular velocity [rad/sec]
ß	Current phase from the positive q-axis [rad]
λ_{pm}	Permanent magnet flux [Wb]
L_d	d-axis inductance[H]
L_q	q-axis inductance[H]
N	Number of turns
γ	Slot pitch [rad]
q	Number of coils in a phase belt
p	Number of poles
S	Number of slots
m	Number of phases
V_i	i-th order harmonic component [V]
u_1	Fundamental component in voltage generated by the modulator
$u_{1six\text{-}step}$	Fundamental component in the voltage at six-step operation
m	Modulation index
V_a	Terminal Voltage [V]
T_{em}	Airgap torque [Nm]
R	Electrical resistance [Ω]
$\mathcal{R}$	Reluctance [A/Wb]
ϕ	Magnetic flux [Wb]
ρ	Electric resistivity [Ω-m]
δ	Skin depth [mm]

Subscripts

$(\ )_s$	Quantity associated to stator
$(\ )_{rf}$	Rotor reference frame

Abbreviations

PMSM	Permanent Magnet Synchronous Machine
SPMSM	Surface Permanent Magnet Synchrnous Machine
IPMSMM	Interior Permanent Magnet Synchrnous Machine
VF-PMSM	Variable Flux Permanent Magnet Magnet Synchrnous Machine
VMP-PMSM	Variable Magnetization Pattern Permanent Magnet Synchrnous Machine
EV	Electric Vehicle
MS	Magnetization State
PWM	Pulse Width Modulation
THD	Total Harmonic Distortion
PC	Permeance Coefficient
MMF	Magnetomotive Force
FEA	Finite Element Analysis
SPP	Slots per Poles per Phase

Introduction

This section provides the background and motivation for this research, key research contributions, and a chapter-by-chapter list of the material discussed in this report.

Background and Motivation

Demands of electric machines have become multi-objective, and the expected operating regions of machines have been expanded, along with the expansion of the applications and the progress of the drive technology in recent years. For instance, when motors are used in commercial applications such as refrigerator compressors, washing machines, and electric vehicles, there is no certain fixed profile regarding the motor operation. Rather, the operating profile highly depends on each user's activity. Hence, machines in such applications need to cover from high-load, low-speed condition to low-load, high-speed condition within a certain amount of losses and pulsating torque.

Nevertheless, the mainstream of today's machine design approaches still stays in the static geometrical modifications optimized to a single rated point or selected few operating points. For instance, over the decades, fixed forms of spatial magnetization pattern aiming at the reduction of losses and torque ripple have been investigated in a surface permanent magnet synchronous machine (SPMSM) designs. Typical practices of shaping the magnetization pattern are to geometrically shape magnets, align small pieces of magnets and magnetize pre-magnetized magnets material using magnetizing fixtures. In any of the methods, the magnetization pattern cannot be changed once the machine is fabricated.

Meanwhile, in an adjacent area of the machine design, hybrid drive systems with the 6-step operation and the sinusoidal pulse width modulation (PWM) has been researched and brought significant impact on the reduction of losses and pulsating torque. By having the capability to

change modulation methods during the operation, drive systems can choose an optimum modulation method to minimize losses according to operating regions. Similar gains can be expected in a machine if no-load back-EMF waveforms from machines have the real-time variable spatial properties.

The motivation driving this research is to introduce variable spatial properties to machines based on these backgrounds. It is highly expected that the controllable dynamic spatial properties in machines allow drive systems to have more flexibility in torque control and loss control.

Research Contributions

The primary contribution of this work is to propose a concept of real-time variable spatial characteristics in machines using magnet material de/re-magnetization property. Technical feasibility of the concept has been verified through theoretical analysis and experiments. Potential benefits of the proposed concepts that can not be achieved by conventional machines have been quantitatively investigated.

In the development process of the analysis, a simplified framework to model spatial demagnetization is establishd extending the conventional magnetic equivalent circuit model. The proposed virtually subdivided magnet model simplifies the complex spatial demagnetization phenomena and provides an intuitive understanding based on the conventional lumped circuit analogy.

A design methodology to add real-time variable spatial characteristics in machines and control schemes to manipulate these additional properties are also developed. Two key design factors for these machines, slot-pole combinations, and material types, are investigated, giving boundaries to the design space for machines. This work identifies the potential factors in a control system that

affect the magnetization pattern change process, particularly, the magnetizing current pulse width, pulsating torque during the magnetization change and the reaction field due to the eddy current in the magnet.

Summary of Chapters

Chapter 1 reviews the state-of-the-art technologies regarding permanent magnets and electric machines using permanent magnets. Existing modulation techniques for inverters are also covered in order to lay a foundation for the discussion regarding the benefits of dynamic variable magnetization patterns. Based on the review results, a concept of the Variable Magnetization Pattern Permanent Synchronous Machines (VMP-PMSMs) is proposed at the end.

Chapter 2 discusses a virtually subdivided magnet model, a framework to model spatial demagnetization, enhancing the conventional magnetic equivalent lumped circuit model. A spatial magnetization pattern change method in permanent magnets in machines is developed using the proposed framework.

Chapter 3 provides a design guide of VMP-PMSMs which utilizes the spatial magnetization pattern change method developed in Chapter 2. Theoretical design space boundaries for these machines in terms of slot-pole combination and material types are suggested based on the analytical investigation.

Chapter 4 investigates the several potential factors in drive systems that may affect the control quality of the magnetization pattern change, such as the magnetizing current vector trajectory, pulsating torque during the magnetization change and the harmonic current due to the pulse width modulation.

Chapter 5 shows the design process and experiment results of a prototype VMP-PMSM. A quantitative evaluation scheme of the magnetization pattern is proposed in this chapter for a systematic machine geometry modification. The measured results of the machine in magnetization pattern change operation and the normal operation are provided in this chapter.

Chapter 6 evaluates the pulsating torque characteristics and loss characteristics of VMP-PMSMs. The combination of the variable current drive and the variable magnetization pattern also examined.

Chapter 7 presents the conclusions, contributions, and recommended future work.

Chapter 1 State-of-the-Art Review

1.1 Magnetic property of Permanent Magnets

1.1.1 Fundamental property of permanent magnets

The materials that can be magnetized are called ferromagnetic. Ferromagnetic consist of soft material and hard material. Magnetically soft materials, such as iron, iron-silicon alloys, and nickel-iron alloys, can be magnetized but the magnetism remains for only a brief moment. Whereas, magnetically hard materials can be magnetized and hold the magnetism persistently, creating the magnetic field. Permanent magnets belong to hard materials. The strength of the remaining magnetism is represented as **M**, magnetization [1], [2] .

The magnetic field that a permanent magnet generates outside of itself has a certain direction from the one end of the magnet to another end of the magnet as shown in Fig.1-1. The end where the magnetic field is flowing out is called a north pole and the end where the magnetic field is flowing in is called a south pole. The permanent magnet also produces the magnetic field inside of itself, which heads from a north pole to a south pole. This magnetic field inside of the permanent magnet is particularly called the demagnetizing field.

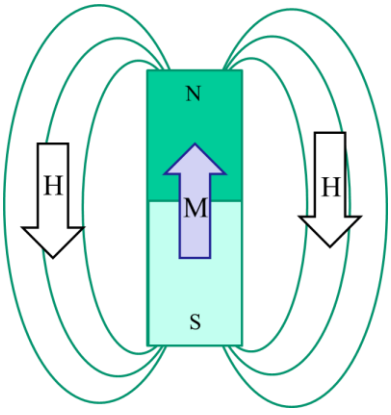

Fig. 1-1. Magnetic field generated by a permanent magnet

The total magnetic field in an area containing the permanent magnets is a summation of the demagnetizing field and the external magnetic field created by the current. The magnetic flux density corresponding to the total magnetic field in the area is proportional to the sum of the total magnetic field and the magnetization of the permanent magnet.

Magnetization **M** or magnetic polarization **J** have a dependency on the total magnetic field **H** as shown in Fig 1-2. This function is often called an intrinsic curve. As shown in Fig. 1-2, within a certain level of the magnetic field, the magnetic polarization keeps a constant value. When the total magnetic field goes beyond specific level in either a negative or positive direction, **J** drops or rise drastically. The drop of **J** is called demagnetization, and the rise of **J** is called (re) magnetization. The point at which **J** becomes zero is called intrinsic coercive force, which corresponds to the magnetic field required to cancel out the magnetization completely. This parameter is quite important for the discussion of the characteristics of the permanent magnet since it indicates how easily the material demagnetize. When the coercive force is high, the material is less likely to demagnetize.

In Fig.1-2, the red line is the magnetic flux density in the air and the blue line is the magnetic flux density due to the magnetization. The resultant green curve, often called the normal curve, represents the magnetic flux density corresponding to the total magnetic field in an area containing a permanent magnet. The intersection of the normal curve and the B-axis in Fig.1-2 is called residual magnetic flux density or remanence, B_r. B_r is a parameter that indicates the magnitude of the magnetic flux density that the permanent magnet can supply when the external magnetic field is zero.

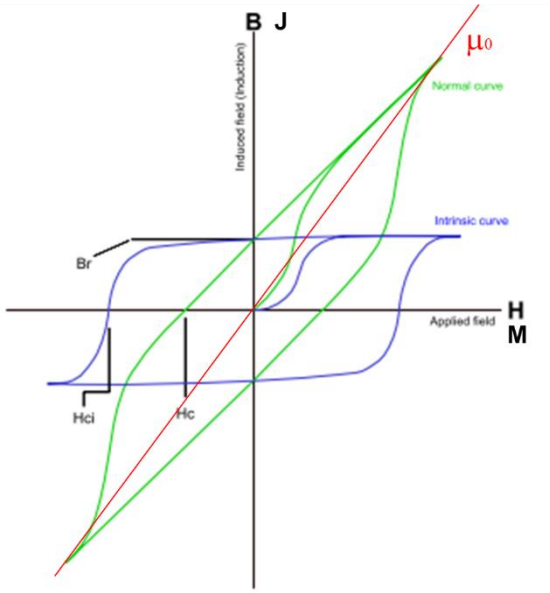

Fig. 1-2. Permanent magnet material property

1.1.2 Initial magnetization

Permanent magnet material is not a magnet before being processed. In the original state, the magnetic dipoles in the magnetic material are quite randomly distributed as shown in Fig. 1-3. When electrons move in free space, they generate a magnetic field. In a magnet, electrons move around the atomic nucleus and generate strong dipole moments. The electrons rotate around themselves thereby generating spin-up or -down momentum. In absence of the applied magnetic field, these momentums are randomly distributed. Applying an external magnetic field leads to partially reversible movement. Increasing the field leads to a sudden irreversible movement of the domain. If the field rises even further, the whole magnet changes its magnetization direction and the magnet becomes fully magnetized. In this state a certain negative field, the coercive field strength H_{cJ}, has to be applied to erace the magnetization [3]. A set of photomicrographs in Fig. 1-4 shows how the magnetic domains grow as the magnetic field increase.

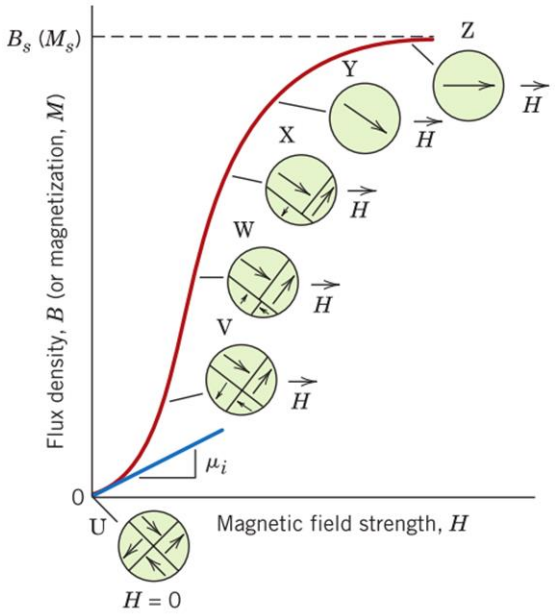

Fig. 1-3. Initial Magnetization [1]

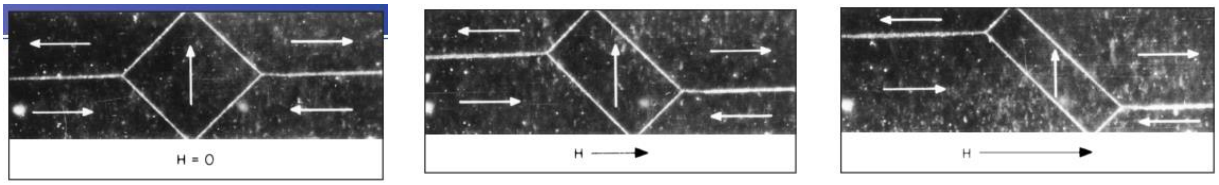

Fig. 1-4. Process of magnetic domain growth [1]

1.1.3 Nucleation/Pinning coercivity mechanism

Coercivity in permanent magnets is governed by one of two mechanisms, either domain wall pinning or domain nucleation. The mechanism which controls the coercivity determines both the shape of the initial magnetization curve and the magnetizing field strength which must be applied within the magnet to ensure saturation. Typical initial magnetization and demagnetization curves for both nucleation and pinning type materials are shown in Fig. 1-5 [3], [4].

Pinning type materials consist of very rigid domain walls which can only be changed when applying a very strong field. Therefore, the coercive field strength rises faster than the remanent flux density Br. Applying this very large field results in rotation of the walls at once. An example of a material in which the magnetization occurs according to the pinning mechanism is Sm2Co17 [4].

In NdFeB and Sm1Co5, that show a nucleation mechanism, these domains contain walls that are easy to move compared to the pinning mechanism. Heating the magnets over the Curie point and cooling them down generate smaller domain regions. The starting point of the magnetization is the so-called nucleation point, which is a favorable discontinuity. Around this point, the domain walls of the adjacent wall move into the favorable direction and allow a single directed remanent flux density. Compared to the pinning mechanism, the remanent flux density rises faster than the coercive field strength, but to fully magnetize the magnet, a high magnetic field is needed to eliminate any unfavorable discontinuities which might be the starting point of demagnetization [4].

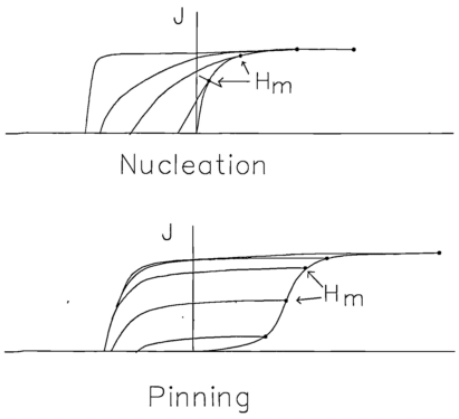

Fig. 1.10 Typical initial magnetization and demagnetization curves for nucleation and pinning coercivity mechanism materials.

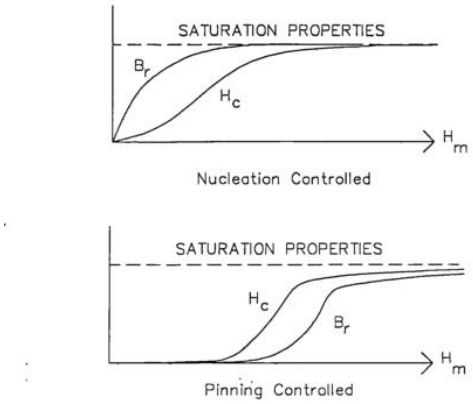

Fig. 1.11 Dependance of remanence and coercivity on the level of magnetizing field for a nucleation and pinning type materials.

(a) Typical initial magnetization curve and demagnetization curve for nucleation and pinning type material

(b) Coercivity and remanence for nucleation and pinning type material

Fig. 1-5. Difference of the nucleation and pinning type material[3]

1.1.4 Operating point of permanent magnets

The operating points of permanent magnets in machines are determined as an intersection of the permanent magnet B-H curve and a load line shown in Fig. 1-6. Corresponding equations of the B-H curve and load line are written as follows, respectively,

$$B = \mu_0 \mu_r(B) \bullet H + B_r \tag{1- 1}$$

$$H = \frac{A_m l_g}{\mu_0 A_g l_m} B + H_{ext} \tag{1- 2}$$

The slope of the load line is determined by the machine geometry while the abscissa of the load line is determined by the external magnetic field supplied through the armature winding current shown in (1-3).

$$H_{ext} = \frac{MMF}{l_g} \tag{1- 3}$$

The intersection of the B-H curve and the B-axis is called remanence (Br). Once the operating point falls below the knee point by the high current injection, the operating point follows the minor loop instead of the outer major loop until the operating point reaches the saturated point. The status that the operating point is located below the knee point is called demagnetized and the recovery of the magnetism by pushing the operating point to the saturated point is called remagnetized.

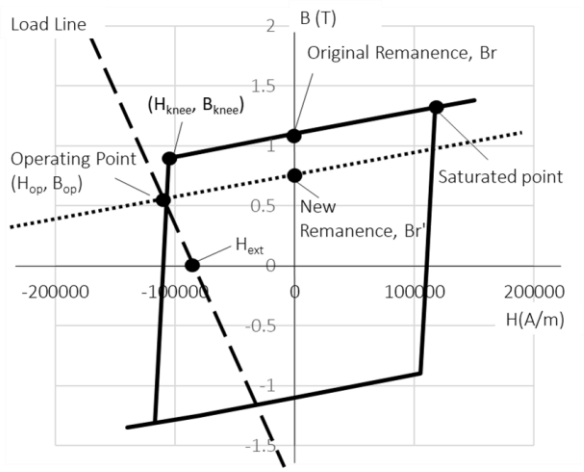

Fig. 1-6 Magnet B-H curve

1.2 Motors with Permanent Magnets

Due to its high energy density, the permanent magnets have been paid attention as the excitation source in electric machines. There two types of electric machines with permanent magnets; one is a DC machine and another is an AC machine. The drive system for the DC motor is quite simple and had been used widely before the AC drive technology became common. However, in terms of the available speed range and the efficiency, AC machine is more advantageous. Hence, as semiconductors technology used in AC drive system advances, DC machines have been replaced by AC machines in many scenes[5].

Permanent magnet synchronous machines (PMSMs) are one of the most widely used AC magnet machines. Figure 1-7 shows the cross sections of this type of motors. In Fig. 1-7, the thin beige color corresponds to the permanent magnets. A PMSM with magnets on the rotor surface as shown in Fig.1-7 (a) is called surface permanent magnet synchronous machine (SPMSM), whereas, a PMSM with magnets buried in a rotor as shown in Fig.1-7(b) is called an interior permanent magnet synchronous machine (IPMSM).

SPMSMs are often used in industrial general-purpose servo machines because of ease of fabrication as well as its lower torque ripple. In general, the machine manufacturing of SPMSMs is easier than IPMSMMs, in which magnets are buried in the steel lamination. In addition to that, because of lower pulsating torque than IPMSMMs due to the absence of the reluctance torque, SPMSMs are often used in the scene where the minimization of pulsating torque is the highest priority, such as electric power steering (EPS) in automobiles [6]–[9].

In the design process of PMSMs, the arrangement of magnets is one of the most important keys. In the case of IPMSMMs, the layout of magnets in the steel lamination core have a large degree of freedom [10]. In contrast, SPMSMs may not necessarily have a wide room for geometrical arrangement of magnets as much as IPMSMMs since they can only be on the surface of steel lamination core as the name suggests. In SPMSMs, instead of the geometrical arrangement, the spatial distribution of magnetization, which can be designed by either geometrical magnet shape, magnet's segmentation or one bulky magnet with non-uniform magnetization distribution, plays a significant role to determine the machine's characteristics.

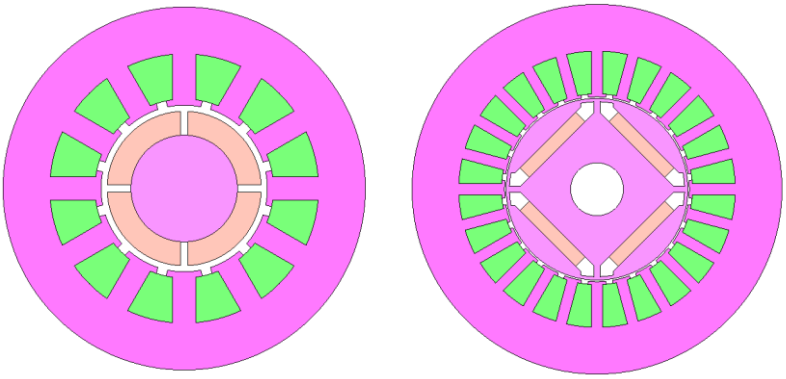

(a) SPMSM (b)IPMSMM

Fig. 1-7 Example of Permanent Magnet Synchronous Machines

1.3 Role of Magnetization Pattern in PMSM Drive System

In this section, fundamental equations that govern the behavior of SPMSMs and the existing magnetization patterns for SPMSMs are briefly reviewed. Afterward, the effect of the magnetization pattern in SPMSMs are summarized from the point of three major machine characteristics; back-EMF, pulsating torque and iron losses.

1.3.1 Governing equation of SPMSMs

In the synchronous d-q coordinates with an electrical angular velocity ω_e, the steady-state voltage equation is expressed as follows:

$$\begin{bmatrix} v^r_{ds} \\ v^r_{qs} \end{bmatrix} = \begin{bmatrix} R & -\omega_e L_q \\ \omega_e L_d & R \end{bmatrix} \begin{bmatrix} i^r_{ds} \\ i^r_{qs} \end{bmatrix} + \omega_e \lambda_{pm} \begin{bmatrix} 0 \\ 1 \end{bmatrix} \tag{1-4}$$

The vector diagram of machine parameters is shown in Fig. 1-8. The d- and q- axis component of the armature current is represented as

$$i^r_{ds} = -I_a \sin\beta, \qquad i^r_{qs} = I_a \cos\beta \tag{1-5}$$

where $I_a = \sqrt{3} I_e$, I_e is the armature current per-phase (rms), and β is the leading angle of armature current from the q-axis.

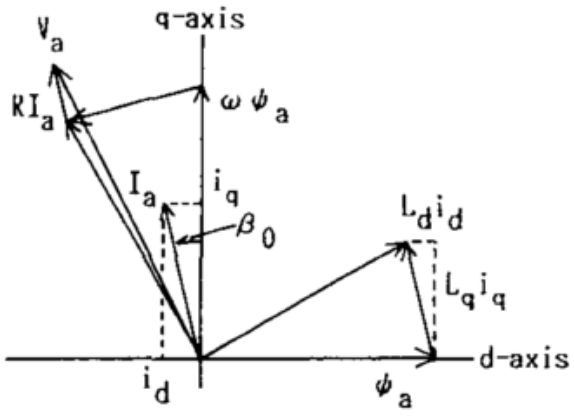

Fig. 1-8 Vector Diagram of Machine Parameters [3]

The torque T_{em} and the terminal voltage V_a are given by

$$T_{em} = \frac{3P}{4}\lambda_{pm}\, i^r_{qs} \tag{1- 6}$$

$$V_a = \sqrt{(\omega_e\lambda_{pm} + \omega_e L_d\, i^r_{ds} + R\, i^r_{qs})^2 + (-\omega L_q\, i^r_{qs} + R\, i^r_{ds})^2} \tag{1- 7}$$

1.3.2 Overview of magnetization spatial distribution

The direction of the magnetic field that the pre-magnet is subjected to determines the direction of magnetization. By changing magnitude and the direction of the magnetic field, several kinds of magnetization distribution are possible as shown in Fig. 1-9. Another way to change the magnetization pattern is to cut a magnet into an arbitrary shape. Figure 1-10 shows SPMSMrotors with different magnet shape and different magnetization distributions inside of the magnets. The magnet alignment in the bottom-most left in Fig. 1-10 is particularly called a Halbach-array, named after an inventor of this arrangement, Klaus Halbach. This arrangement makes the magnetization distribute in a manner so that it can gradually change the polarity as shown in Fig.1-11. As a result, magnetic field distributes only on the outside of the magnet and inside of the magnet has almost no magnetic field.

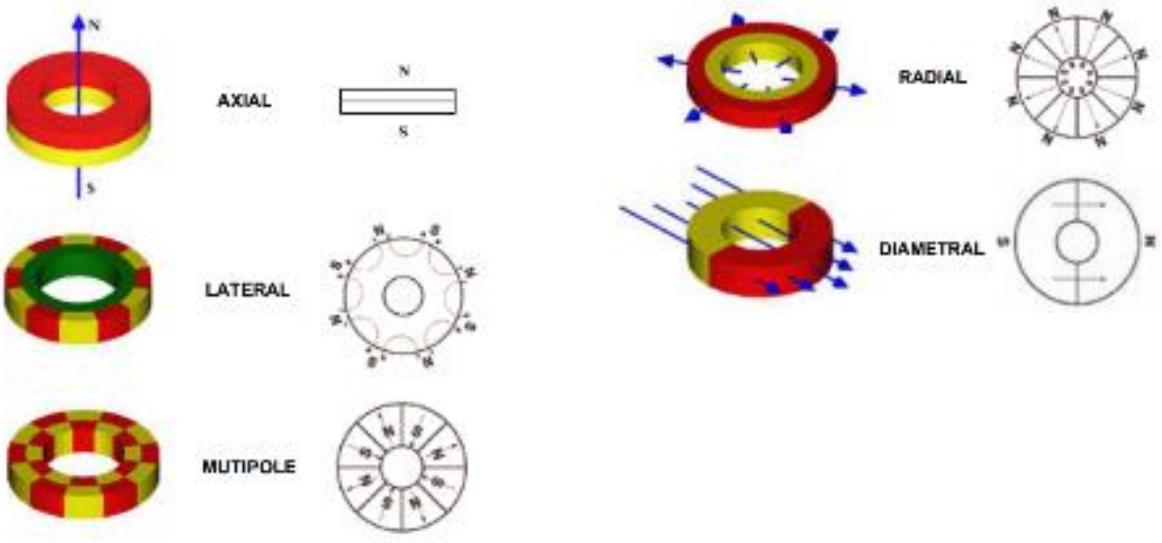

Fig. 1-9. Magnetization Pattern shaped by Direction of Magnetizing Magnetic Field

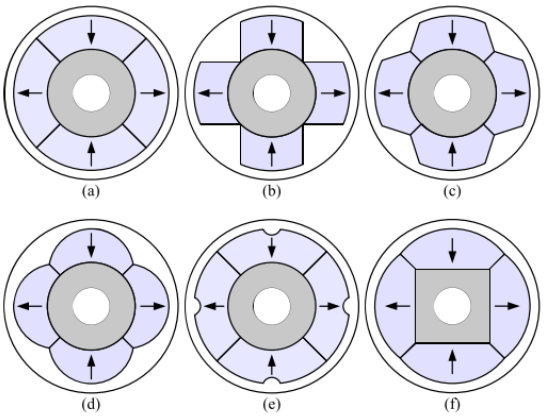

Fig. 1. Typical magnet geometrical shaping. (a) Radial sided arc-shaped. (b) Parallel sided arcshaped. (c) Tapered edge. (d) Sinusoidal shaped. (e) Auxiliary slots. (f) Loaf-shaped.

(a) Geometrically shaped magnetization pattern

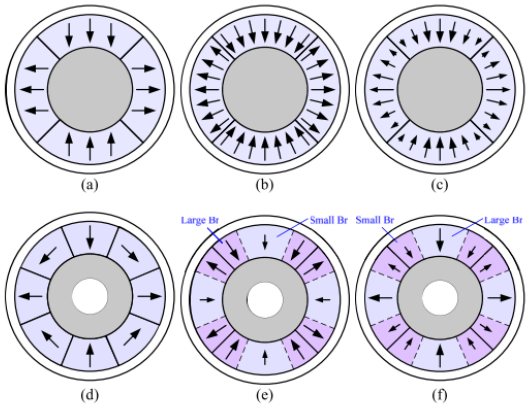

Fig. 2. Typical magnet shaping in material properties. (a) Parallel magnetization. (b) Radial magnetization. (c) Sinusoidal magnetization. (d) Halbach. (e) Mixed material for square airgap field. (f) Mixed material for sinusoidal airgap field.

(b) Segmented Magnet and gradation in a piece of magnet

Fig. 1-10. Magnetization Pattern created by geometrical shape, segmentation and distribution inside of magnets [11]

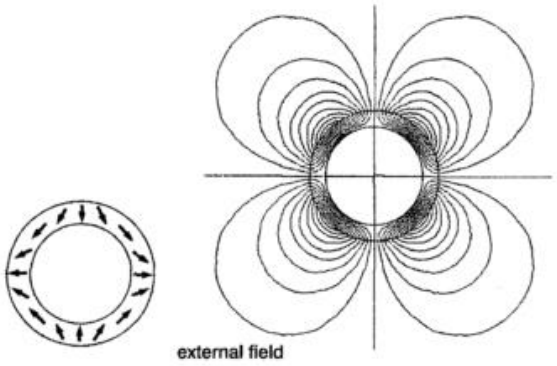

Fig. 1-11. Halbach-Array [12]

1.3.3 Back-EMF

As magnets move relative to the windings in a motor, the magnetic flux due to the magnets linking to the windings varies. The change ratio of linkage flux with respect to time appears as the back-EMF at the terminals of winding.

Harmonics components in back-EMF are one of the major factors to cause the pulsating torque and iron losses as reviewed in the following section. Thus, tremendous amounts of effort to make it closer to pure sinusoidal, such as distributed stator winding, optimization of the magnet pole-arc, skewing of the stator/rotor, have been made [12].

Most commonly taken approach is to design winding configuration in the stator. Although the assembling process of the distributed windings is more troublesome than the concentrated winding, the distributed windings are preferred in the general-purpose machines since it can create nearly sinusoidal back-EMF.

Another approach is to change magnetization distribution in magnets in a rotor [13]–[15]. Magnets with curvature surface, such as bread loaf shape magnets or sinusoidal shape magnets, have a gradual change of magnetization with respect to the circumferential direction of the rotor.

Figure 1-12 is an example of segmented pseudo-Halbach magnets arrangement in SPMSMs. From A to D, the piece of magnet becomes smaller. E is perfect Halbach and F is a parallel arrangement. Figure 1-13 is the resultant magnetic flux density and back-EMF. It is shown that as the piece of magnet becomes smaller, the back-EMF contains fewer harmonics. The back-EMF from the pure Halbach, E, does not contain harmonics whereas the radial magnet shows trapezoidal back-EMF.

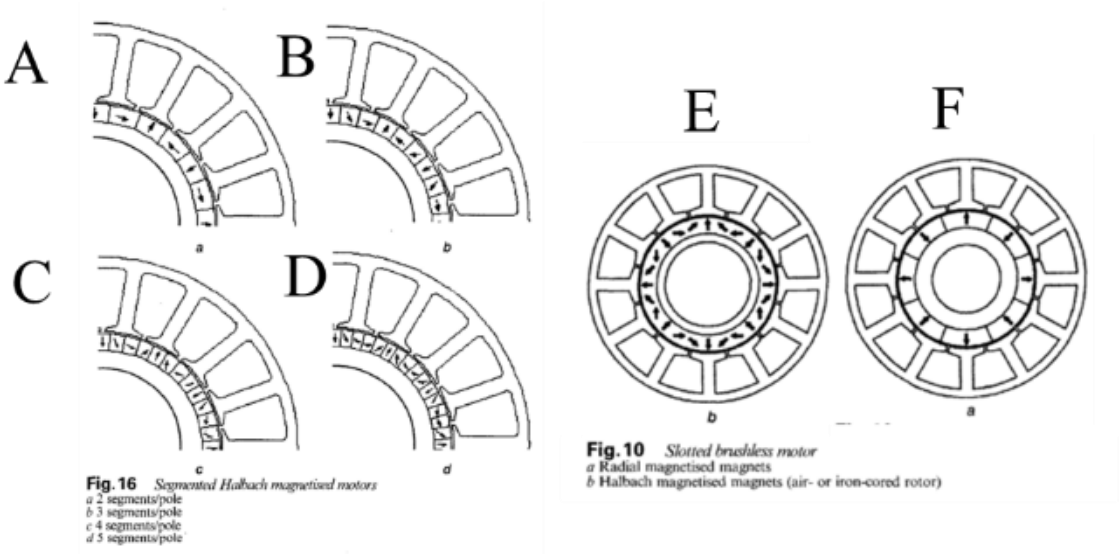

Fig. 1-12. Test set to verify Halbach-Array [12]

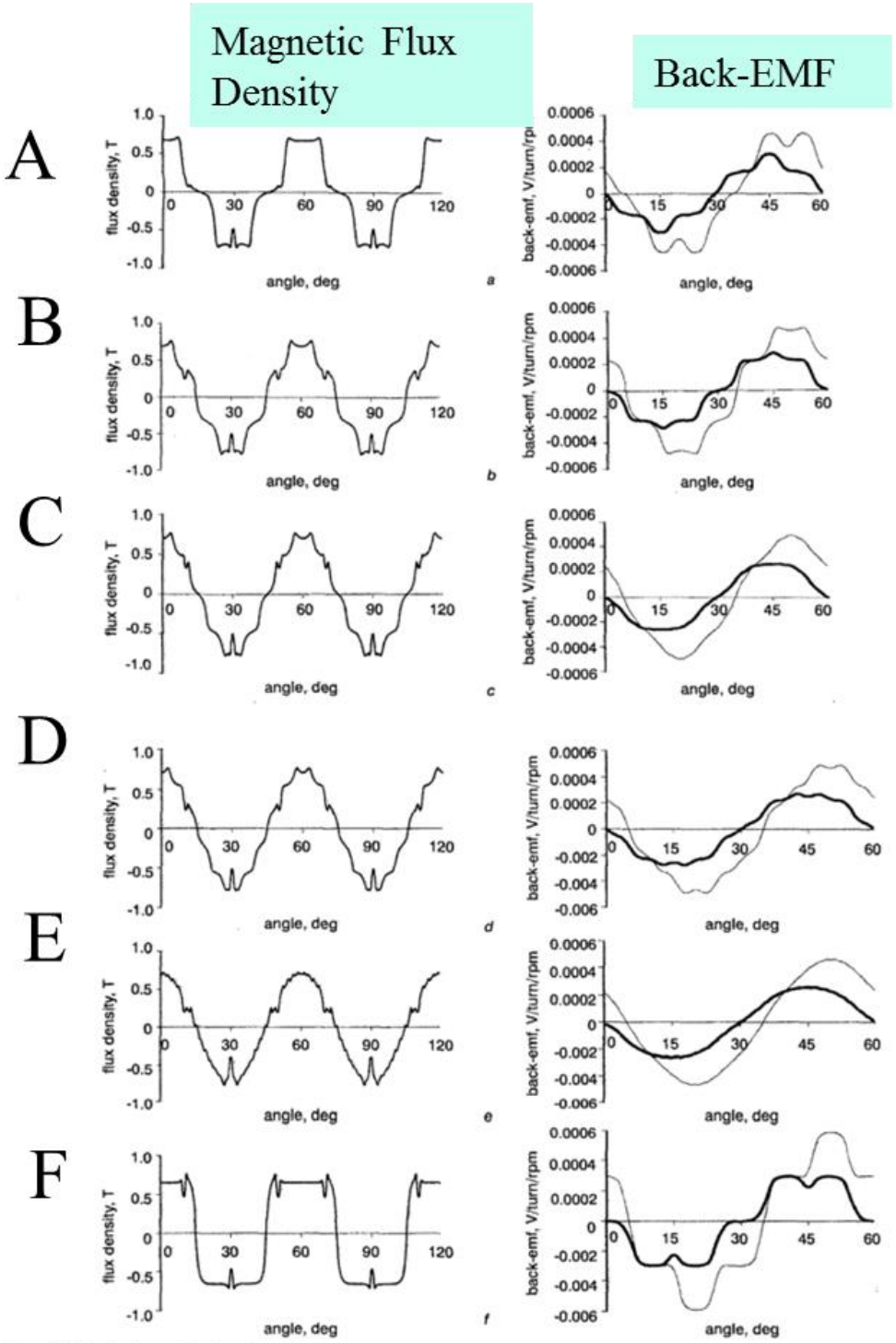

Fig. 17 *Airgap field distributions and back-emf waveforms*
phase emf
line emf
a 2 segments/pole
b 3 segments/pole
c 4 segments/pole
d 5 segments/pole
e ideal Halbach magnetisation
f radial magnetisation

Fig. 1-13. Resultant magnetic flux density and back-EMF [12]

1.3.4 Pulsating torque

Pulsating torque is normally not preferred and treated as a disturbance to the motor drive system except for few numbers of applications. The pulsating torque observed when a machine is spinning under zero current condition is particularly called a cogging torque meanwhile the pulsating torque appeared in machines when the load current is injected to is called load torque ripple [7].

Cogging torque is generated by the spatial variance of the attractive force between a rotor and a stator[16], [17]. There are two causes for the spatial variance of the attractive force. One is permeability in a circumferential direction. Another is the gradient of the tangential magnetic flux density in the circumferential direction of the airgap. Maximum cogging torque is observed when an edge of a magnet enters into or come out from under a tooth tip, which corresponds to a moment when a gradient of the tangential component of magnetic flux density shows the maximum.

Cogging torque can be reduced by minimizing the spatial distribution of permeability. For instance, in machines with closed slots, cogging torque is not observed since permeability between magnets and the stator are always constant in such structure. However, the increase of the leakage flux due to the closed slots essentially leads to lower output torque compared to machines with open slots, thus, closed slots are not a practical option for cogging torque reduction. As an alternative solution, manipulation of the magnetization spatial distribution is often employed. For instance, shaped magnets with curvature surface, such as bread loaf shape magnets or sinusoidal shape magnets, are typical magnetization pattern arrangements to a realize gradual change of the tangential component of the magnetic flux density in the circumferential direction.

Load torque ripple is mainly caused by harmonics components in back-EMF and current. Harmonics components of current and back-EMF can contribute to increasing average torque, but, at the same time, it brings additional ripples to the torque. Hence, the reduction of the harmonic components of back-EMF which is reviewed in the last section substantially leads to the load torque ripple reduction as well.

Regarding pulsating torque reduction, Zhu et.al [18] has reported a comparison of three magnets; Square, sinusoidal and sinusoidal plus third harmonics injection from the point of the pulsating torque reduction as shown in Fig.1-14. By cutting a magnet to a sinusoidal shape, torque ripple dramatically decreased, however, the average torque is sacrificed since the fundamental component in the back-EMF from the sinusoidal shape magnet is lower than from the square shape magnet. In their research, the decrease of the average torque is compensated by adding third harmonics shape to the magnet.

Another example is mitigating the torque ripple by changing the gap width between magnets (Fig. 1-15) [19]. Since the magnet arrangement is not symmetric, this machine inherently has a risk of high unbalanced magnetic pull. Another attempt of torque ripple reduction by changing magnet arrangement is to use a segmented magnet (Fig.1-16) [20]. By combining pieces of a magnet with different grade, height, and orientation, authors replicate the pseudo-Halbach array. Segmented magnet arrangement in the axial direction shown in Fig.1-17 has been proposed in [21]. This technique can fundamentally achieve the cogging torque reduction, minimizing the total usage of the permanent magnet material.

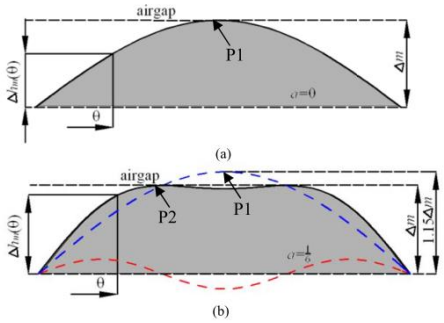

Fig. 3. Theoretical PM shapes for Sine and Sine with third harmonic. (a) Sine shaped. (b) Sine+3rd shaped.

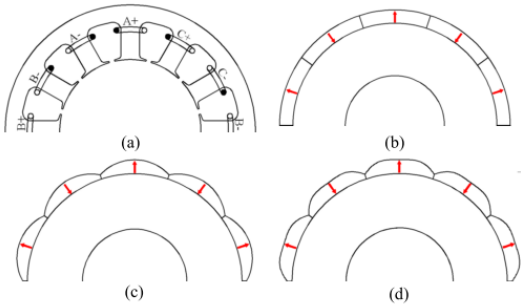

Fig. 1. 12-slot/10-pole SPM machines with different PM shapes. (a) 12-slot stator. (b) Conventional rotor. (c) Sine rotor. (d) Sine+3rd rotor.

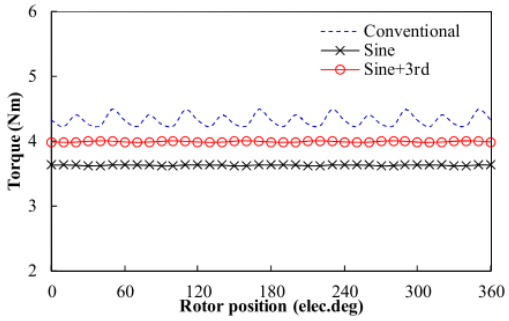

Fig. 13. Variation of torque with rotor position, $I_{peak} = 25$ A.

Fig. 1-14. Permanent magnet with third harmonics [18]

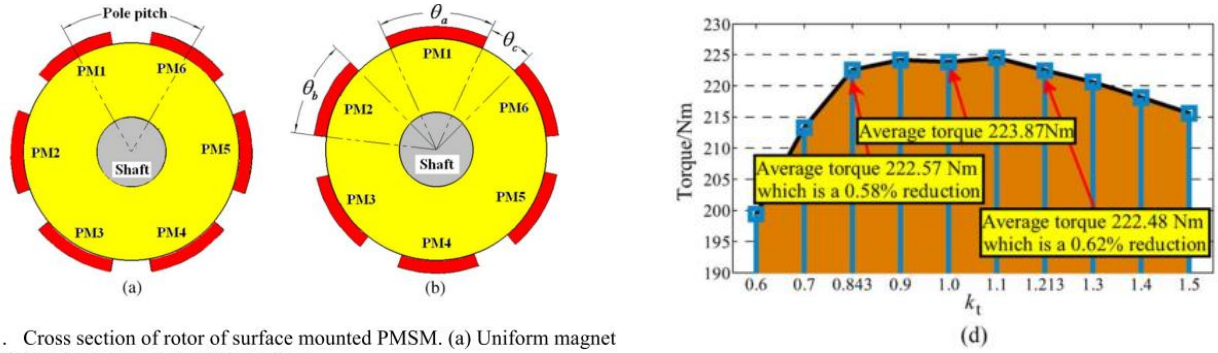

Fig. 1. Cross section of rotor of surface mounted PMSM. (a) Uniform magnet rotor. (b) Different magnet widths method.

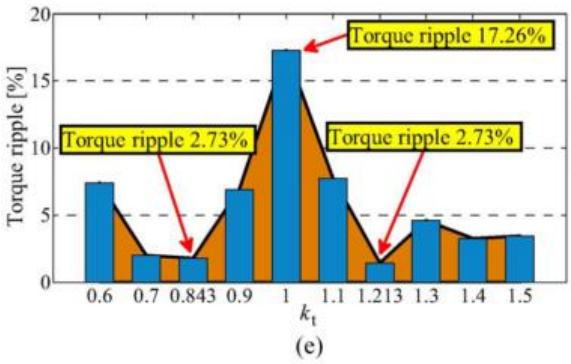

Fig. 1-15. SPMSMwith uneven width magnets [19]

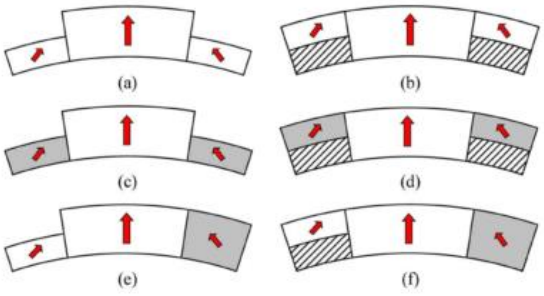

Fig. 1. Configurations of conventional and modular Hat- and T-type magnet poles. (a) Conventional Hat-type. (b) Conventional T-type. (c) Modular Hat-type ESMH. (d) Modular T-type ESMH. (e) Modular Hat-type USMH. (f) Modular T-type USMH.

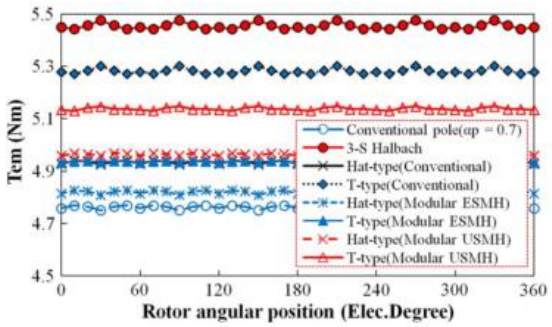

Fig. 10. Comparison of analytically predicted $T_{co.}$ waveform between 12-slot/10-pole PM brushless machines having conventional, optimized three-segment Halbach, conventional Hat- and T-type magnet poles, and modular Hat- and T-type magnet poles.

Fig. 1-16.SPMSMwith mixed grade and height magnets [20]

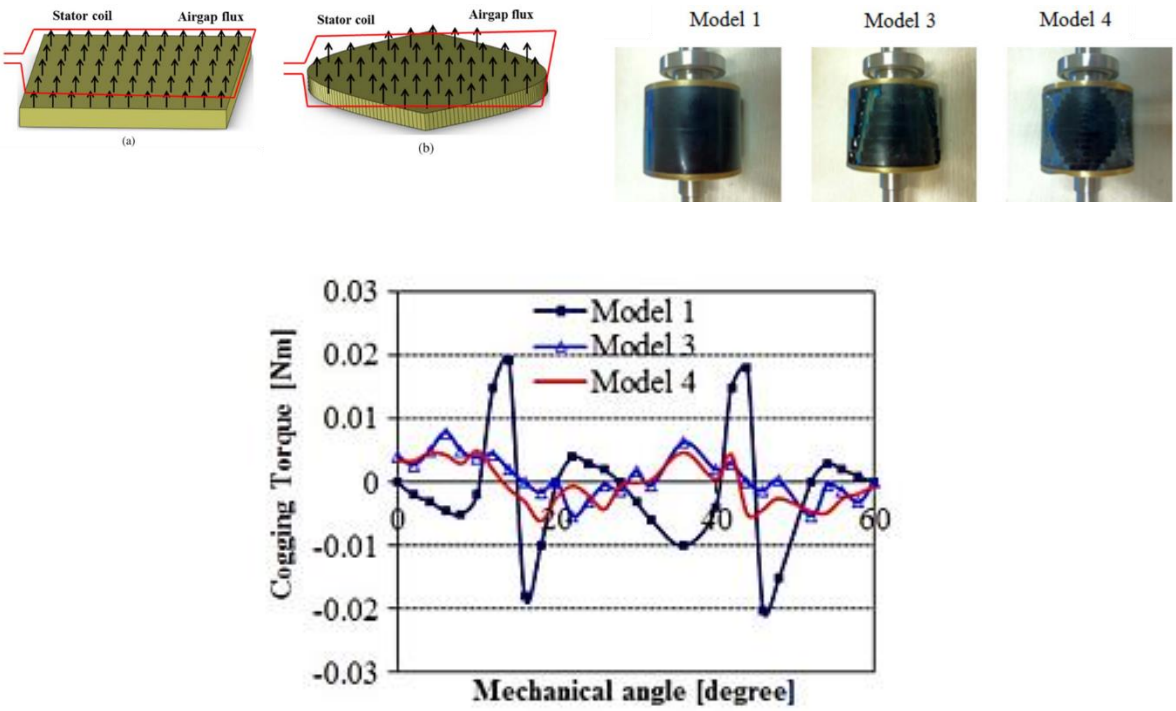

Fig. 1-17. SPMSMwith axially arranged magnets [21]

1.3.5 Iron losses

Losses caused in the steels subjected to an alternating magnetic field are called iron losses or core losses. There are three types of losses in iron losses; hysteresis loss, eddy current loss and excess loss.

Hysteresis loss is defined as the consumed energy in the process of re-aligning the magnetic domains of a magnetic material in an alternating magnetic field. The total hysteresis loss that the iron core loses during one cycle of the alternating magnetic field is proportional to the area of the closed loop that the operating point's trajectory of the iron core makes in B-H curve. If the given magnetic field contains multiple harmonic components besides the fundamental frequency, the magnetic field with such harmonic components generates multiple closed loops in B-H curve.

Thus, the hysteresis loss due to the non-sinusoidal magnetic field is larger than the hysteresisi loss due to the sinusoidal magnetic field.

Eddy current loss is defined as the Ohmic loss due to the electric conductivity to induce the electric current flowing in the iron core subjected to the alternating magnetic field. Electromotive force (EMF) is induced due to the magnetic field in the iron core following Faraday's law of induction. Since the iron core itself is a conductor, the eddy current flows in the iron core. The squared of this eddy current and resistivity of the iron core generate the Ohmic loss. In general, the eddy current loss is proportional to the squared of the frequency of the given alternating magnetic field.

Research of loss reduction by modifying magnet shape in SPMSMs [22] [23] is quite active since it is an essential concern of machines as energy converters. For instance, Fig.1-18 is an example of a study about the magnet's shape optimization in terms of the iron losses using a square shape magnet and an arch shape magnet. It has been shown in this research that a machine with the arc shape magnets has lower losses than with the square shape magnet since the iron losses due to the permanent magnets in the machine with the arc shape magnet is essentially contains only the fundamental component, hence it can be lower than the square magnet. Figure 1-19 is an example of a study of Halbach array arrangement in terms of iron losses in a rotor core. It has been shown that, although the losses due to a stator teeth harmonic remain, the Halbach array arrangement substantially reduces iron losses in the rotor core.

Yamazaki [24] classified causes of iron losses with respect to winding configurations as shown in Fig.1-20. It has been depicted reported in [24] that the losses due to the harmonics component in the magnet are more dominant in a machine with the distributed winding than with the concentrated winding because of the narrower teeth inherited by the nature of the distributed

winding. The magnetic flux density caused by a magnet in a rotor is chopped down by the narrow teeth when it enters into the stator of the distributed winding machine, so it tends to have additional harmonics that are not seen in the concentrated winding machine. In addition to that, the report shows that the magnet harmonics become the major component in the cause of the iron losses particularly in the flux weakening region since the fundamental component of magnetic flux is weakened in that region causing the reduction of the iron losses due to the fundamental component. In other word, the iron losses due to the magnet harmonic component become dominant relative to the fundamental component as machine speed increases.

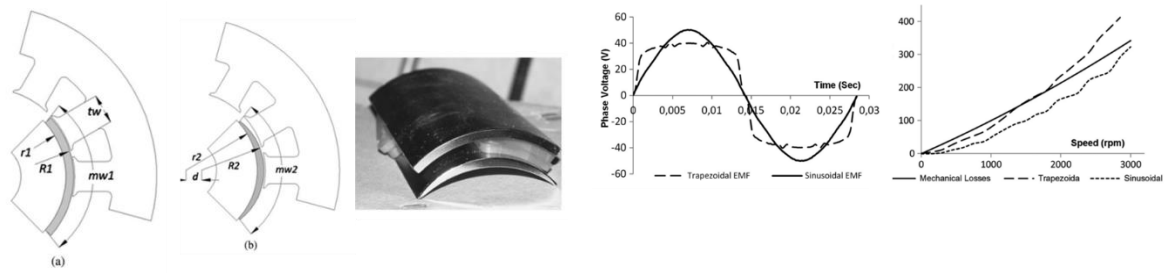

Fig. 1-18. Iron loss comparison with geometrically shaped magnets [22]

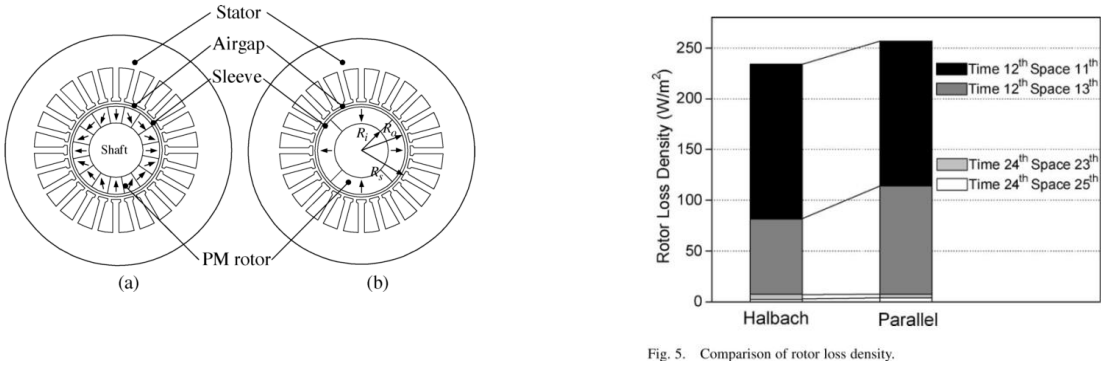

Fig. 1-19. Iron loss in machines with ring magnets and Halbach array magnets [23]

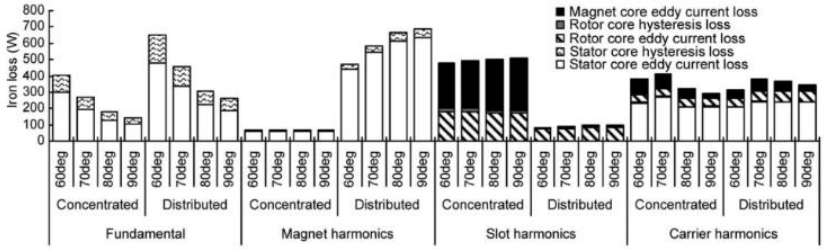

Fig. 8. Classified iron losses due to their origins in motors with concentrated and distributed windings ($I_\alpha = 300$ A, 6000 min^{-1}).

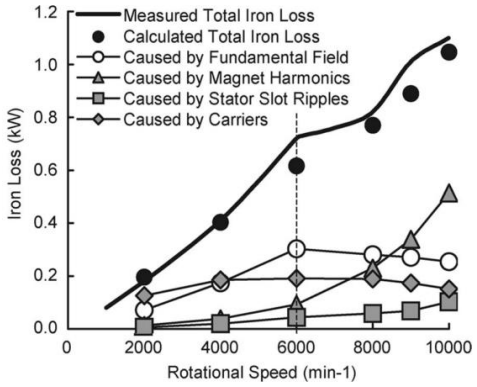

Fig. 10. Calculated and separated iron loss and measurement.

Fig. 1-20. Iron loss segregation [24]

1.4 Magnetization Pattern Shaping Technique

Typical magnetization pattern shaping method is shown in Table.1-1. The most intuitive method of magnetization pattern shaping is to cut magnets into the required shape in the manufacturing process and then attach them to the surface of the machine core [9], [13], [22], [25], [26]. It is most commonly used in industrial products.

The use of the segmented magnet is often discussed in the academic field [27]–[31]. The most siginificant advantage of this approach is the availability of the Halbach arrangement. This technique is not common in the actual assembly since the attaching small pieces of the magnets on the rotor core is merely onerous.

Another technique is to make a gradient in magnetization distribution in each piece of magnets. It can be realized by arranging the design of magnetizing fixtures used to magnetize the

pre-magnetized magnetic material. However, in general, the homogeneous magnetization distribution in the permanent magnets are predominantly aimed in the manufacturing process in order to fully utilize the magnet volume, thus, the discussion in academia regarding this technique are normally targeting the complete magnetization or uniform magnetization. The magnetization distribution with an unexpected gradient is called incomplete magnetization distribution and rather are treated as the failed pattern. As an extension of this method, magnetizing the magnet material in the machine core has been studied in [32]–[36]. The magnetization pattern shaping in the initial magnetizing process is essentially inseparable from the techniques to magnetize magnets discussed in the next section, regardless of the use of the fixture or machine cores. Hence, this technique is explored further.

The primary drawback of these conventional magnetization shaping methods is that the magnetization pattern cannot be changed once the machine is fabricated.

Table 1-1. Typical magnetization pattern shaping method

Methods		Pros	Cons
Change Magnets' Geometric Shape	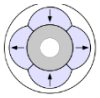	Intuitive Relatively easy to assemble	Cannot change after machine assembly
Arrange Segmented Magnets	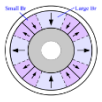	Halbach Array is possible	Cannot change after machine assembly Assembling is onerous
Make Gradient in Magnetization Distribution in Each Piece of Magnet	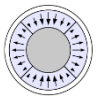	Can change after machine assembly	

1.5 Techniques to Magnetize Permanent Magnets

Techniques to magnetize a piece of non-magnetized permanent magnets for PMSMs can fall into three categorizations based on the timing when magnets are magnetized, as shown in Table 1-2.

The first technique is called the pre-assembly magnetization. In this method, magnetize a piece of magnetic material prior to assembly, then glue it on rotor a core. This technique is rarely used since handling the post magnetized magnet is troublesome.

The second technique is the subassembly magnetization. In this case, first, a pre-magnetized magnet is set on a rotor core using glue, then put the rotor with the pre-magnetized magnet in a magnetizing fixture. This technique is most commonly used to magnetize the magnets in commercial motors. Design of magnetizing fixture is a key to shape the desired magnetization pattern through this method. From that point of view, reference [37] compares advantages of several fixture topologies and documents a design methodology, presenting a case study of the homopolar magnetization of annular isotropic NdFeB ring magnets used in a tubular, linear permanent-magnet actuator.

The third method is to use stator winding for magnetizing current injection. A stand-still magnetization using a reconfigured two-phase stator winding connected to DC power source shown in Fig.1-21 [34] is proposed by H., Min-Fu. In the initial stage of their work, the uniform magnetization of the entire surface area of magnets was defined as the challenge since inherently the two-phase winding can only cover two-thirds of one pole pair of magnets. Later, this challenge was overcome by the same group with two shots of current while spinning the rotor during the magnetization [32] (Fig.1-22). A common point in the initial and the later work is that both need a DC power source connected to two phases. For this topology, the winding

configuration when magnetizing magnets needs to be different from normal operation, thus, the method is applicable only before running the machine. In addition, both aim to create full and uniform magnetization and the possibility of creating a non-uniform magnetization pattern has not been discussed.

Wu.,T[38] has proposed an in-motor magnetization pattern shaping method in SPMSMs. This work developed an arbitrary non-uniform magnetization pattern shaping method using ideal low coercive magnet materials without changing machine winding configuration. Key ideas of this method are summarized as follows.

- A profile of the external magnetic field for one electrical cycle is used as a basic unit of the magnetization manipulation.
- Shape the magnetization distribution into an arbitrary shape by sequentially applying multiple units of the magnetic field as the machine spins.
- Required magnitude and phase angle of each unit of the magnetic field are pre-calculated considering the airgap permeance distribution so that the magnetic field can locally demagnetize a portion of the magnet to a certain level of remanence.
- The required magnetizing current is back-calculated from the desired magnitude and the phase angle of the magnetic field.

The magnetization contour during the magnetization pattern shaping process using this method are shown in Fig. 1-23. It has been demonstrated in that this method can achieve several magnetization patterns such as sinusoidal, sinusoidal + DC offset and uniform (Fig1-24). This shows the possibility of the in-motor magnetization pattern shaping. Although the development and the verification of this method assume an ideal low coercive magnet material, some points

made by this work, such as an identification of the magnetic field as a control variable in the magnetization pattern change system, are insightful and have provided a solid basis of practical implementations.

Table 1-2. Assembly method of permanent magnets in PMSM

Methods		Description
Pre-assembly magnetization	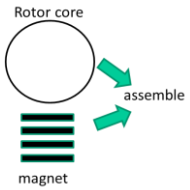	Set the post-magnetized magnet on the rotor. Rarely used.
Subassembly magnetization	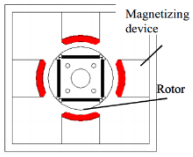	Set the pre-magnetized magnet on the rotor then magnetized using a fixture. Most commonly used.
Post-assembly magnetization	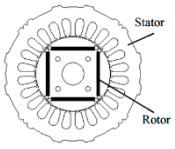	Set the pre-magnetized magnet on the rotor then magnetized using stator winding.

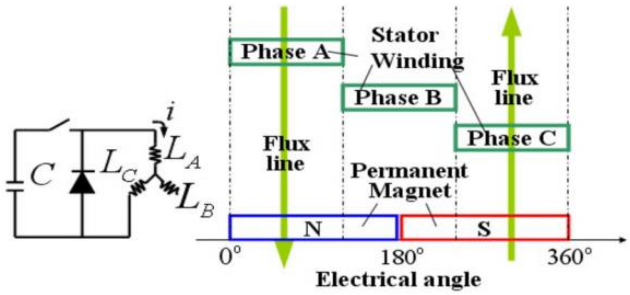

Fig. 2. Post-assembly magnetization using two phases.

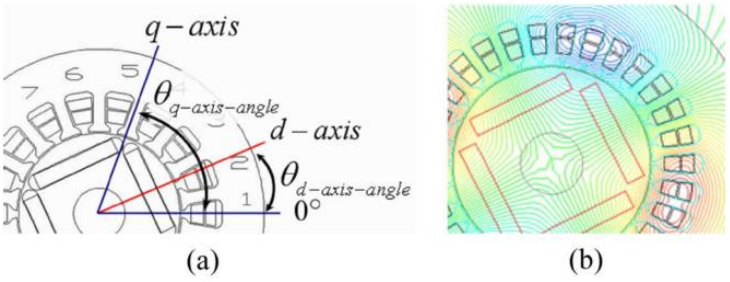

Fig. 3. (a) Rotor position for correct magnetization, and (b) flux distribution at magnetization instant.

Fig. 1-21. Post-assembly magnetization in IPMSMM using DC circuit [34]

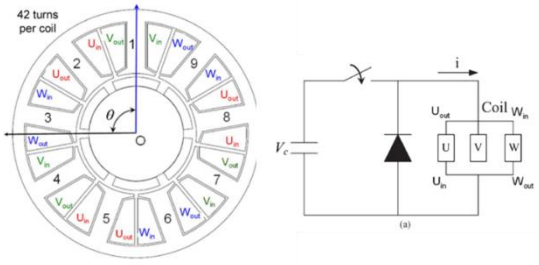

Fig. 4. Motor cross section and phase winding arrangement: 6-pole 9-slot arrangement of three-phase windings showing one slot coil pitch (coil wound around one tooth).

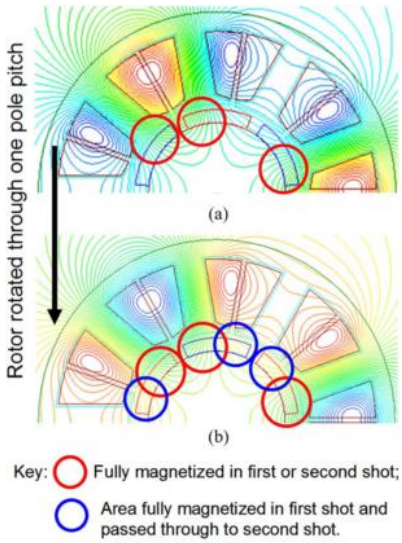

Fig. 6. First and second pulse arrangements with two-phase connections illustrating areas of magnetization in each shot. (a) First pulse. (b) Second pulse.

Fig. 1-22. Post-assembly magnetization in SPMSMusing DC circuit [32]

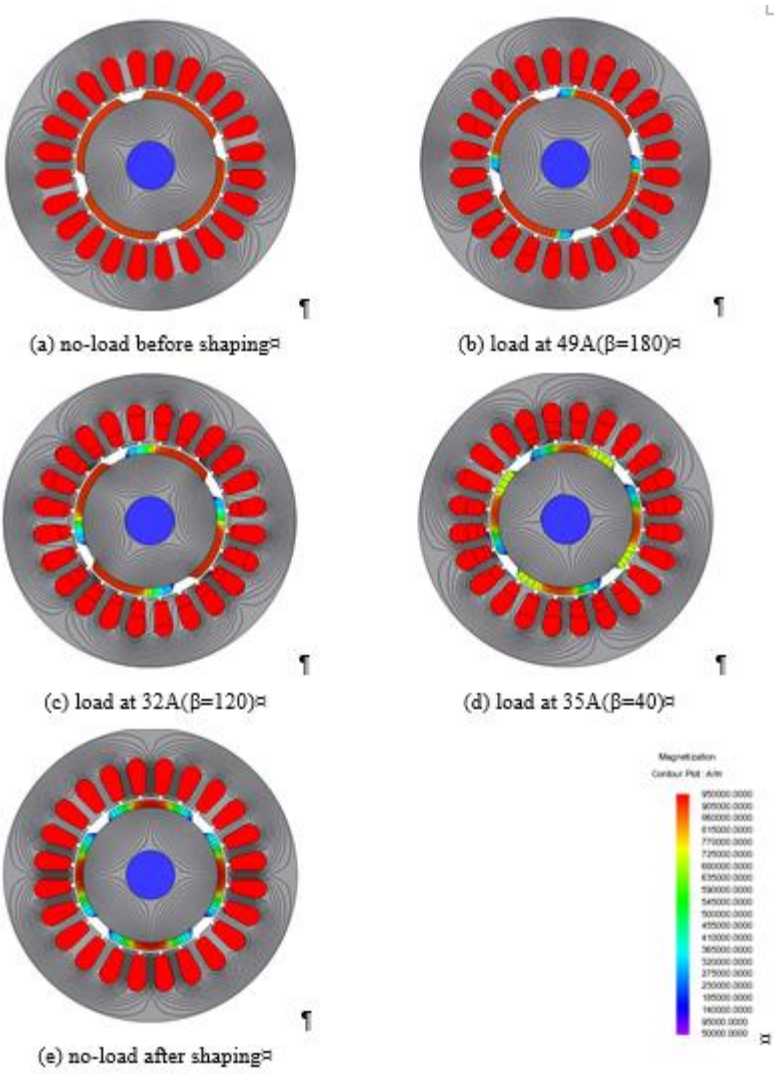

Figure 3.2.10. FEA magnetization distribution and flux paths during IMPS process for sinusoidal commanded magnetization pattern using calculated current vectors¤

Fig. 1-23. Magnetic flux line and magnetization counter during magnetization pattern shaping process [38]

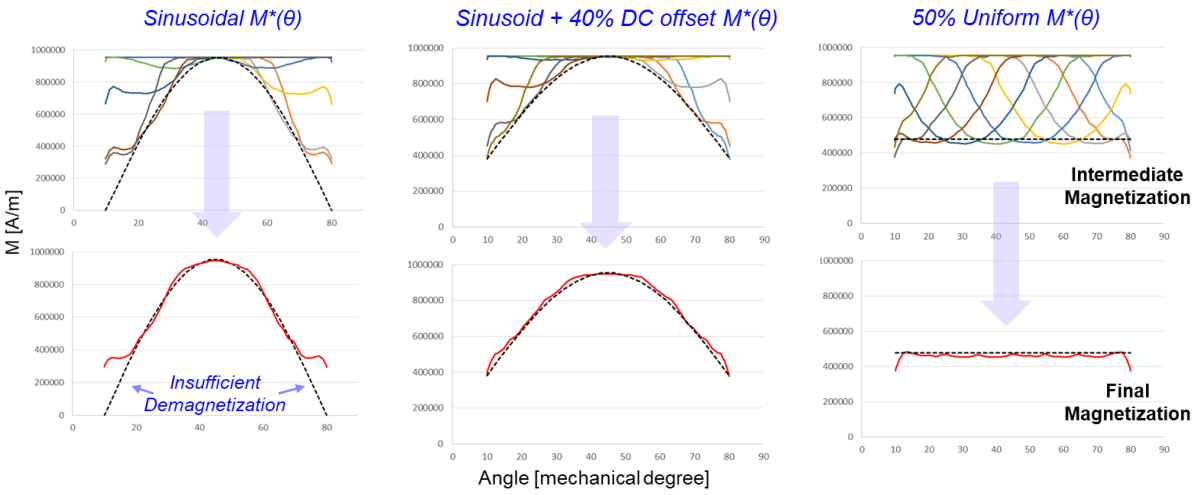

(a) Sinusoidal Magnetization Pattern (b) Sinusoidal Magnetization + 40 % DC (c) 50 % Uniform Magnetization Pattern

Fig. 1-24. FEA results of magnetization pattern shaping [38]

1.6 Demagnetization Analysis

In the conventional approach, the magnetization spatial distribution is often discussed in a context of unwanted demagnetization of permanent magnets. In this section, the existing studies regarding the prevention, detection and the estimation of the demagnetization are summarized, aiming to transfer the knowledge to the active magnetization pattern control.

In general, the magnitude of the demagnetization depends on the external magnetic field that a magnet is subjected to and the temperature in the machine. Larger current than the rated current that can be generated in accidents and losses that leads to temperature rise in machines need to be considered in the machine design process. From that consideration, G.Choi [39] provides a comprehensive design guideline to mitigate unexpected demagnetization in PMSMs based on the analysis of the stator winding and the rotor configurations.

Jin Hur [40] proposes a method to detect demagnetization due to faults from the spatial harmonics spectrum of back-EMF of BLDC in off-line. When the permanent magnet is partially

demagnetized, the back-EMF contains additional harmonic components compared to the original back-EMF as shown in Fig. 1-25 and 26. The authors calculate the harmonic spectrum of the several demagnetized magnets in PMSMs and identify the correlation between the degree of the demagnetization and the distribution of the harmonic components.

Another report by Jin Hur [41] analyzes demagnetization under the locked rotor condition and the load condition using 6-pole 9-slot SPMSMand IPMSMM as shown in Fig. 1-27 and 28. This research does not describe the details of the physical mechanism of the demagnetization. However, the approach to demagnetization with a clear distinction between the locked rotor and the spinning condition, which is not considered in other researches in this area, is quite insightful.

Won, S. H [42] has proposed a modeling method of incomplete magnetization using non-uniform recoil permeability distribution in BLDC. Partial demagnetization caused by the incomplete magnetizing process due to the fringe effect on the ring magnet is discussed in this paper. The calculated cogging torque becomes reasonably closer to the measured cogging torque by considering the recoil permeability distribution caused by the partial demagnetization.

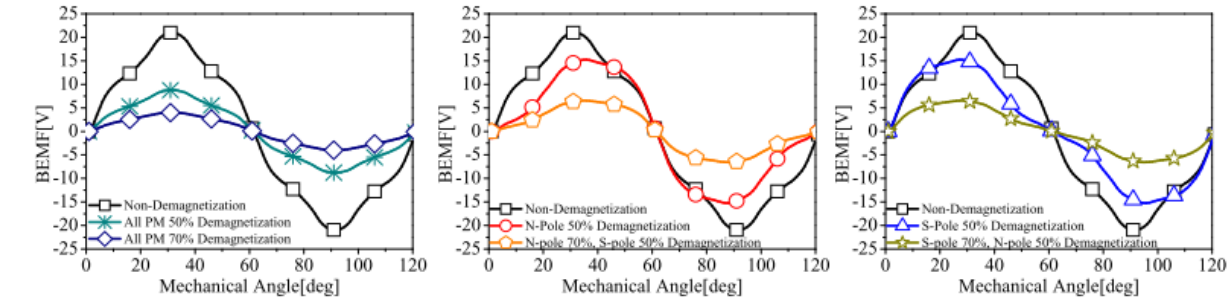

Fig. 1-25. Back-EMF in time domain for demagnetization fault detection [40]

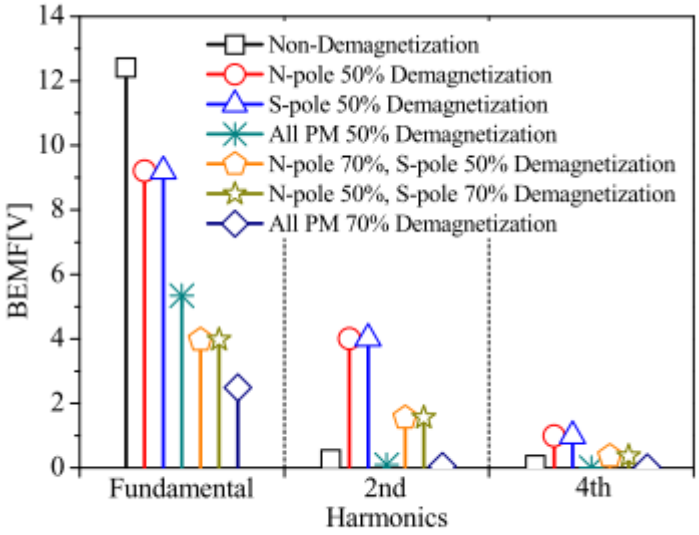

Fig. 9. Result of harmonics characteristic according to demagnetization patterns

Fig. 1-26. Back-EMF in frequency domain for demagnetization fault detection [40]

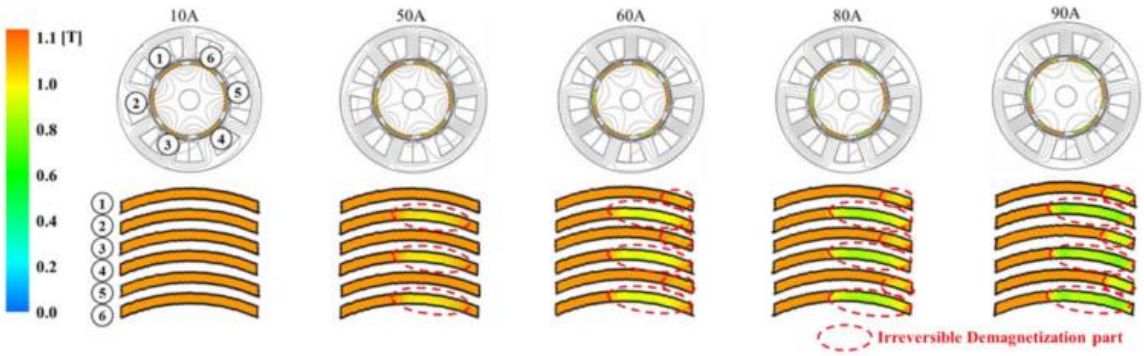

Fig. 5. Irreversible demagnetization result at static analysis in SPM model.

Fig. 1-27. Partial demagnetization due to the current with different magnitude [41]

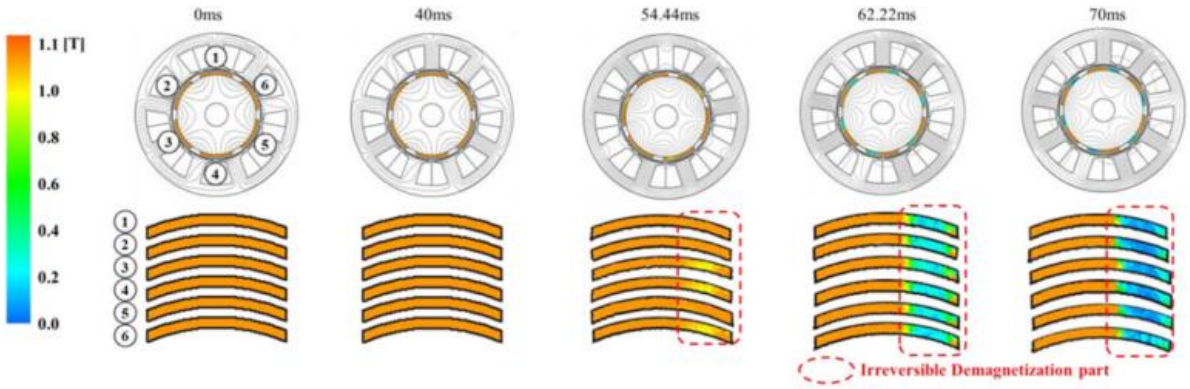

Fig. 8. Comparison of demagnetization ratio relative to current in SPM model.

Fig. 1-28. Partial demagnetization due to the current with different time width [41]

1.7 Effect of Eddy Current in Magnetization Process

Permanent magnets are conductive materials with electric resistivity. When the PWM inverter is used to operate machines, the harmonic magnetic field caused at the PWM frequency induces the non-negligible eddy current in the permanent magnets. The eddy current in the permanent magnet is often discussed in the context of loss analysis in the machine design area [43][44][45]. Also, the magnetization state estimation using the eddy current distribution in permanent magnets are also studied in the machine drive area [46]. In the research area of the magnetizing fixture and in-motor magnetization, the reaction field caused by the eddy current have been focused a lot.

The reaction field due to the eddy current has the opposite direction from the external magnetic field created by the stator winding current [44], [47]–[49]. The conceptual explanation of the origin of the reaction field is shown in Fig. 1-29. The circle and the cross in the magnets in Fig. 1-29 represent the eddy current in the permanent magnet and the arrows are the reaction field caused by this eddy current. Figure 1-30 shows the segregated magnetic field calculated using frozen permeability method[50]–[52]. Since this example uses NdFeB, which has

relatively high electric resistivity, the reaction magnetic field is much lower than the external magnetic field. Note: The marker of the external magnetic field in Fig 1-30 is 2 T, whereas the marker of the reaction field is 2mT.

The reaction field works as a disturbance in the magnetization process, causing the discrepancy between the desired magnetic field and the actual magnetic field that the permanent magnet is subjected to. Jewell addresses the reaction field from the point of view of the magnetizing fixture setup in [49]. It is summarized in reference [49] that a high-voltage magnetizer is suitable to multipole magnetization in general, since it results in shorter pulse duration, and hence lower fixture temperature rises for a given peak MMF. Nevertheless, high capacitance, low-voltage magnetizers are a better choice if a longer pulse duration is required to minimize eddy current effects.

Hemeida et.al [53] proposes an analytical solution of the eddy current in the permanent magnets taking the reaction field into account. In their approach, the surface and the inside of the permanent magnet is represented using an electric network model shown in Fig. 1-31. The inductances are introduced to describe the reaction field of the eddy currents flowing through a permanent magnet and also the skin effect.

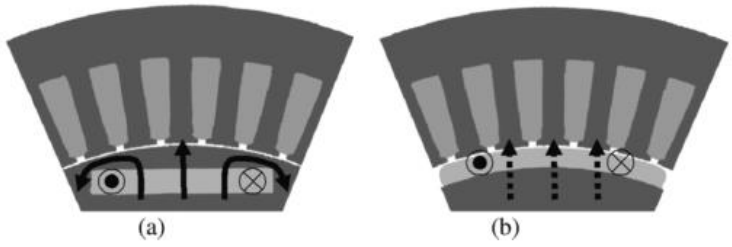

Fig. 7. Reaction field by magnet eddy currents. (a) IPM. (b) SPM.

Fig. 1-29. Reaction field by magnet eddy current [44]

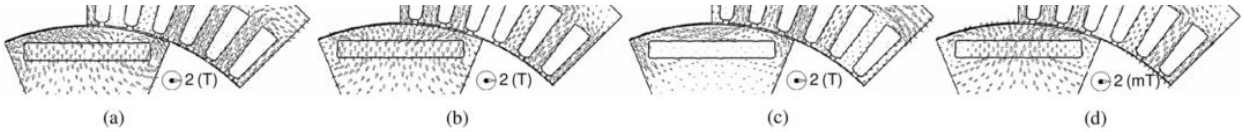

Fig. 9. Decomposed fluxes due to origins (IPM motor). (a) Total flux. (b) Magnetization flux. (c) Armature flux. (d) Reaction flux by eddy currents.

Fig. 1-30. Segregation of fluxes in an IPMSMM motor[44]

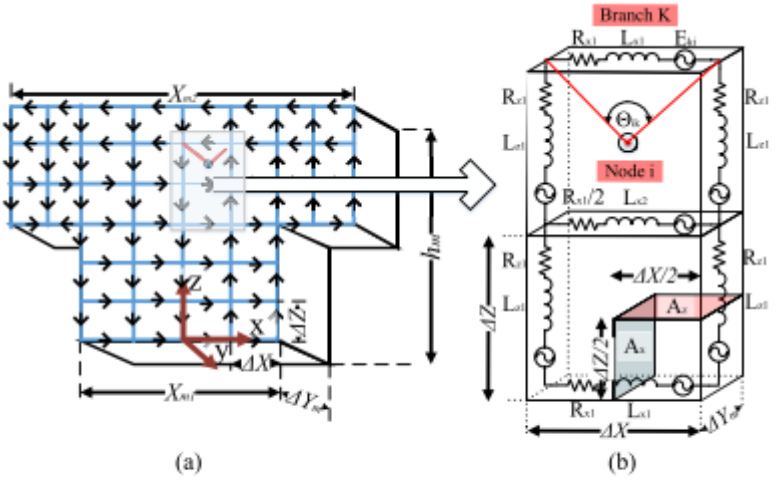

Fig. 7. Electric network distribution consisting of induced voltage, resistances, and inductances (self and mutual inductances). (a) PM complete circuit network. (b) One section of two nodes of the network.

Fig. 1-31. Analytical solution of the eddy current in magnets considering the reaction field[53]

1.8 Permanent Magnet Model in Numerical Analysis

Machine analysis relating to the magnetization in the research level often employs finite element analysis. In this section, the necessity of the finite element analysis in the magnetization analysis and the high-level explanation about how the characteristics of the permanent magnet are considered in the finite element analysis are summarized. Also, topics explored in recent academia in terms of the permanent magnet modeling in numerical analysis are covered.

1.8.1 Lumped circuit model of permanent magnet

The magnetism in an electromagnetic system including magnet material is often modeled using lumped parameter magnetic equivalent circuit. The interrelationships between the

magnetic and the electrical circuits are shown in Fig. 1-32. The analogy between the magnetic and electrical circuit are summarized in Table.1-3. In Fig. 1-32, the Magnetomotive Force, MMF (F) is supplied by the current in the coil winding around a steel core. The small magnetomotive force drop in steel is often neglected in a similar manner with the voltage drop in wires in the electric circuit.

In Fig. 1-33, a permanent magnet is substituted to supply MMF. In the lumped circuit model, a magnet is modeled with a series of MMF source and reluctance. The MMF source corresponds to the permanent magnet can be defined as (1-8) [54].

$$MMF = H_{op} l_m = \frac{1}{\mu_0} \frac{A_m l_g}{A_g} B_{op} \qquad (1\text{-}8)$$

Although the length and the surface area of the permanent magnet can be considered in the lumped circuit model, the magnetization spatial distribution inherently cannot be captured. It is because the lumped circuit model is a method to simplify the spatially distributed physical quantity into constant discrete entities.

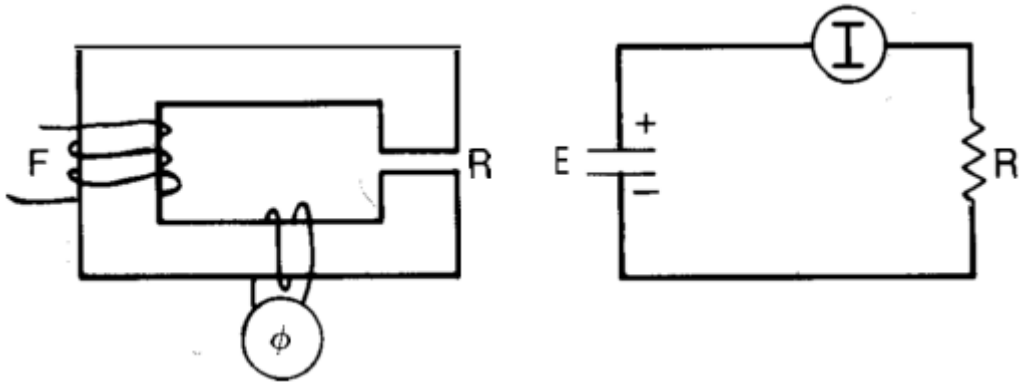

Fig. 1-32. Interrelationships between the magnetic and the electrical circuits [55]

Table 1-3. Analogy between the magnetic and electrical circuit

Electrical		Magnetic	
Resistance	$R = \frac{l}{\sigma A}$	Reluctance	$\mathcal{R} = \frac{l}{\mu_0 \mu_r A}$
Current	I	Magnetic Flux	ϕ
EMF	E	MMF	F

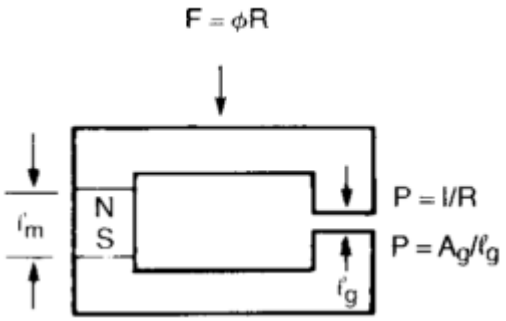

Fig. 1-33. Magnetic equivalent circuit with permanent magnet[55]

1.8.2 Analytical solution based on Biot-Savar's law

The magnetic flux density at an arbitrary point is uniquely determined by the magnetization of the magnet. Analytically, the magnetic flux density at an arbitrary point in an area including a permanent magnet shown in Fig. 1-34 is obtained as follows by following Biot-Savar's law,

$$\mathbf{B}(x,y,z) = \frac{\mu_0}{4\pi}\int_{V_0} \nabla\cdot\mathbf{M}(x',y',z')\cdot\frac{\mathbf{r}-\mathbf{r}'}{|\mathbf{r}-\mathbf{r}'|^3}\,dv' + \frac{\mu_0}{4\pi}\int_{S_0}\mathbf{M}(x',y',z')\cdot\mathbf{n}\cdot\frac{\mathbf{r}-\mathbf{r}'}{|\mathbf{r}-\mathbf{r}'|^3}\,ds' \qquad (1\text{-}9)$$

The first component in the right-hand side is a volumetric integration of divergence of magnetization, whereas the second component of the right-hand side is a surface integration of magnetization and a normal vector of the surface.

If the magnetization distribution is uniform, the first component becomes zero. In this case, only the magnetization distribution on the surface effects the phenomena, hence the calculation can be simplified. Meanwhile, if the magnetization distribution is not uniform, all of the magnetization inside of the magnet volume need to be taken into account. Especially, when the magnetization in the permanent magnet is not homogeneous in any direction, manual calculation of the volume integral in the first component is difficult. In such case, the numerical calculation becomes an almost vital tool to solve the problem. It should be noted that when a numerical

model is built for this problem, the resolution of geometrical discretization of the model affects accuracy due to the divergence in the first component [54].

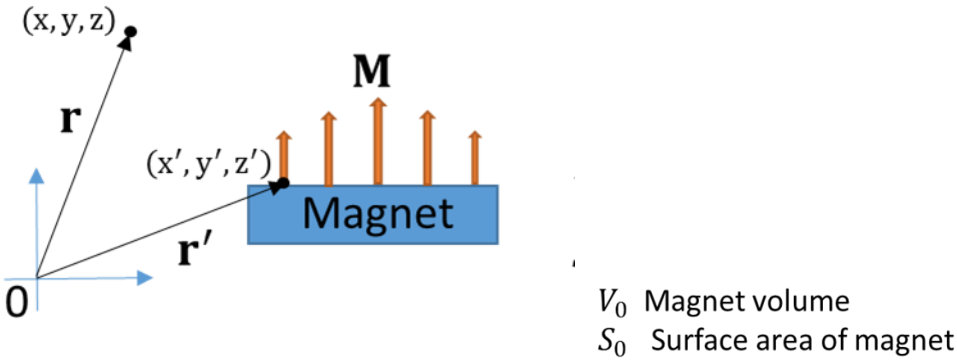

Fig. 1-34. An arbitrary point in an area including a permanent magnet

1.8.3 Calculation flow of FEA including magnetization characteristics

Electromagnetic FEA is a numerical calculation method to solve the spatially and temporally discretized Maxwell equation as taking vector potentials as unknown values. Typical calculation flow of time transient electromagnetic FEA is shown in Fig. 1-35. The material property of the permanent magnet is considered in the hysteresis calculation loop. In order to solve the Maxwell equation including the permanent magnet, essentially, the magnetization **M** is needed as an input of equations. However, the magnetization changes dynamically depending on the magnetic flux density obtained from the vector potentials, that are unknown variables of the system. Therefore, an iterative process using a nonlinear material curve essentially happens in FEA calculation to determine the operating point of magnets.

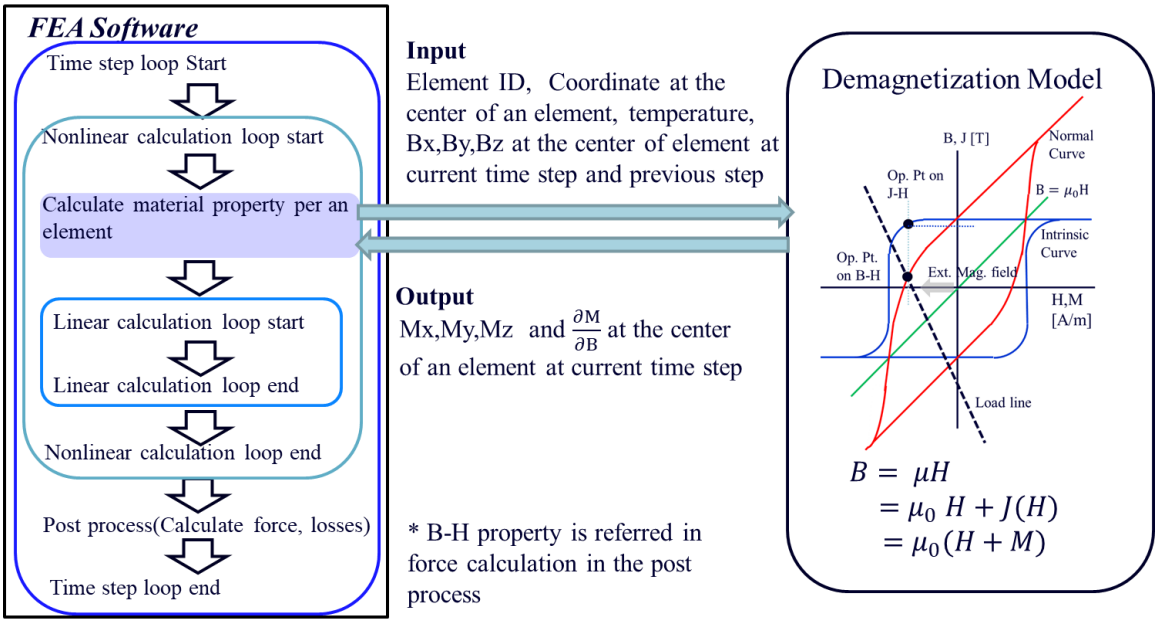

Fig. 1-35. Flow-chart for typical finite element analysis considering the demagnetization [56], [57]

1.8.4 Representation of B-H characteristics

The modeling of the B-H property of the permanent magnet is an inherently critical factor in the analysis of de/re-magnetization of magnets in machines. Although the demagnetization caused by temperature is quite interesting and important topics in the machine designs, the demagnetization by the current is primarily discussed here to focus on the research subject. Demagnetization modeling due to the current can be categorized into four models; limit model, linear model, exponential model and Hysteresis model [58]–[60].

The limit modes shown in Fig.1-36(a) is the simplest model among four models. It is also called the coercivity limit model. In this model, the B-H curve is a straight line up to a certain limit, corresponding to the intrinsic coercivity J_{Hc} [61].

Linear models shown in Fig.1-36(b) are often used for the conceptual explanation of the demagnetization. It defines the demagnetization using two straight lines, one is from remanence

to the knee point and another is from the knee point to the coercivity. The curve's roundness around the knee point is not considered in this case [62].

An exponential model using the full demagnetization curve created by a sort of the curve fitting as shown in Fig. 1-37 has been proposed by Ruoho[61], [63]. Eriksson [64] experimentally verified the exponential model using the magnetizing fixture for the case the permanent magnet is partially demagnetized by the excessive current. They claim that the maximum deviation of simulation and experiment is 3% for the most part of the tested permanent magnets.

Hysteresis model contains more complicated mathematical process and measurement data are required in this model to replicate the material's behavior. However, it has received attention since it can provide relatively accurate minor loop behavior among the existing demagnetization modeling methods [59], [65]–[68]. The Preisach model is one of the hysteresis modeling methods and is widely applied for magnetic material modeling from the soft magnetic material to the hard-magnetic material. Preisach theory describes the hysteresis of ferromagnetic material as an infinite set of magnetic dipoles which have rectangular hysteresis loops shown in Fig. 1-38.

K.T. Chau et.al [65] have reported the general expressions of the Preisach hysteresis model of the AlNiCo used in the time-stepping finite element method. They have developed the algorithm to generate B-H minor loops based only on the input data of the major loop, without involving statistically distributed parameters or empirical adjustment. The minor loops for AlNiCo obtained through their algorithm is shown in Fig. 1-39.

Yu, C et al. [66] have shown a performance comparison of the Preisach model and the linear model with an experimental result obtained from a machine with AlNiCo-5. Comparative study regarding the B-H modeling of AlNiCo in machines are not often seen so this is a

relatively rare report. They claim that the linear model shows adequate matching with the Preisach model and the experimental result as shown in Fig.1-40.

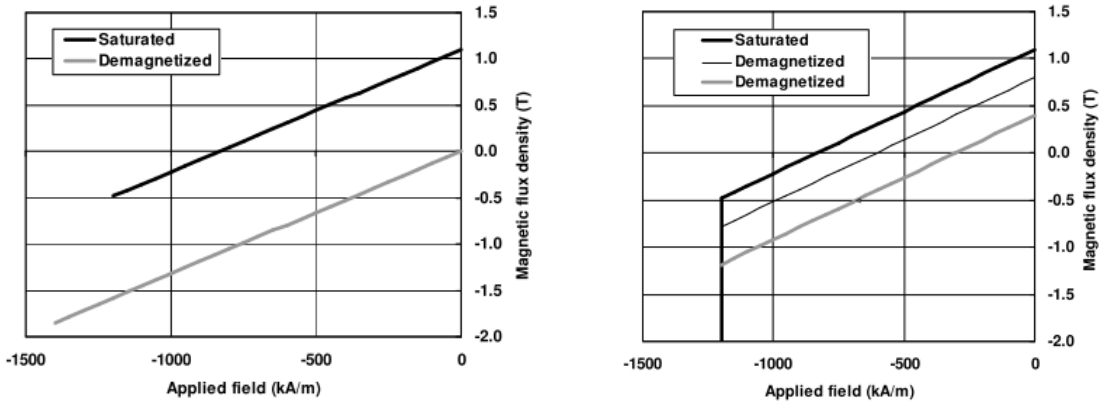

(a) Limit Model (b) Linear Model

Fig. 1-36 Simplified demagnetization model [61], [63]

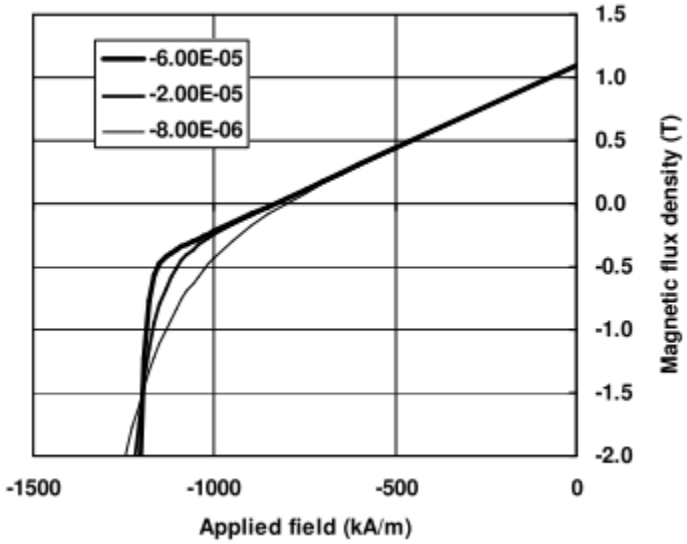

Fig. 1-37 Demagnetization model considering the roundness around knee point [63]

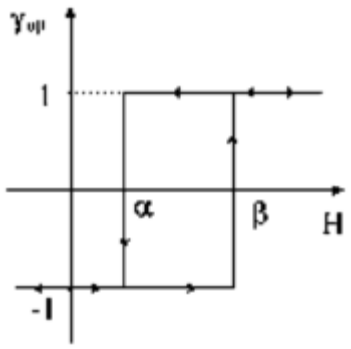

Fig. 1-38 Rectangular hysteresis loops [59]

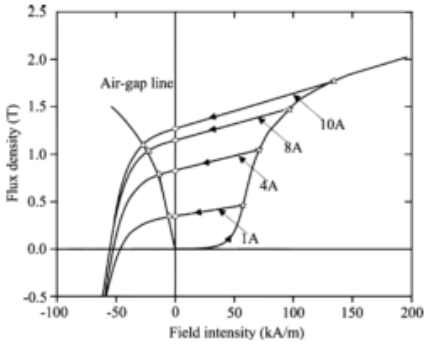

Fig. 7. Trajectories of AlNiCo-PM under various magnetizing currents.

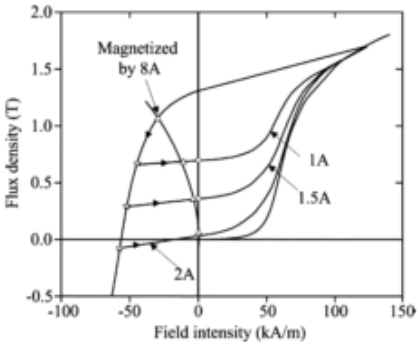

Fig. 9. Trajectories of AlNiCo-PM under various demagnetizing currents.

(a) Magnetization (b) Demagnetization

Fig. 1-39 Minor loops in AlNiCo [65]

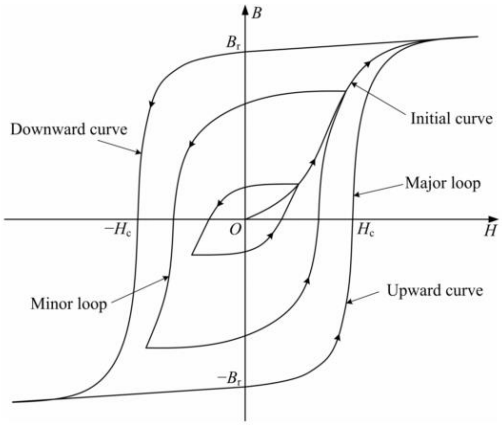

Fig. 2. Preisach hysteresis model.

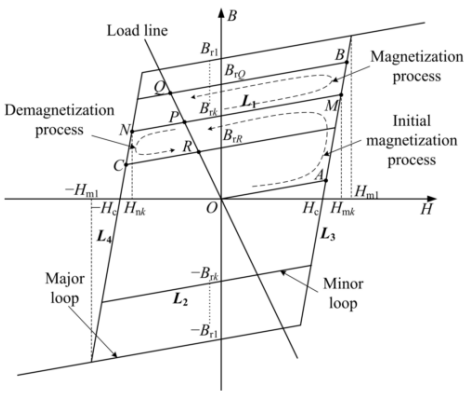

Fig. 3. Linear hysteresis model.

(a) Preisach hysteresis model (b) Linear hysteresis model

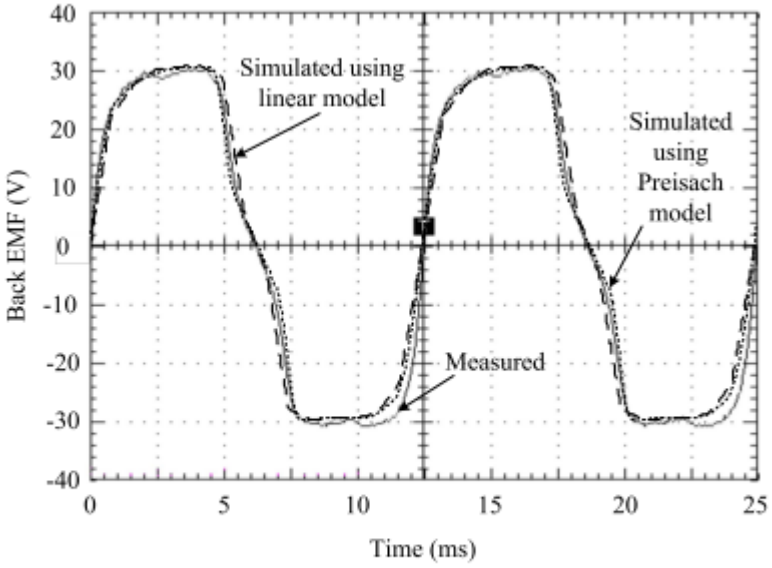

Fig. 6. Simulated and measured back EMF waveforms at 600 r/min.

(c) Back-EMF from linear model, Preisach model and measurement

Fig. 1-40 Minor loop representation [66]

1.9 Variable Flux Machines

In this section, variable flux permanent magnet (VF-PMSM) machines or memory flux machines are reviewed as an example of applications actively utilizing permanent magnet de/re-magnetization.

1.9.1 Fundamental ideas

VF-PMSMs have been proposed as one of the attempts to operate PMSMs with lower losses in variable speed applications. As PMSM variable drive technique evolves, applications of PMSM have spread out in the market, resulting in demands for wider operating area. For instance, traction motors for electric vehicles (EVs) need to be capable from the short distance drive in the city area with frequent stops to the long-distance drive in a highway with continuous high speed. Or, in-home appliance, washing machines with dryer functions have to be able to operate with variable loads according to the operating process. e.g. Heavy load in low speed is required in the washing process and the light load in high speed is required in the dryer process after draining out water as shown in Fig.1-41. Conventionally, machines are designed so that the machine's operating point can fit in the minimum loss region. However, in the case of the variable speed application revied here, the operating points may not necessarily be located in the minimum loss area.

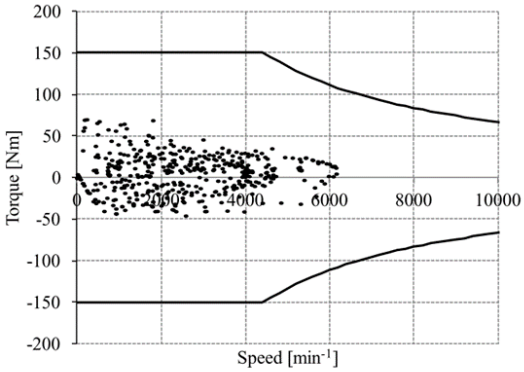

Fig. 2. Speed versus torque plots of an EV motor operation point in JC08 mode driving cycle.

(a) Automobile with JC08 mode driving cycle

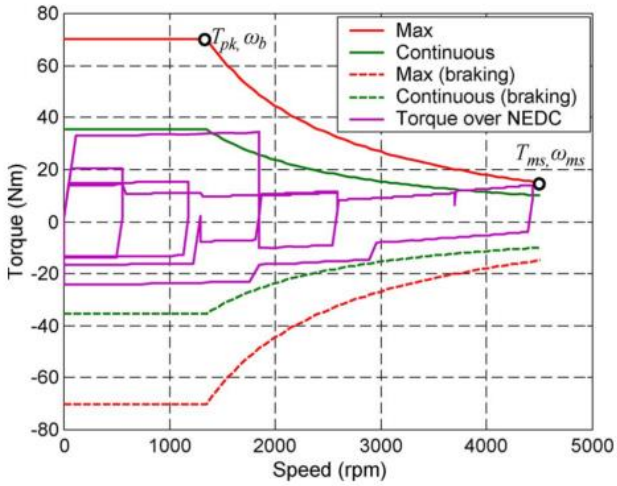

Fig. 2. Torque speed envelope.

(b) Automobile with NEDC driving cycle

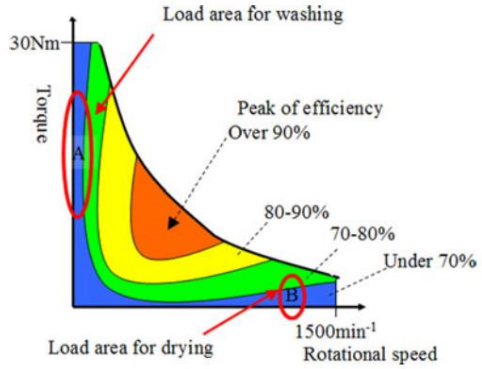

Fig. 3. Load areas of the washing machine for washing and drying are clearly divided.

(c) Operating region for washing machine the

Fig. 1-41. Operating points distribution and N-Curves of the several applications [69]–[71]

The original idea of VF-PMSMs is to reduce the copper loss caused by the continuous flux weakening current by changing the magnetization level of the permanent magnet. In the conventional machines, negative d-axis current is continuously injected to mitigate the magnet flux in the high speed so that the induced voltage caused by the spin of the magnet does not exceed the DC bus voltage. This technique is called flux weakening and has been widely used. By employing the flux weakening scheme, the available speed of PMSM has been remarkably extended [72], [73]. However, injecting additional continuous d-axis current to weaken flux results in the increase of the copper loss. In the case of VF-PMSMs, the available speed is

extended by demagnetizing permanent magnet through the high impulse current, instead of using the continuous low flux weakening current (Fig. 1-42 and 43). Since it does not need sustained flux weakening current, it indeed contributes to reducing the copper loss while achieving a similar or higher maximum speed with the conventional PMSMs (Fig. 1-44). In addition to that, it has been shown that VF-PMSMs can achieve lower iron losses than the conventional fixed magnetization pattern machines in [74]. It is because VF-PMSMs can reduce not only the fundamental component but also the harmonic components of magnet flux, unlike the flux weakening technique that only weakens the fundamental component in the magnet flux.

1.9.2 Machine topologies

The first VF-PMSMs proposed by Ostovici [75] and studied by Pillay [76]–[78] employ the spoke type topology with AlNiCo in order to avoid the uncontrolled demagnetization during the normal operation (Fig.1-45 (a)). In this topology, the magnetization vector in the permanent magnets is set in the tangential direction, so that the q-axis current by the armature current does not penetrate permanent magnet. Hence, this structure allows making the magnet wider in the radial direction without taking risk of the demagnetization during the normal operation enabling high magnetic flux density in the airgap.

Natee and his fellow group [74], [79]–[84]has proposed VF-PMSMs with radially magnetized magnets using fractional distributed winding from a consideration of the inverter rating aiming traction machine for EV. Since the current required to change magnetization state is essentially higher than the current for normal operation, the use of a high rating inverter is an unavoidable consequence of VF-PMSM drive system. In order to operate the overall system with lower losses, the machine topology using lower current for the magnetization state change is studied in [82], showing the machine configuration with radially magnetized magnets is advantageous to

reduce the inverter rating compared to spoke type machines. A choice of the arrangement of the radially magnetized magnet creates a constraint regarding the magnet width to avoid the demagnetization by the load current, bringing the limitation to the achievable magnetic flux density in the airgap [81]. Later they have compensated this limitation by arranging high coercive magnet, NdFeB, together with a low coercive magnet, SmCo [85] (Fig.1-45(b)).

An outer rotor type VF-PMSM with fractional concentrated winding shown in Fig. 1-45(c) has been proposed by Toshiba [71] and commercialized. Although the concentrated winding machine is more advantageous than the distributed winding machine in terms of the lower copper losses due to the short end windings, rich harmonic components in the concentrated winding bring a challenge to the fundamental mechanism of VF-PMSMs. In order to achieve the uniform magnetization state change, the entire surface of the magnet needs to be uniformly subjected to a certain level of demagnetizing MMF. However, the existence of the harmonic components in concentrated winding causes a deviation in the spatial distribution of MMF. The machine proposed in [71] has a relatively high number of poles and slots (48 poles 36 slots) compared to other VF-PMSMs, resulting in wider stator core teeth than the magnet's width. This structure enables to fully de/re-magnetize magnets even with the concentrated windings containing rich harmonics. A penalty of this structure is, essentially it needs to inject two current pulses to uniformly change the magnetization state as changing the rotor position since the number of slots per poles per phase (SPP) of this machine is 1 by 2.

Overall, rotor designs have been most discussed in this field from the points of view to minimize magnetizing current while maintaining the full re-magnetizing capability, high torque capability and constant power capability over the entire speed range. Meanwhile, stator design has not been discussed as much as rotors. Therefore, fundamental questions regarding the design

of machines using an active magnetization change technique, such as applicable slot pole combinations and winding configurations, have not been clearly answered yet in this field. Although there are a few reports about the comparison of the slot pole combination from the point of the minimization of the magnetizing current [77], [78] , these discussions have not reached general comprehensive guidelines.

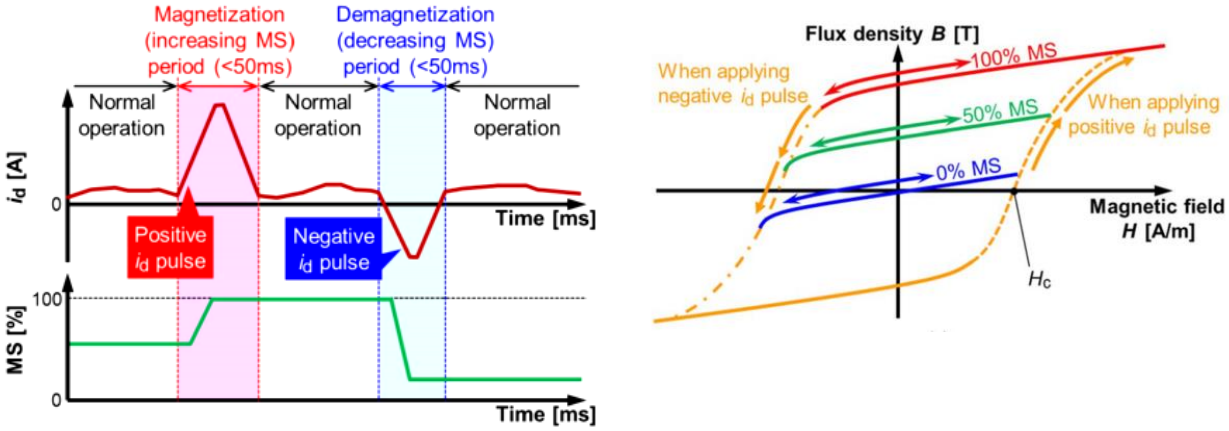

Fig. 1-42. Current trajectory and the conceptual B-H history in VF-PMSMs [81]

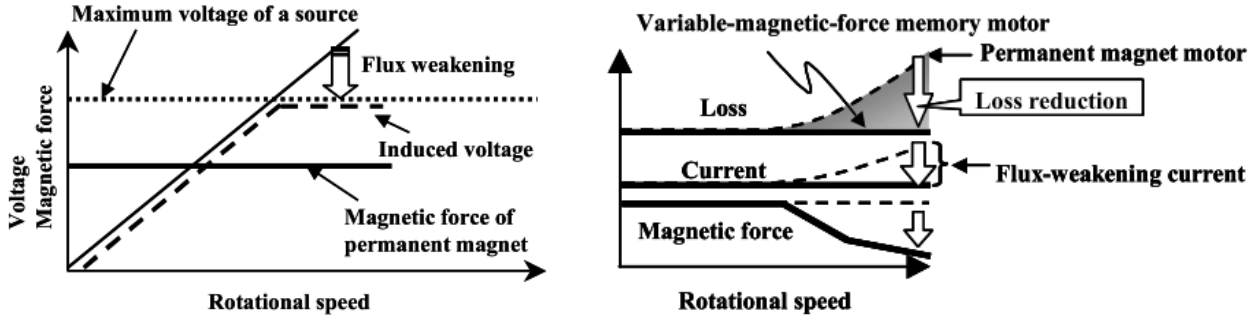

Fig. 1-43. Mechanism of loss reduction in VF-PMSMs [86]

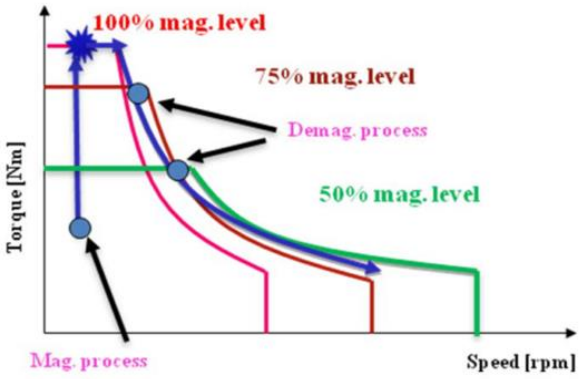

Fig. 1-44. Mechanism of operating area expansion in VF-PMSMs

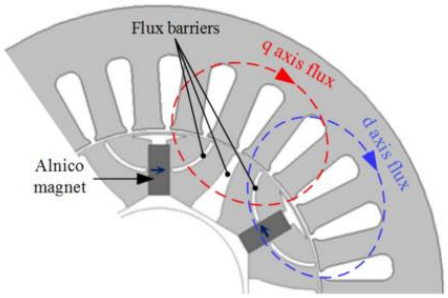

Fig. 2. Illustration of the *d*- and *q*-axis flux paths in the tangentially magnetized variable flux machine.

(a) VF-PMSM with spoke type magnet and distributed winding [77]

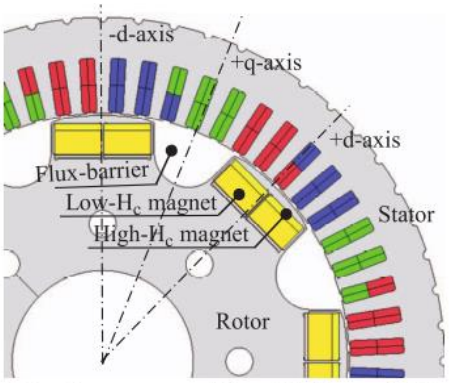

(a) Geometry of the fabricated VF-PMSM machine

(b) VF-PMSM with radial type magnet and distributed winding [74]

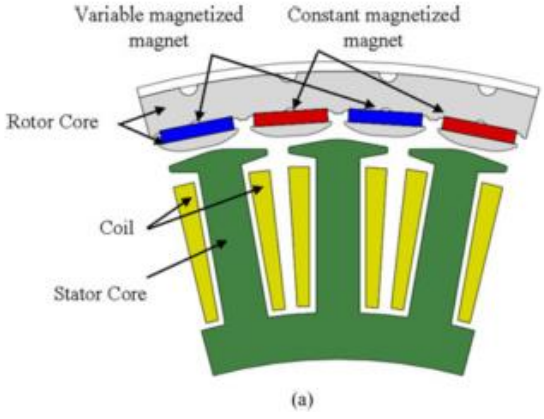

(c) VF-PMSM with radial type magnet and concentrated winding [71]

Fig. 1-45. Topology of VF-PMSMs

1.9.3 Permanent magnet materials

Magnet material characteristics are one of the most critical factors in machines using an active magnetization change technique. There are several different kinds of low coercive magnets materials and the choice of magnets predominantly determines the performance of the machines. Nevertheless, comprehensive design methodology including the material selection has not been published.

For instance, an insightful analytical design guide of VF-PMSMs is provided in [115], however, the discussion there is limited within an assumption that the magnet material is already selected. Similarly, the optimal magnet material curve to meet the desired machine spec is obtained in [74] by adjusting the ratio of the low coercive force magnet and the high coercive force magnet, but the magnet materials and the rotor geometry there are given in that optimization process.

Reference [116] compares three different type of low coercive magnets, Ferrite, AlNiCo and SmCo in a VF-PMSM predominantly using finite element analysis (FEA). This study is keenly aware of the importance of the magnet property in active magnetization change techniques, however, in their discussion, all magnets have the same dimension and the remagnetizing current is not considered.

1.9.4 Magnetization state change technique

Magnetization state change technique has two inherent unique challenges. One is pulsating torque the during magnetization change process, another is high-speed capability. When a high pulse current is injected into the machine to change the magnetization state, severe pulsating torque can be produced in VF-PMSMs due to the sudden increase of the reluctance torque by current injection and the magnet torque by MS change [83]. At the same time, large pulse

current causes high induced voltages which can be violating the inverter voltage limit. This concern limits the maximum speed at which the magnetization state change can happen [87]. An example of the speed limit of the magnetization change in the current vector control system is shown in Fig. 1-46.

In order to avoid the pulsating torque, the magnetization state manipulation is often implemented at zero speed, zero load conditions or by using pre-defined current vector trajectory lookup tables under non-zero speed and loaded condition [88]. An observer-based current decoupling method without current trajectory look-up tables is proposed by [83] . However, it still needs a pre-defined look-up table of magnetization state (MS) as a function of magnetizing current. Also, magnet flux in [83] is controlled by the open loop.

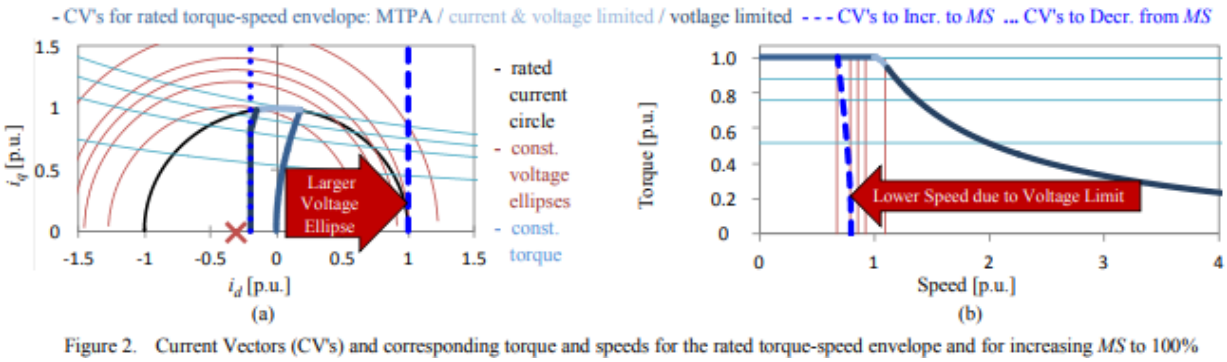

Figure 2. Current Vectors (CV's) and corresponding torque and speeds for the rated torque-speed envelope and for increasing *MS* to 100%

Fig. 1-46 The speed limitation found in magnetization state change [89]

In [89], closed-loop MS control system with deadbeat-direct torque and flux control (DB-DTFC [90]) using nearly zero lag MS estimator has been proposed. The MS estimator is able to instantaneously capture the wide variation of inductances depending on operating points by having a structured neural network (SNN) inside of the system. Such instantaneous parameter estimators enable to implement DB-DTFC algorithm in MS feedback control system. Since both

torque and stator flux are simultaneously controlled in DB-DTFC, inherently the MS control system using DB-DTFC maintain smooth torque even during the magnetization change process. The experimental evaluation from [89] is shown in Fig. 1-47.

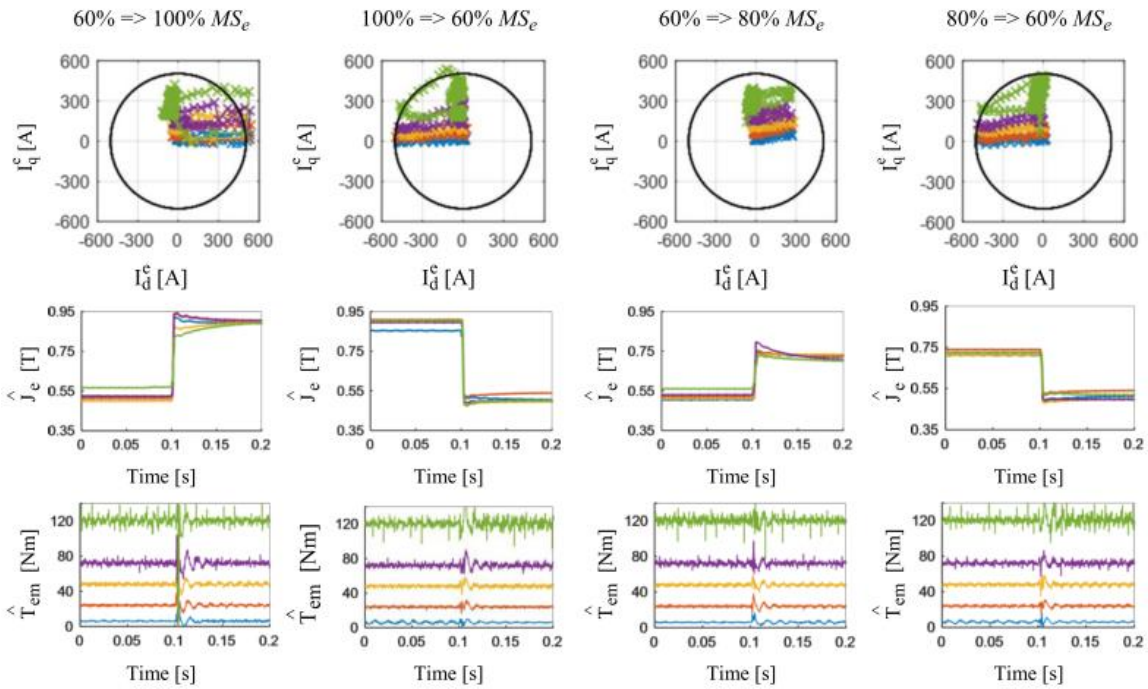

Fig. 11. Experimental evaluation of closed-loop J_e control under various load conditions, at close to base speed (2000 rpm)
- 120 Nm, - 60 Nm, 48 Nm, -24 Nm, - 6 Nm, - rated current circle

Fig. 1-47. Closed-loop MS control system with DB-DTFC [89]

Reference [80] proposes a method to extend the speed capability of VF-PMSMs by designing suitable flux trajectories based upon the direct flux control scheme. The straight line stationary frame flux linkage trajectory (SLλ^2T) developed in their research achieves the maximum possible speed capability by optimally utilizing the inverter bus voltage and an extremely short MS trajectory duration as shown in Fig. 1-48. The drawback of this method is a significantly large pulsating torque. In the case of the automobile application, in which [80] aims to use the proposed method, the high frequency pulsating torque in the high-speed region is absorbed by

the vehicle dynamics system, hence, it practically does not bring problems. In low speed, the pulsating torque is still a non-negligible problem, hence, other magnetization change methods are required in that operating region.

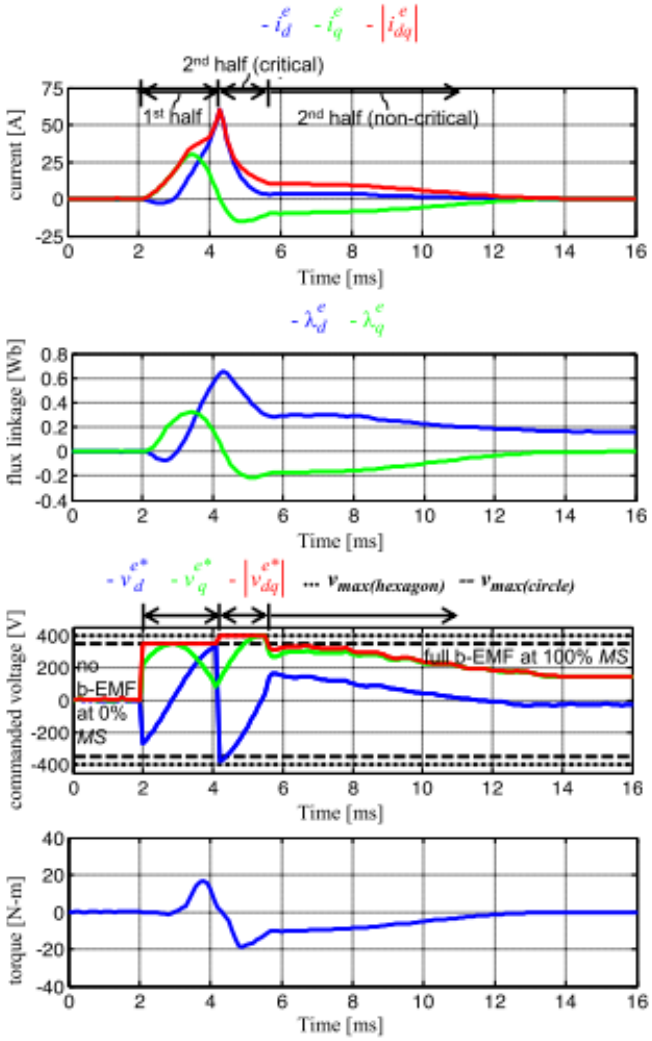

Fig. 11. Experimental evaluation of synchronous reference frame currents, flux linkages, commanded voltages, and torque in time domain for the SLλ^sT to increase MS from 0% to 100% at 3350 R/Min (1.52 p.u.) Speed, 600 V_{DC} bus, starting and ending at zero current.

Fig. 1-48. straight line stationary frame flux linkage trajectory (SLλ^2T) method proposed in [80]

1.10 Modulation Techniques for Inverters

In previous sections, technologies relating to machines with permanent magnets have been reviewed from the viewpoint of the spatial distribution of magnetization, implicitly assuming modulation technique of inverters is fixed during the operation. However, in recent progress in the inverter technology, machine drive systems capable of changing modulation methods during operation are becoming popular subjects. In this last section in the state-of-the-art review, existing publications regarding the variable current waveform drive are summarized in order to reconsider the meaning of the variable feature in machine drive systems.

Sinusoidal pulse width modulation (PWM) inverter is commonly used for PMSM drives. In this modulation technique, the commanded voltage magnitude is replicated by adjusting the output width of DC bus voltage within one switching period. Since this modulation method is able to construct the pseudo-sinusoidal current waveform in machine windings, it is well fit to the ideal AC machine theory based on an assumption of the sinusoidal current waveform.

However, from the standpoint of the utilization of DC bus voltage and switching loss reduction, this modulation technique may not be the best choice.Instead, the modulation technique so-called six-step operation, square wave drive or overmodulation drive in which the turning on and off of switches happen for 120 electrical degrees per cycle is superior in terms of the modulation index and less frequent switchings [91], [92].

The modulation index is the normalized fundamental voltage, defined as

$$m_{index} = \frac{u_1}{u_{1six\text{-}step}} \qquad (1\text{-}10)$$

Where u_1 is the fundamental component in voltage generated by the modulator and $u_{1six\text{-}step} = 2/\pi\ U_d$ the fundamental component in the voltage at six-step operation. In the case of the

sinusoidal PWM where the reference is a sinusoidal voltage between phase and neutral, the fundamental component is U_d / 2. Therefore, the maximum modulation index m_{index} = 0.785 is obtained. In the case of the six-step operation, m_{index} =1 is achieved [91].

Although six-step operation causes more pulsating torque and more iron losses in machines compared to sinusoidal PWM as shown in Fig. 1-49, it can contribute to enhancing the operating region of the drive due to the high modulation index as shown in Fig. 1-50. In addition, it also can reduce the losses caused by switching. In short, there is no clear ranking between PWM and six-step methods, rather, the design decision regarding the drive system need to be made considering the tradeoff between each modulation technique [93].

For instance, the combined use of the sinusoidal PWM in the low speed and the six-step operation in the high speed have been proposed for the traction PMSM drive in EVs and HEVs [94]. The pulsating torque in low speed is a high-priority problem in the automobile application, thus, the choice of the sinusoidal PWM operation is out of the question in that operating region. In contrast, in high speed, the pulsating torque can be absorbed by the inertia of the motor itself. Therefore, the operating expansion by the six-step operation is a quite realistic and reasonable option in such an operating region.

In the case of the motors used in the household electric appliances, the opposite approach has been taken. Reference [95] reports an example of PMSM drive used in compressors in refrigerators that employs sinusoidal current drive for the high-speed operation and six-step drive for the low-speed operation. The main focus of [95] is to minimize total losses in entire operation by balancing the trade-off between the iron loss due to the rich harmonic component in six-step operation and switching loss from sinusoidal PWM operation.

Although these two examples reviewed here eventually select the opposite combination of the modulation and the speed, the main shared idea is to utilize the variable feature of the modulation method in order to optimize the performance of the total drive system according to the priority imposed to each application.

As an extension of discussion regarding modulation technique, Miyamasu [96] reports interesting attempts. In general, BLDC machines (SPMSMs with a fixed trapezoidal back-EMF) and BLAC machines (SPMSMs with a fixed sinusoidal back-EMF) are designed assuming that the drive current waveform matches to each no-load back-EMF shape as shown in Fig.1-51 (a) [7]. Merging the knowledge from this machine design and modulation technique [96] have been empirically verified that drive systems using same waveform shape in the current and in the back-EMF achieve better efficiency than drive systems that use different waveform shape in current and back-EMF as shown in Fig. 1-51 (b). This suggests that the modulation change techniques reviewed through [94] and [95] can bring more benefit in terms of loss reduction if they are combined with dynamic variable back-EMF waveform changes.

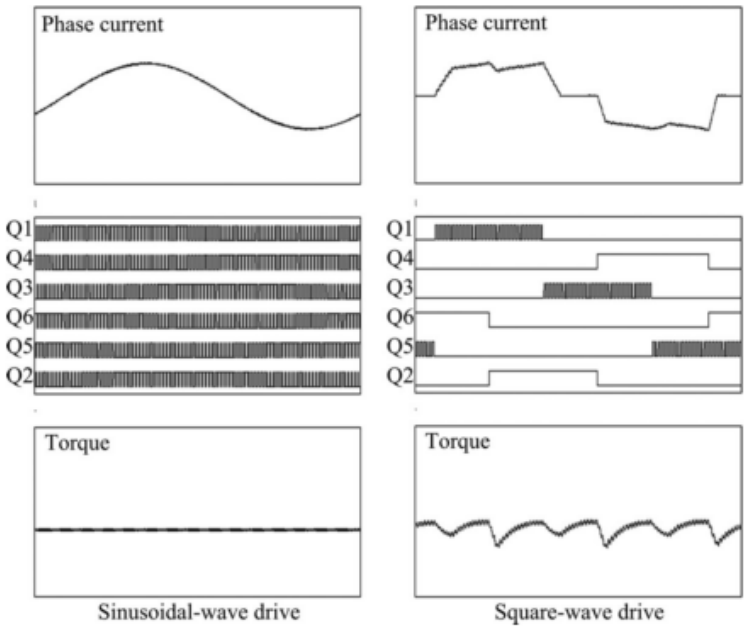

Fig. 1. Comparison of phase current, gating signals, and generated torque of the PMSM according to the driving mode.

Fig. 1-49. Current, gate signal and torque from sinusoidal-wave and square-wave drive [95]

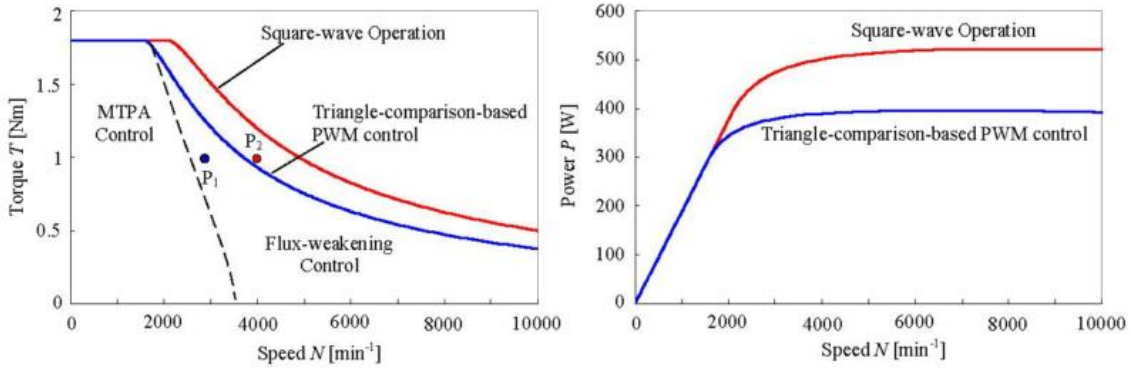

(a) Torque versus speed characteristics. (b) Power versus speed characteristics.

Fig. 1. Comparison of torque and power characteristics for two kinds of inverter control schemes.

Fig. 1-50. Operating area expansion by square wave operation [97]

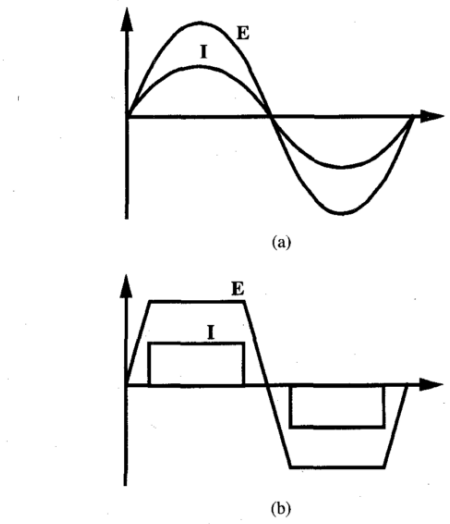

Fig. 1. Idealized phase excitation waveforms for the two major classes of PMAC machines. (a) Sinusoidal. (b) Trapezoidal.

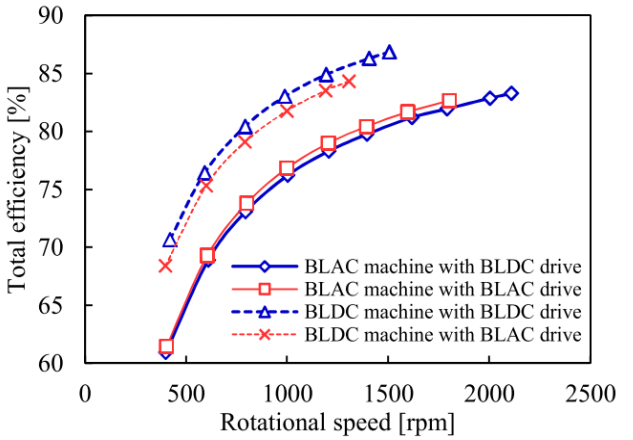

Fig. 15 Experimental results of the total efficiency of BLDC machine and BLAC machine with BLDC drive and BLAC drive.

(a)Operation of BLAC and BLDC [7] (b)Total efficiency of BLAC/DC machine and drive [96]

Fig. 1-51. Benefit of BLAC and BLDC

1.11 Summary of Research Opportunities Identified

The following research opportunities have been identified in the state-of-the-art review:

- **Machines with dynamic variable spatial properties**

A large amounts of efforts has been paid in the machine design area to shape the magnetization pattern in a static manner to achieve “better” back-EMF to reduce the pulsating torque and losses. However, since demands on machines in modern applications have become multi-objective and the expected operating region have been expanded, these static geometrical modifications may not satisfy all requirements regarding losses and torque in modern applications. Meanwhile, in the machine drive area, the hybrid drive systems using six-step operation and sinusoidal PWM have been already realized, achieving the loss reduction and the operating area expansion. Similar gains are

obviously expected if the back-EMF waveform can dynamically change by shaping magnetization pattern.

- **Method to dynamically manipulate the spatial magnetization distribution in operating motors**

  In-motor type magnetization manipulations in existing publications including VF-PMSMs show the possibility of dynamic spatial property change in machines. However, their common goal in existing reports is only to achieve the uniform magnetization distribution. Hence, the manipulation of spatial distribution has not been evolved there. A conceptual attempt to shape arbitrary magnetization patterns exists but the practical feasibility has not been clarified.

- **Machine design methodology to enable dynamic magnetization pattern manipulation**

  Passive machine design methodology to realize dynamic variable properties in permanent magnets is not established. One of the most basic considerations in the conventional SPMSMdesign process is to prevent the unintentional demagnetization during the normal load operation. In the case of the design of SPMSMs with a variable magnetization pattern shaping capability, in addition to such conventional concerns, intentional de/re-magnetization during the magnetization change operation needs to be considered.

- **Machine control methodology to enable dynamic magnetization pattern manipulation**

  In order to elevate VF-PMSMs from the concept level to the rigorous technology that can be used in the practical scene, not only the machine design but also the control

system needed to evolve further. The pulsating torque during the magnetization change process and the high-speed capability are unavoidable inherent challenges in magnetization state change techniques since the magnetizing current is essentially higher than the rated load current. In the case of the VF-PMSMs, solutions to these challenges are proposed from the control side. Machines with a variable magnetization pattern shaping capability also need to have solutions to these inherent problems.

- **Modeling method of demagnetization property of permanent magnet for the magnetization state control considering the spatial magnetization distribution**

  Discussion regarding machines with an active magnetization state change inherently needs to incorporate the demagnetization modeling since the hysteresis behavior of permanent magnets governs the variable characteristics of such machines. As a common practice, a low-cost hysteresis modeling such as a lumped parameter representation with MMF and flux is often used in the conceptual explanation of VF-PMSMs. In the case of the machines with a variable magnetization pattern shaping capability, the fidelity level of the conceptual model must be beyond the conventional lumped parameter since the spatial attribute needs to be considered.

Chapter 2 Dynamic Manipulation of Spatial Magnetization Distribution

2.1 Introduction

In this chapter, the fundamental idea of dynamic manipulation of magnetization patterns in the permanent magnet is developed based on an analytical model. The in-motor magnetization pattern manipulation method[38] is refined using the proposed model. The prototype model is designed based on the fundamental principal and experimentally tested.

2.2 Concept of Dynamic Manipulation of Magnetization Pattern

In order to represent the spatial demagnetization in permanent magnets in SPMSMs, a virtually subdivided permanent magnet model shown in Fig.2-1 is used in this work. Figure 2-2 is an equivalent magnetic circuit for the subdivided permanent magnet model. In this model, the permanent magnet and the stator winding MMF are virtually subdivided into pieces in the circumferential direction. Assuming that the magnetization orientation is radial, each segment can be represented as magnetically independent from the adjacent segments.

In the situation shown in Fig.2-1, segments in the left edge of the permanent magnet are subjected to the positive MMF, that is high enough to keep the operating point of the segments above the knee point in B-H curve. Meanwhile, the segments in the right edge of the permanent magnet are subjected to the negative MMF that pushes the operating points of the segments below the knee point. As a result, the left side of this bar magnet does not experience the demagnetization, but the right side is demagnetized. Consequently, the magnetization distributes in an non-homogeneous manner in this bar magnet.

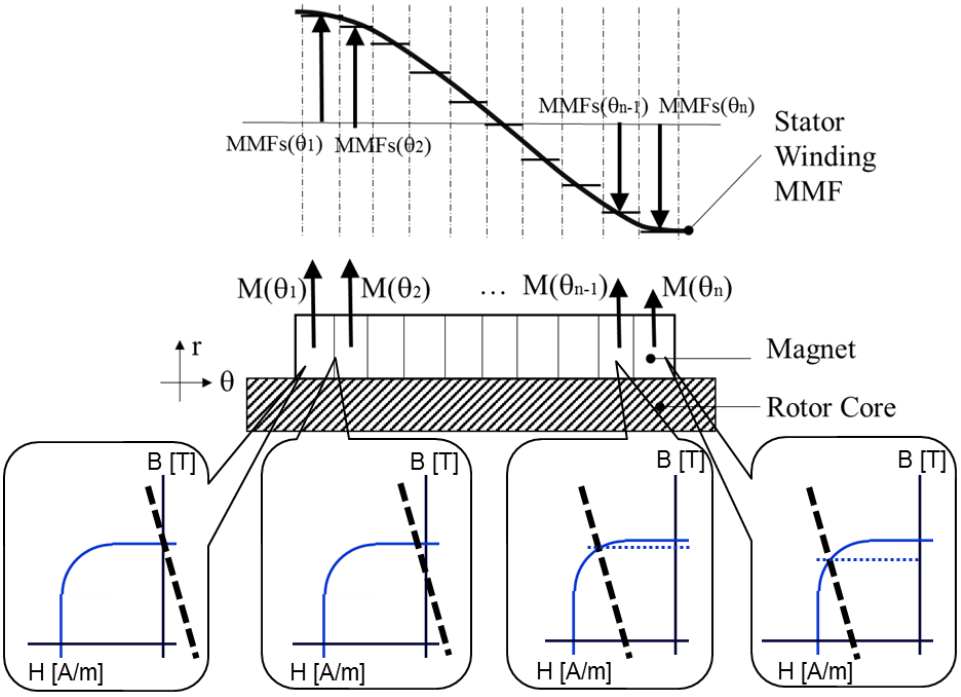

Fig. 2-1. Virtually subdivided magnet model

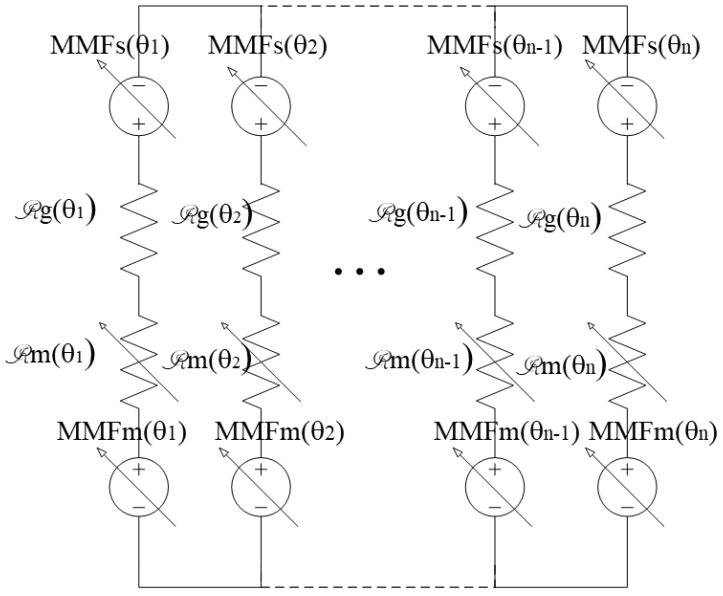

Fig. 2-2. Equivalent magnetic circuit for virtually subdivided magnet model

This model expresses that the demagnetized area is governed by the phase angle of the stator MMF. It other words, the demagnetized area moves along with the phase angle of the current vector injected into a machine since the stator MMF is a function of winding current.

The expected ideal stator MMF distributions in a machine corresponding to two types of the current vector injection are shown Fig.2-3. In the case of the negative d-axis current vector injection, the peak of the sinusoidal stator MMF is located at the center of the magnet (Fig.2-3(a)). This current vector injection is used in the global uniform magnetization state change in the conventional VF-PMSMs. Meanwhile, when the current vectors are injected twice, in the first quadrant and the fourth quadrant respectively, the peak of the stator MMF is not located at the center of the magnet (Fig.2-3(b)). Rather, both edges of the permanent magnet are subjected to the higher stator MMF in the negative direction. If this stator MMF at both edges is high enough so that it can cause demagnetization, this magnet has high magnetization state at the center and low magnetization state at both edges. Machines with dynamic variable spatial properties, referred to as Variable Magnetization Pattern Permanent Synchronous Machines (VMP-PMSMs) in this document are developed based on this idea.

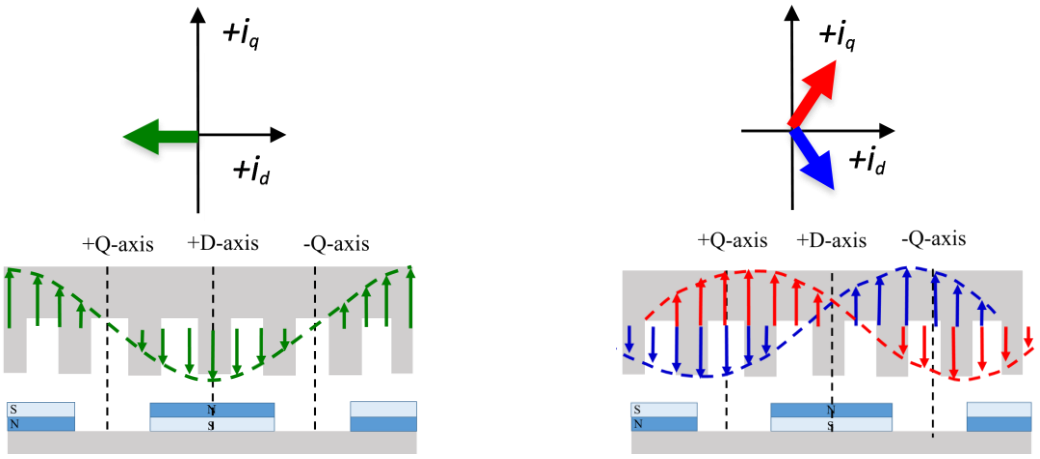

(a) (b)

Fig. 2-3. Magnetic field distribution by i_d and i_q

Both the global uniform magnetization state change and the magnetization pattern change are subsets of the active magnetization change techniques as shown in Fig. 2-4. The characteristics of the magnetization pattern change can be more organized when it is compared with the global uniform magnetization state change for VF-PMSMs as shown in Table. 2-1.

The main focus of global uniform magnetization state change is on a one-dimensional quantity, permanent magnet flux, whereas the target of the magnetization pattern change is to change the two-dimensional attribute, magnetization pattern. In the case of the VF-PMSMs, in order to assure that the entire surface of the magnet is subjected to the certain level of the stator MMF by the d-axis current injection, relatively narrower magnet is chosen. However, in the case of the VMP-PMSMs, the wider permanent magnets are chosen so that it can have more room to change the magnetization state. Only the d-axis current is used as a magnetizing current vector in the VF-PMSMs, while both d- and q-axis current are used as magnetizing current vectors in the VMP-PMSMs.

The benefits brought by each technique are also different. The global uniform magnetization state change contributes to expanding the operating area as well as to reduce the copper loss and the iron loss by reducing the fundamental component of the magnetic flux density. In the case of the magnetization pattern change, in addition to these benefits achieved by the global uniform magnetization state change, the further iron loss reduction and pulsating torque reduction can be expected because it can reduce the harmonic components in the magnetic flux density by the magnetization pattern shaping.

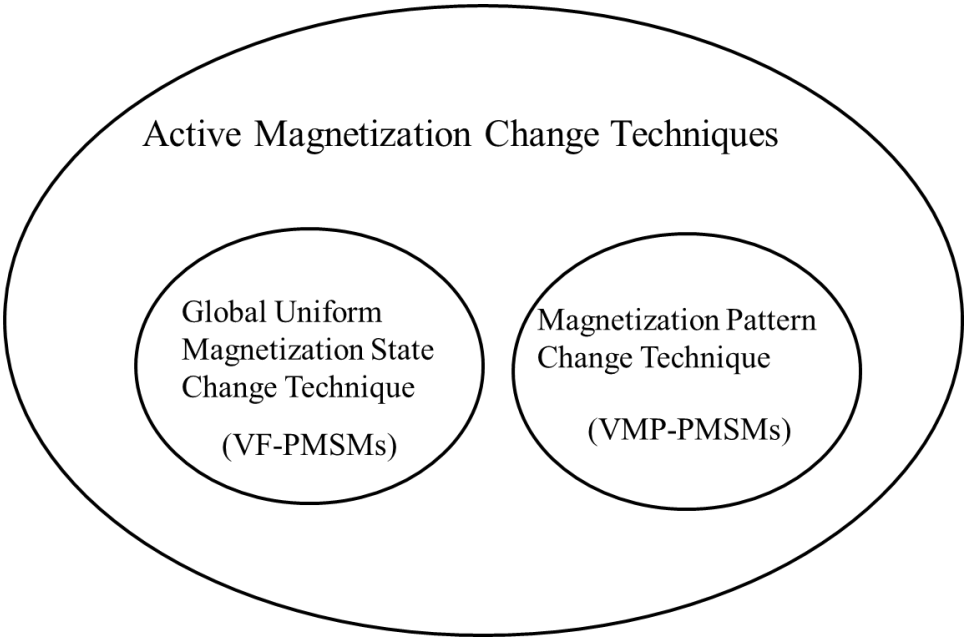

Fig. 2-4 Categorization of active magnetization techniques

Table 2-1. Comparison of global uniform magnetization change and magnetization pattern change

	Global Uniform Magnetization Change	Magnetization Pattern Change
Application	VF-PMSM	VMP-PMSM
Variable attribute	Magnet flux (1-D)	Magnetization distribution (2-D)
Magnet width (In the case of non-spoke type magnet configurations)	Narrower	Wider
Magnetizing current	d-axis only	d- and q- axis
Benefits	• Operating area expansion, • Copper loss reduction, • Iron loss reduction (fundamental)	• Operating area expansion, • Copper loss reduction, • Iron loss reduction (fund + harmonics component), • Torque ripple reduction

2.3 Analysis of Demagnetization Mechanism in Machines

In order to discuss the demagnetization in the surface permanent magnet using the virtually subdivided magnet model, the analytical model of demagnetization and the stator winding MMF need to be developed. A key to connecting these two models is a transformation of the stator winding MMF to the external magnetic field in the airgap. In this section, the demagnetization model in magnets and the stator winding MMF model are developed, then the relationship between MMF and the external magnetic field is investigated especially from the perspective of demagnetization in magnets.

2.3.1 Demagnetization model in subdivided magnets

The operating point of each segment of the permanent magnet is determined as the intersection of the material B-H curve and the load line shown in Fig.1-6, and their equations are,

$$B_{op}(\theta) = H_{op}(\theta)\mu_0\mu_r(B_{op}(\theta)) + B_r(\theta) \tag{2-1}$$

$$H_{op}(\theta) = \frac{A_m(\theta)l_g}{\mu_0 A_g(\theta)l_m} B_{op}(\theta) + H_{ext}(\theta) \tag{2-2}$$

Where, B_{op} is the magnetic flux density at an operating point [T], μ_0 is permeability of free space [H/m], μ_r is the relative permeability, H_{op} is the magnetic field strength at an operating point [A/m], B_r is the remanence[T], A_m is the area of the segmented permanent magnet [m^2], l_g is the airgap effective length [m], A_g is the area of the airgap corresponding to the segmented magnet [m^2], l_m is the magnet thickness [m] and H_{ext} is the external magnetic field strength [A/m].

The slope of the load line is determined by the machine geometry while the abscissa of the load line is determined by the external magnetic field supplied through the stator winding MMF shown in (2-3).

$$H_{ext}(\theta) = \frac{MMF_{s\_rf}(I_m, ß, \theta, t)}{l_g(\theta) + l_X(\theta)} \tag{2-3}$$

Where, l_X is the distance from the magnet surface to the sampling point in the magnet[m].

A linear hysteresis model is chosen to model de/re-magnetization here since the first priority here is to establish the handy low-cost model for intuitive understanding and not to build up high fidelity high-cost model. In the linear hysteresis model, when the external magnetic field $H_{ext}(\theta)$ is larger than the demagnetization boundary H_{BC}, the new remanence is calculated as follows using the symbols in Fig. 1-6.

$$B_r'(\theta) = \mu_1 H_{op}(\theta) + B_{op}(\theta) \tag{2-4}$$

Where, $H_{op}(\theta) = \frac{A_m(\theta) l_g}{\mu_0 A_g(\theta) l_m} B_{op}(\theta) + H_{ext}(\theta)$ and $B_{op}(\theta) = B_{knee} - (H_{knee} - H_{op}(\theta))\mu_2$

Therefore,

$$B_r'(\theta) = \frac{\mu_0 A_g(\theta) l_m}{\mu_0 A_g(\theta) l_m - \mu_2 A_m(\theta) l_g} (\mu_2 H_{ext}(\theta) + B_{knee} - \mu_2 H_{knee}) \{ \mu_1 \frac{A_m(\theta) l_g}{\mu_0 A_g(\theta) l_m} + 1 \} + \mu_1 H_{ext}(\theta) \tag{2-5}$$

2.3.2 Analytical model of stator MMF

Consider the three-phase sinusoidal currents expressed as (2-6) in the coordinate system shown in Fig.2-5,

$$i_a = I_m \sin(\omega_e t + ß), \; i_b = I_m \sin(\omega_e t + ß - \frac{2\pi}{3}), \; i_c = I_m \sin(\omega_e t + ß + \frac{2\pi}{3}) \tag{2-6}$$

Where, I_m is the magnitude of the stator winding current [A], ω_e is the excitation angular velocity [rad/sec], t is the time [sec] and ß is the current phase from the positive q-axis.

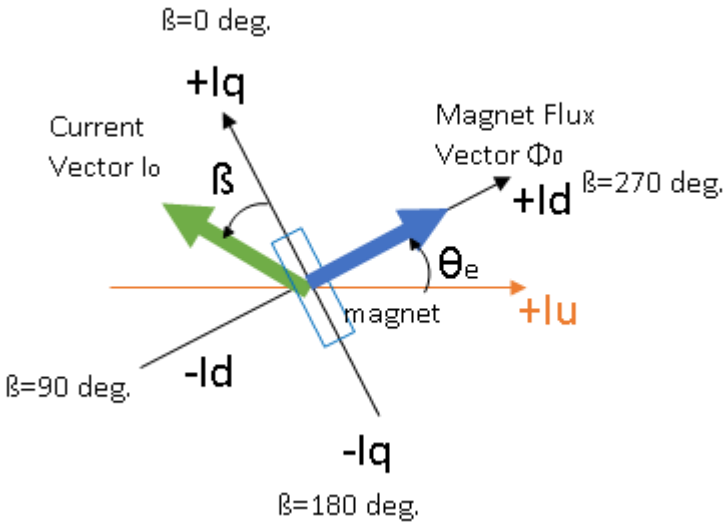

Fig. 2-5. Definition of coordinate

Assuming that the three coils are wound identically and placed in the machine at 120 degrees intervals, the MMF of the three windings a, b and c in the stationary reference frame are written as,

$$MMF_{sa}(\theta) = \frac{4}{\pi}\frac{N\, i_a}{2}\sum_h \frac{1}{h} k_{ph}\, k_{dh}\, \cos(h\,\theta)$$

$$MMF_{sb}(\theta) = \frac{4}{\pi}\frac{N\, i_b}{2}\sum_h \frac{1}{h} k_{ph}\, k_{dh}\, \cos\left(h\,\theta - \frac{2\pi}{3}\right) \qquad (2\text{-}7)$$

$$MMF_{sc}(\theta) = \frac{4}{\pi}\frac{N\, i_c}{2}\sum_h \frac{1}{h} k_{ph}\, k_{dh}\, \cos\left(h\,\theta + \frac{2\pi}{3}\right)$$

Where, N is the number of turns, h is the harmonics order and k_{ph} is the pitch factor while k_{dh} is the distribution factor which both follow (3). k_{ph} is the pitch factor while k_{dh} is the distribution factor which both follow (2-8).

$$k_{ph} = \cos\left(h\frac{\gamma}{2}\right), \quad k_{dh} = \frac{\sin\left(\frac{hq\gamma}{2}\right)}{q\sin\left(\frac{h\gamma}{2}\right)} \tag{2-8}$$

Since the interest of this work is in the effect of MMF on the permanent magnet on the rotor, transform it into the rotational reference frame, that is represented as (2-9) [98],

$$MMF_{sa\_rf}(I_m, ß, \theta, \omega_e t) = \frac{4}{\pi}\frac{N i_a}{2}\sum_h \frac{1}{h} k_{ph} k_{dh} \cos\left[h\left(\theta + \omega_e t \frac{2}{p}\frac{S}{m}\frac{1}{q}\right)\right]$$

$$MMF_{sb\_rf}(I_m, ß, \theta, \omega_e t) = \frac{4}{\pi}\frac{N i_b}{2}\sum_h \frac{1}{h} k_{ph} k_{dh} \cos\left[h\left(\theta + \omega_e t \frac{2}{p}\frac{S}{m}\frac{1}{q} - \frac{2\pi}{3}\right)\right] \tag{2-9}$$

$$MMF_{sc\_rf}(I_m, ß, \theta, \omega_e t) = \frac{4}{\pi}\frac{N i_c}{2}\sum_h \frac{1}{h} k_{ph} k_{dh} \cos\left[h\left(\theta + \omega_e t \frac{2}{p}\frac{S}{m}\frac{1}{q} + \frac{2\pi}{3}\right)\right]$$

Where, q is the number of coils in a phase belt, p is the number of poles, S is the number of slots, m is the number of phases.

The net stator winding MMF acting in the machine,

$$MMF_{s\_rf}(I_m, ß, \theta, \omega_e t) = MMF_{sa\_rf}(I_m, ß, \theta, \omega_e t) + MMF_{sb\_rf}(I_m, ß, \theta, \omega_e t) + MMF_{sc\_rf}(I_m, ß, \theta, \omega_e t) \tag{2-10}$$

Equation (2-10) can be reduced to as follows,

$$MMF_{s\_rf}(I_m, ß, \theta, \omega_e t) = \frac{3}{2}\frac{4}{\pi}\frac{N I_m}{2}\left[\sum_{h=1\ 7\ 13....}\frac{1}{h} k_{ph} k_{dh} \cos\left[h\left(\theta + \omega_e t \frac{2}{p}\frac{S}{m}\frac{1}{q}\right) - \omega_e t\right]\right.$$

$$+ \sum_{h=5\ 11\ 17....} \frac{1}{h} k_{ph}\, k_{dh} \cos[h(\theta - \omega_e t \frac{2}{p}\frac{S}{m}\frac{1}{q}) + \omega_e t] \ ]$$

(2-11)

Organize the right hand side about $\omega_e t$,

$$MMF_{s\_rf}(I_m, ß, \theta, \omega_e t) = \frac{3}{2\pi}\frac{4}{2}\frac{N I_m}{2}[\sum_{h=1\ 7\ 13....} \frac{1}{h} k_{ph}\, k_{dh} \cos[h\theta + \omega_e t (h\frac{2}{p}\frac{S}{m}\frac{1}{q} - 1)]$$
$$+ \sum_{h=5\ 11\ 17....} \frac{1}{h} k_{ph}\, k_{dh} \cos[h\theta - \omega_e t (h\frac{2}{p}\frac{S}{m}\frac{1}{q} + 1)] \ ]$$

(2-12)

When $\frac{2}{p}\frac{S}{m}\frac{1}{q} = 1$, equation can be rewritten to,

$$MMF_{s\_rf}(I_m, ß, \theta, \omega_e t)$$

$$= \frac{3}{2\pi}\frac{4}{2}\frac{N I_m}{2}\{ k_{p1}\, k_{d1} \cos(\theta + \omega_e t) + \sum_{h=6\ 12....} \frac{1}{h} k_{ph}\, k_{dh} (\cos[h(\theta + \omega_e t)] + \cos[h(\theta - \omega_e t)]) \}$$

(2-13)

This equation shows that MMF in a machine in the rotor reference frame contains the harmonic components that have the order of integer multiple of six.

2.3.3 Analytical MMF for six slots per one pole distributed winding

As an example of the stator MMF equation developed in the last section, 6 slots per 1 pole pair distributed winding shown in Fig 2-6 is calculated here. Assuming the current density in each slot is uniform, stator winding MMF with instantaneous current $i_a = 0A$, $i_b = -0.866A$ and $i_c = 0.866A$ are calculated using (2-9) as shown in Fig.2-7. The total MMF is obtained using (2-10) as Fig.2-8 by adding up MMF from each phase.

It should be noted that the distribution of the MMF in a staircase manner is a result of an approximation that the current is represented as a dot with infinitely small coil area and the integral path for the Ampere's law in between the dot and the dot does contain any source of the magnetic field as shown in Fig. 2-9[99].

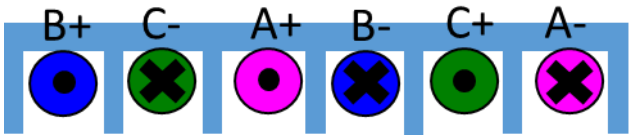

Fig. 2-6. 6 slots per 1 pole pair distributed winding

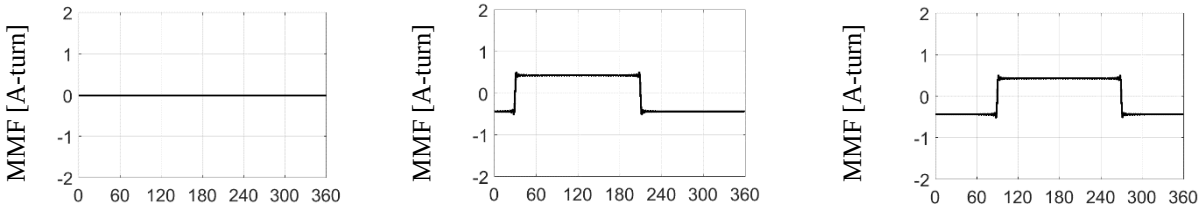

(a) A-phase (b) B-phase (c) C-phase

Fig. 2-7. MMF for each phase with i_a = 0A, i_b = -0.866A and i_c = 0.866A

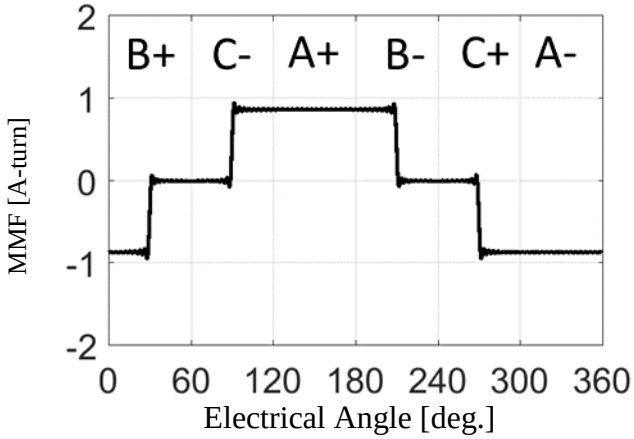

Fig. 2-8. Combined total MMF

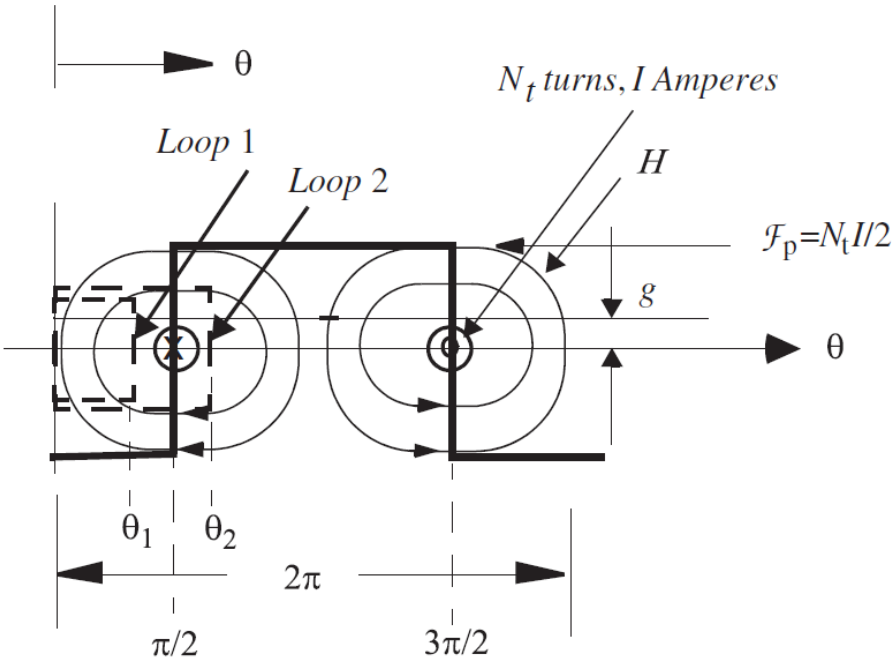

Fig. 2-9. MMF and filed intensity of a full-pitch coil [99].

2.3.4 Magnetic field by FEA for a simplified model of six slots per one pole distributed winding

The magnetic field in a simplified model of 6 slots per 1 pole distributed winding is calculated using FEA to verify the analytical solution in the previous section. Assuming each stator winding current in one slot can be represented as a dot, FEA model is built up as shown in Fig.2-10 (a). For the simplification, the surroundings of each dot are treated as air in this model. The resultant magnetic field by instantaneous current i_a = 0A, i_b = -0.866A and i_c = 0.866A are calculated as shown in Fig.2-10 (b). The first line is located to close to the current, and another line is located far from the current. The resultant vertical magnetic field near the current shows staircase waveform as seen in Fig. 2-11(a) whereas the resultant magnetic field far from the

current shows sinusoidal-like waveform as seen in Fig. 2-11 (b). As Ampere's Law shows, the magnetic field is decayed as the distance from the MMF source is increased. Hence, the magnetic field far from the current loses harmonic components.

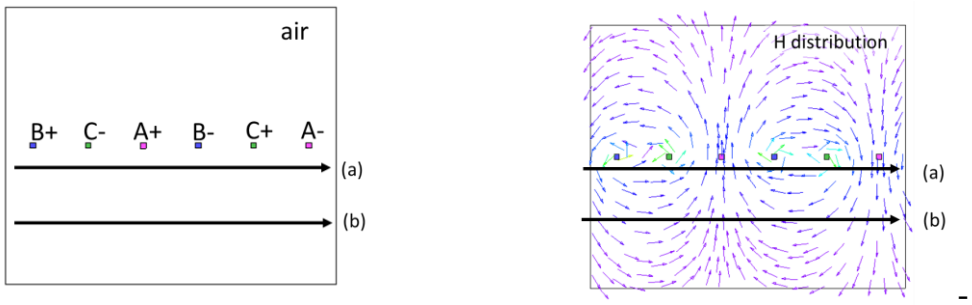

(a) FEA model (b) Resultant magnetic field distribution

Fig. 2-10. Magnetic field in simplified model of 6 slots per 1 pole distributed winding.

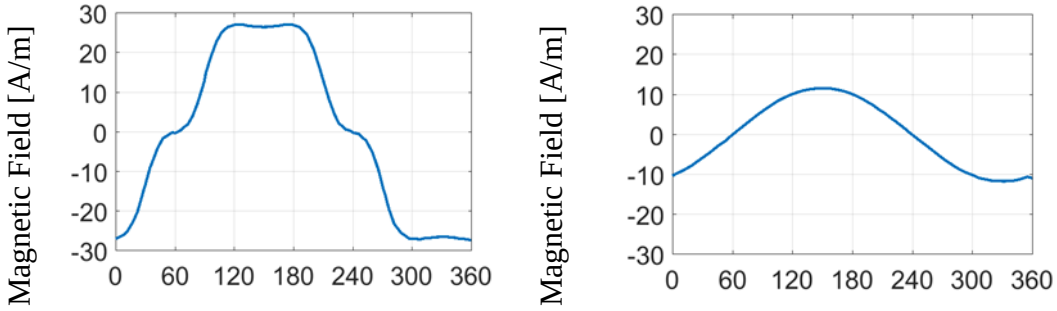

(a) Close to MMF source (b) Far from MMF source

Fig. 2-11 Magnetic field in simplified model of 6 slots per 1 pole distributed winding.

2.3.5 Magnetic field by FEA for a motor model with six slots per one pole distributed winding

The magnetic field in a motor model with the same slot pole combination with the previous simplified model is calculated using FEA in order to examine the magnetic field behavior in the realistic model. The test motor model is designed as Fig. 2-12 assuming a 400W general purpose motor. Constant relative permeability μ_r=1000 is set on the stator core and the rotor core. The

parts corresponding to magnets are defined as the air since the purpose of this test is to examine the magnetic field due to the stator winding so the magnetic field due to the magnet is removed. The current inside of slots is assumed to be uniformly distributed.

The radial component in the resultant magnetic field with current i_a = 0A, i_b = -0.866A and i_c = 0.866A are calculated as shown in Fig.2-13. The magnetic field at the surface of the magnet part shows a staircase waveform as seen in Fig. 2-13(a) whereas the resultant magnetic field at the middle of the magnet part shows sinusoidal-like waveform as seen in Fig. 2-13(b). This indicates that the magnetic field filters out the harmonics in a similar manner with the simplified model.

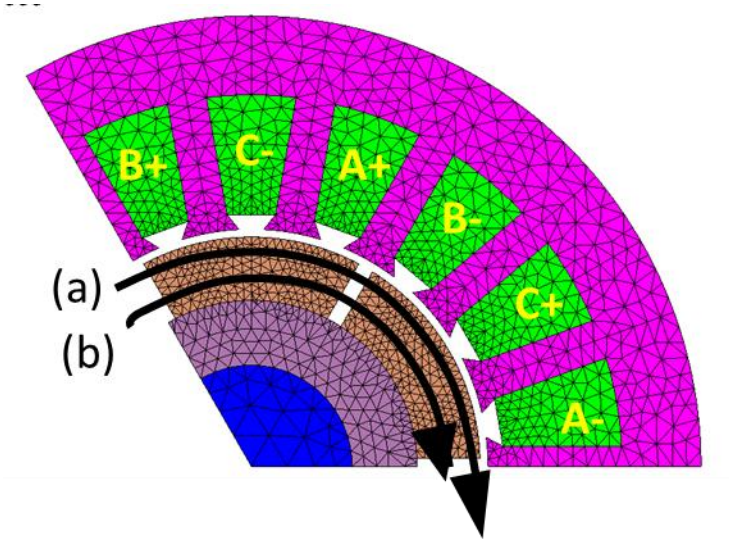

Fig. 2-12. FEA model of 6 slots per 1 pole motor with distributed winding

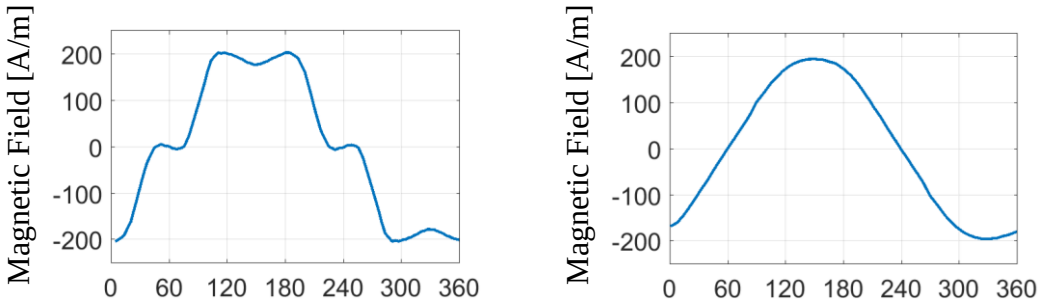

(a) Close to MMF source (b) Far from MMF source

Fig. 2-13 Magnetic field in 6 slots per 1 pole distributed winding motor

2.3.6 Magnetic field in distributed winding machines and concentrated winding machines

In the previous section, MMF and the magnetic field distribution at an instantaneous moment are calculated to study the correlation of MMF and the magnetic field without considering the permeance distribution in the airgap depending on the slot openings. These are useful examples to obtain theoretical understanding but are lacking the practical constraints. For instance, in reality, the instantaneous pulse current with infinitely small width cannot be implemented. Therefore, the magnetic field due to the current pulse with finite time width is studied in this section to get more insights about how the external magnetic field demagnetize the magnets in the real machine.

Figure 2-14 shows an example of airgap magnetic field in 6-poles 18-slots distributed winding machine. Since Fig. 2-14 (a) is in the stationary reference frame, the magnetic field moves along with time. The interest of this work is in how the magnets on a rotor are exposed to the magnetic field, hence, convert the field into the rotor reference frame as shown in Fig. 2-14(b). Due to the synchronization of the rotor speed and the excitation frequency, the magnetic field from every instantaneous moment in the rotor reference frame overlaps each other in the rotor reference frame. The resultant magnetic field becomes time-invariant sinusoidal function.

Figure 2-15 shows an example of airgap magnetic field in 6 poles 9 slots concentrated winding machine. Fig. 2-15 (a) is the result in the stationary reference frame. Since it is the concentrated winding machine, unlike the distributed winding, the resultant magnetic field contains rich harmonics. In the case of the concentrated winding, even in the synchronous speed, the magnet sees different magnetic field depending on time due to the harmonic components. However, when it is represented in the rotor reference frame as shown in Fig. 2-15 (b), it can be found that the envelopes of the magnetic field profile for one electrical cycle is always same at any cycle. It is because the resultant magnetic field profile in the rotor reference frame is a superimposition of a time-invariant fundamental component and harmonic components as shown in Fig. 2-16.

By combinining this analysis result with a demagnetization property of the permanent magnets, an important principle in magnetization change can be found. The magnetization change is an irreversible phenomenon, hence, once a magnetization level in a segment of the magnet is changed by the large magnetic field, it will not change unless larger de/re-magnetizing magnetic field is subject to that portion. Therefore, only the maximum and the minimum value of the magnetic field for one pulse duration regulate how significantly the segment of the permanent magnet is demagnetized[38]. The magnetic field between the maximum and the minimum during the pulse do not affect the resultant magnetization (as long as the linear demagnetization model is valid). In other words, only the envelope of the magnetic field profile for one electrical cycle determines the demagnetization level.

When the magnetic field with harmonic components is given to a spinning magnet for less than one electrical cycle, the resultant magnetization varies depending on timing and duration that the magnetic field is injected. It is because the envelopes of the magnetic field profile within that

pulse varies depending on that timing and duration. Hence, a control system of the magnetization using current pulse for less than one electrical cycle needs infinitely fine time resolution and the large amount of the database about the possible magnetic field profile that the pulse current can make. However, if it is allowed to hold the magnetizing current for one electrical cycle, which can bring the time independent fixed magnetic field envelopes, magnetization can be manipulated by a control system with finite time resolution In summary, as long as the magnetizing current is held for one electrical cycle, the virtually subdivided magnet model assuming the sinusoidal magnetic field is realistic enough even in a concentrated winding machine.

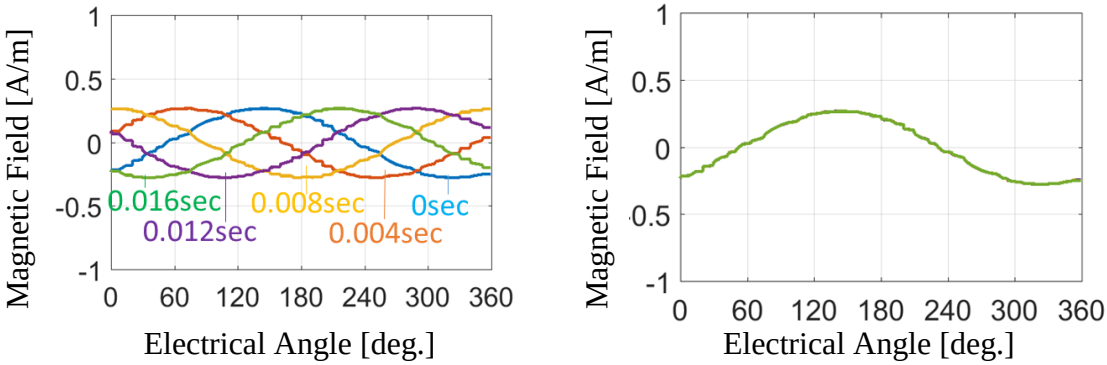

(a) Stator reference frame (b) Rotor reference frame

Fig. 2-14 Magnetic field in 6 poles 18 slots distributed winding motor

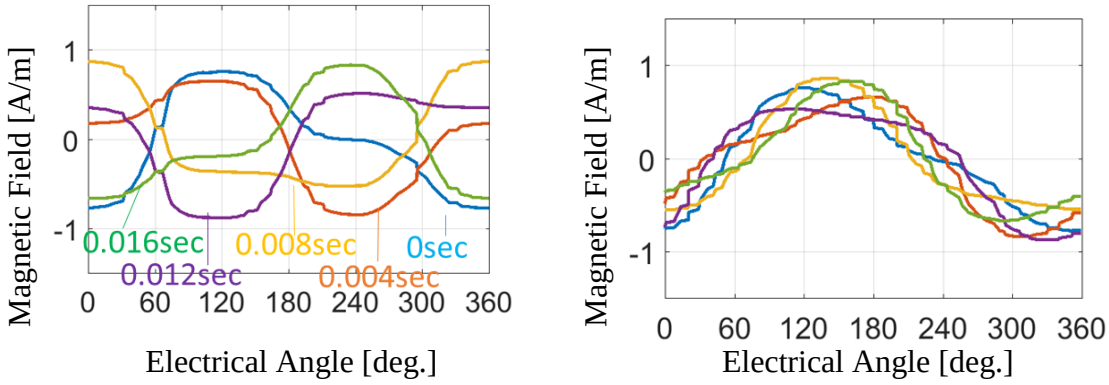

(a) Stator reference frame (b) Rotor reference frame

Fig. 2-15 Magnetic field in 6 slots 9 poles concentrated winding motor

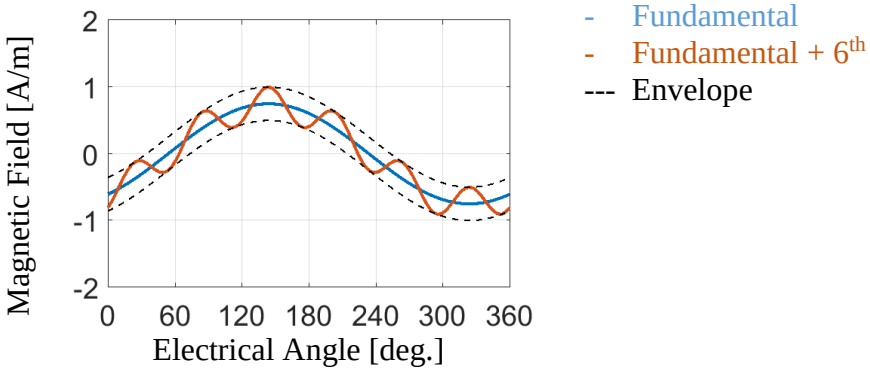

Fig. 2-16 Magnetic field due to fundamental and 6th components

2.4 Analytical System Identification between Magnetization Distribution and Stataor Winding Current

In this section, the system between the magnetization distribution and the stator winding current is formulated by combining the analytical model of the spatial demagnetization and the MMF distribution based on the observations derived so far.

From 2.3.1, a spatial distribution of the remanence after demagnetization has happened can be written as (2-14).

$$B_r'(\theta) = \{\frac{A_m(\theta)l_g(\theta)}{\mu_0 A_g(\theta)l_m(\theta) - \mu_2 A_m(\theta)l_g(\theta)}\ \mu_1\mu_2 + \mu_1 + \mu_2\}H_{ext}(\theta) + \frac{\mu_1 A_m(\theta)l_g(\theta) + \mu_0 A_g(\theta)l_m(\theta)}{\mu_0 A_g(\theta)l_m(\theta) - \mu_2 A_m(\theta)l_g(\theta)}(B_{knee} - \mu_2 H_{knee}) \quad (2\text{-}14)$$

Meanwhile, from 2.3.2, the net stator winding MMF acting in the machine in the rotor reference frame is expressed as (2-15).

$$MMF_{s\_rf}(I_m, ß, \theta, \omega_e t) = \frac{3}{2}\frac{4}{\pi}\frac{N I_m}{2}\left[\sum_{h=1\ 7\ 13....}\frac{1}{h}k_{ph}k_{dh}\cos[h\theta + \omega_e t\,(h\frac{2}{p}\frac{S}{m}\frac{1}{q} - 1)] + \sum_{h=5\ 11\ 17....}\frac{1}{h}k_{ph}k_{dh}\cos[h\theta - \omega_e t\,(h\frac{2}{p}\frac{S}{m}\frac{1}{q} + 1)]\right] \quad (2\text{-}15)$$

As stated in 2.3.6, only the maximum and the minimum value of the MMF profile at each location on the magnet determines the demagnetization level. The minimum and the maximum of the MMF for one electrical cycle can be defined as (2-16) and (2-17).

$$MMF_{s\_rf\_min}(I_m, ß, \theta) = Min\{ MMF_{s\_rf}(I_m, ß, \theta, \omega_e t) \} \quad (2\text{-}16)$$

$$MMF_{s\_rf\_max}(I_m, ß, \theta) = Max\{ MMF_{s\_rf}(I_m, ß, \theta, \omega_e t) \} \quad (2\text{-}17)$$

Finally, the demagnetization physical system that takes stator current as input and the remanence as output is found as (2-18) and (2-19) by substituting (2-15) and (2-16) into (2-14).

$$B_r'(\theta) = \{\frac{A_m(\theta)l_g(\theta)}{\mu_0 A_g(\theta)l_m(\theta) - \mu_2 A_m(\theta)l_g(\theta)}\ \mu_1\mu_2 + \mu_1 + \mu_2\}\frac{MMF_{s\_rf\_min}(I_m, ß, \theta)}{l_g(\theta) + l_x(\theta)} + \frac{\mu_1 A_m(\theta)l_g(\theta) + \mu_0 A_g(\theta)l_m(\theta)}{\mu_0 A_g(\theta)l_m(\theta) - \mu_2 A_m(\theta)l_g(\theta)}(B_{knee} - \mu_2 H_{knee}) \quad (2\text{-}18)$$

$$B_r'(\theta) = \{\frac{A_m(\theta)l_g(\theta)}{\mu_0 A_g(\theta)l_m(\theta) - \mu_2 A_m(\theta)l_g(\theta)}\ \mu_1\mu_2 + \mu_1 + \mu_2\}\frac{MMF_{s\_rf\_max}(I_m, ß, \theta)}{l_g(\theta) + l_x(\theta)} + \frac{\mu_1 A_m(\theta)l_g(\theta) + \mu_0 A_g(\theta)l_m(\theta)}{\mu_0 A_g(\theta)l_m(\theta) - \mu_2 A_m(\theta)l_g(\theta)}(B_{knee} - \mu_2 H_{knee}) \quad (2\text{-}19)$$

Equation (2-18) represents the distribution of the remanence in N-pole whereas (2-19) represents the distribution of the remanence in S-pole. These equations show that the remanence at each location of the magnet is uniquely determined from the stator winding current vector. All remaining component in these equations besides MMF functions are static parameters defined by geometries and materials.

The proposed spatial magnetization change method is based on this demagnetization physical system represented in (2-18) and (2-19). A basic unit of this manipulation method is the magnetic field for one electrical cycle. As described so far, the instantaneous magnetic field that the permanent magnet is subjected to is a function of the magnitude and the angle of the stator winding current vector as well as time (2-13). In contrast, the envelope of the magnetic field profile becomes independent of time when the magnetizing current is held for one electrical cycle.

2.5 Concept Verification using FEA

2.5.1 Example of demagnetization by single current pulse

In this section, FEA simulation result of the non-uniform demagnetization in 6-pole 9-slot concentrated winding machine by a single current pulse is provided. The objective of this calculation is to clarify the relationship of the phase angle of the injected current vector and the demagnetized area in permanent magnets.

Figure 2-17 shows the simulated magnetic field distribution in the airgap due to the stator winding current in a spinning 6-pole 9-slot concentrated winding machine. Each line with a different color in Fig. 2-17(a) means the magnetic field at a different time. The operating point histories shown in Fig. 2-18 indicate that the magnetic field shown in Fig. 2-17 demagnetizes edges of each piece of the magnet with the same magnitude in the opposite direction.

Figure 2-19 shows how the magnetizing current vectors shape the magnetization pattern and the no-load back-EMF. When the current vector is on the positive d-axis (ß = 270°), any portion of the permanent magnet is not demagnetized. As the current phase is lagged, the permanent magnet starts to demagnetize from the edge. For instance, when ß = 240°, the left edge of each piece of the magnet is demagnetized. When the current phase angle is decreased further to ß = 180°, half of the surface area of each piece of the magnet is demagnetized.

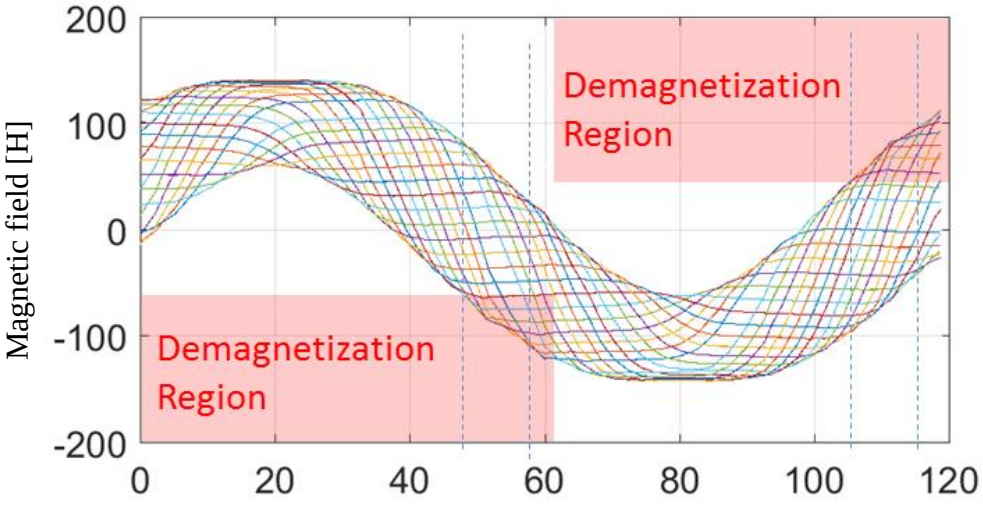

(a) Magnetic field for one electrical cycle in the rotor reference frame

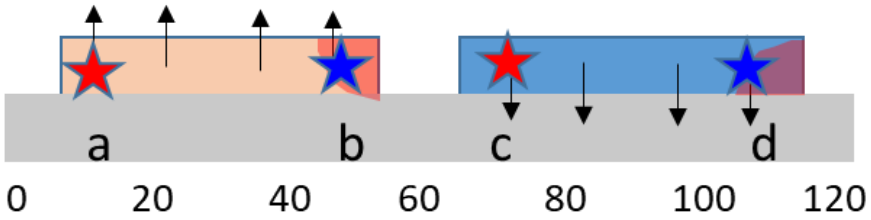

(b) Permanent magnets subjected to magnetic field in (a)

Fig. 2-17. External magnetic field in permanent magnets

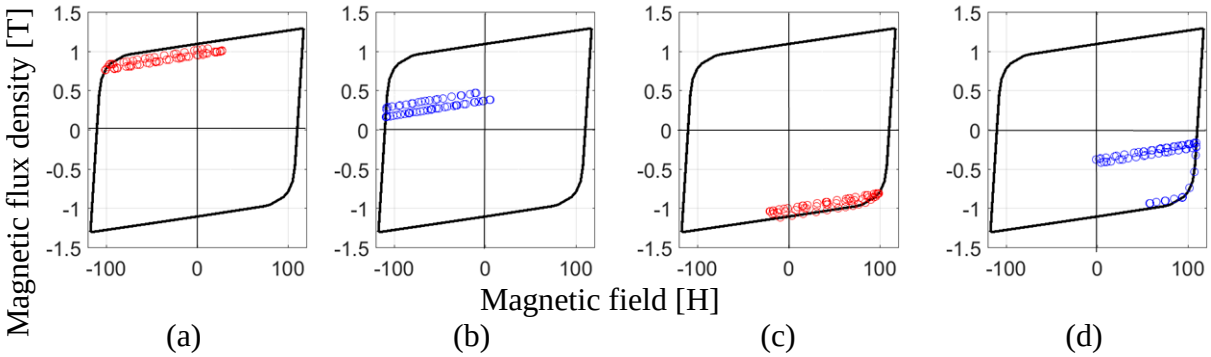

(a) (b) (c) (d)

Fig. 2-18. Operating point histories at points marked with stars in Fig.2-16(b)

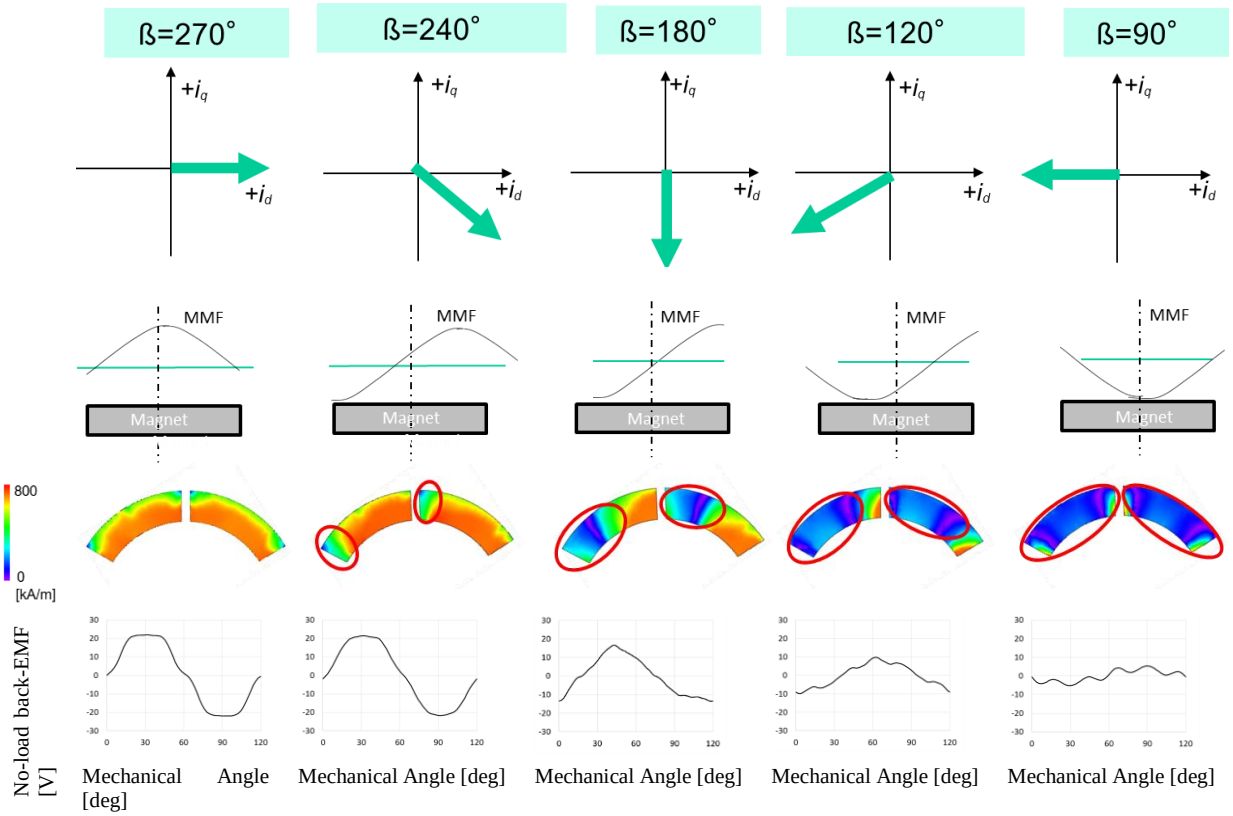

Fig. 2-19. Magnetizing current vector and resultant magnetization pattern

2.5.2 Example of demagnetization by double Current pulse

In this section, FEA simulation results of the non-uniform demagnetization in 6-pole 9-slot concentrated winding machine by two current pulses is provided. In the previous section, the correlation of the magnetizing current phase angle and the demagnetized area are visually provided. Practically useful magnetization pattern can be created by combining these single current pulses. For instance, symmetric magnetization pattern with different effective magnet arc can be made by demagnetizing both edge of a magnet by two pulses.

Figure 2-20 shows an example of two current pulse injections to a 6-pole 9-slot concentrated winding machine. In this example, the magnetizing current vectors are injected in the fourth quadrant of the dq-plane for the first one electrical cycle, then is injected in the first quadrant for the next one electrical cycle. By the first current injection, the left side of the magnet is

demagnetized. Subsequently, the following second injection demagnetizes the other side of the magnet. These magnetizing current vectors can be formulated as (2-20).

$$\begin{cases} I_1 = I \angle ß_1 & ß_1 = 270° - \varepsilon \\ I_2 = I \angle ß_2 & ß_2 = 270° + \varepsilon \end{cases} \quad (2\text{-}20)$$

Where ε is a manipulated current angle offset.

As increasing ε, the q-axis component in the magnetizing current vector is increased as shown in Fig.2-21. Resultant no-load back-EMF by the magnetization pattern created through two current pulse injections is shown in Fig. 2-22. When ε = 0, the permanent magnet is not demagnetized. Hence, the no-load back-EMF maintains the original trapezoidal waveform. As ε is increased, the demagnetized area expands from both edges of the permanent magnets, thus, the no-load back-EMF also changes. At ε = 27°, the resultant no-load back-EMF becomes close to a sinusoidal waveform. Afterward, the no-load back-EMF waveform gets deteriorated along with the increase of ε.

These magnetization pattern changes cause the change in the magnetic flux density in the airgap as shown in Fig.2-23. The harmonic spectrum of the airgap magnetic flux density along with the change of ε is shown in Fig. 2-24 (a). It shows that the fundamental component decreases as the increase of ε in a nonlinear manner whereas the harmonic components show an upside-down behavior approximated to trigonometric functions.

This harmonic spectrum is analogous to the change of the geometrical magnet arc. Figure 2-24(b) is an analytical calculation result of magnet MMF with respect to the pole coverage ratio of the permanent magnet by reference [100]. Here, the pole coverage ratio means the ratio of the permanent magnet arc by the pole arc. In this report, the authors calculate the analytical solution of the magnet MMF following equations developed by Z.Q. Zhu and D. Howe [101]. This

analytical result in Fig.2-24(b) shows an identical behavior with Fig.2-24(a) which is obtained through the magnetization pattern change.

This analogy with the geometrical arc change of the magnet can be interpreted in a way that the magnetization pattern shaping using two pulse injections substantially changes the effective magnet arc. Therefore, it is expected that benefits obtained by changing the geometrical pole arc in the conventional machine design, such as back-EMF with lower harmonics and lower cogging torque, can be achieved by creating magnetization patterns through the two current pulse injection.

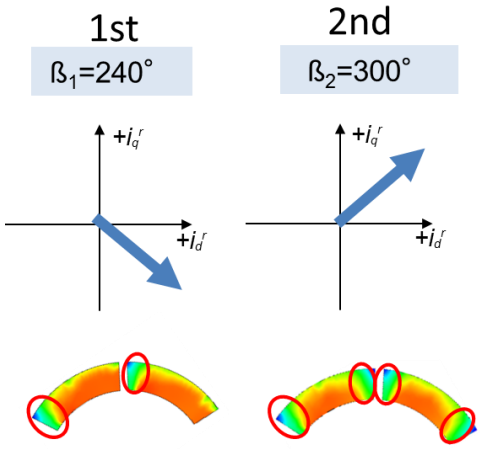

Fig. 2-20. Two sequential magnetizing current vector and resultant magnetization pattern

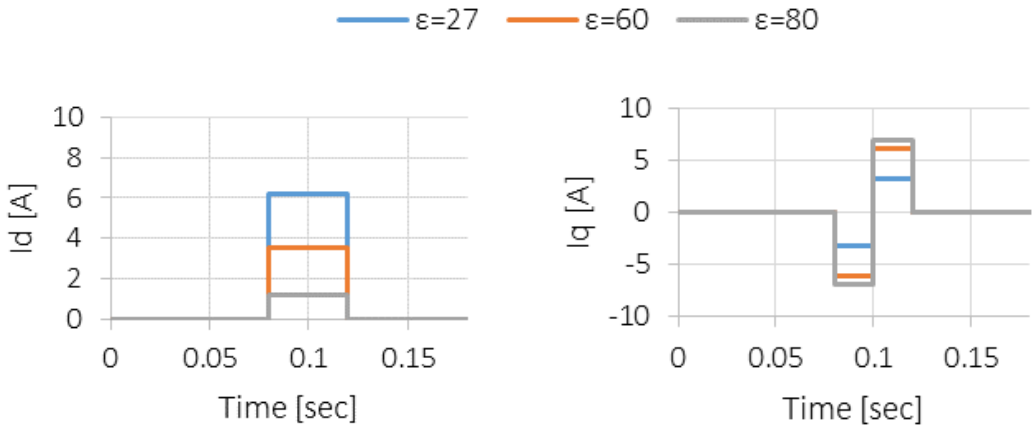

Fig. 2-21. Magnetizing current trajectory for double pulse shot

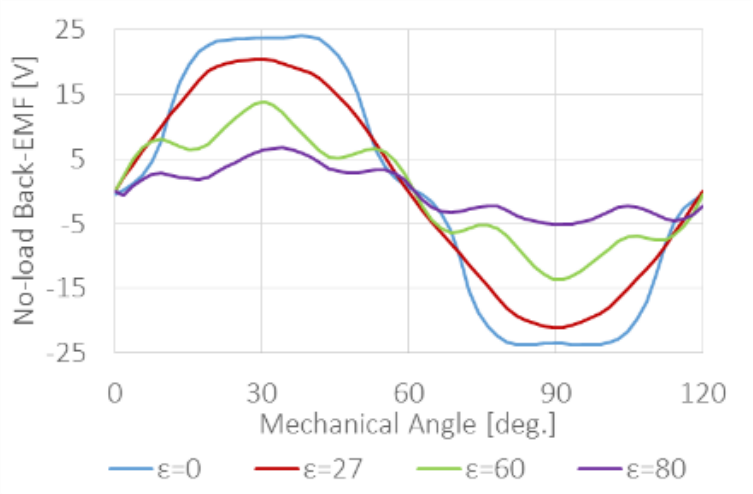

Fig. 2-22. Resultant back-EMF after magnetization pattern shaping

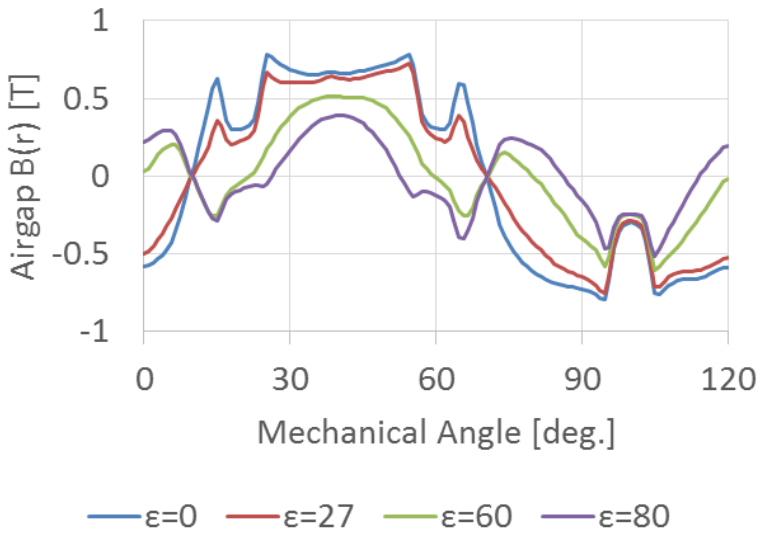

Fig. 2-23. Resultant airgap magnetic flux density after the magnetizing current injection

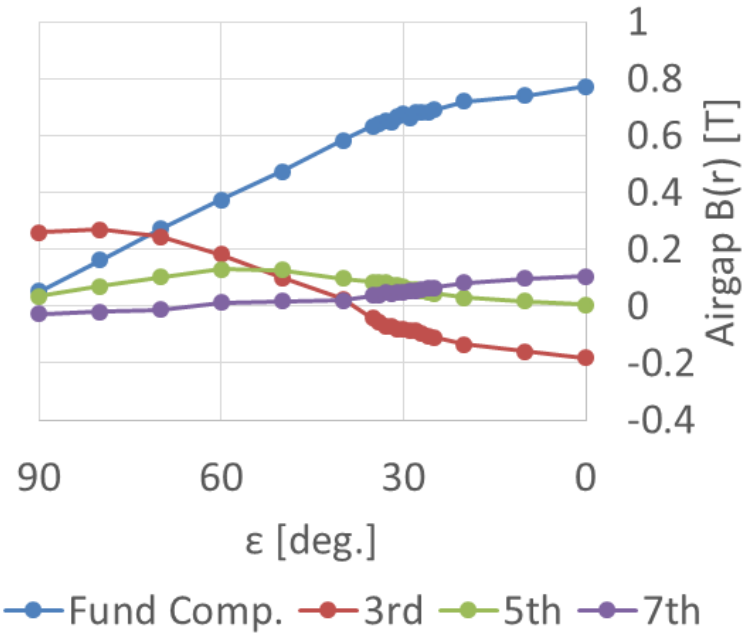

(a) Due to magnetization pattern shaping

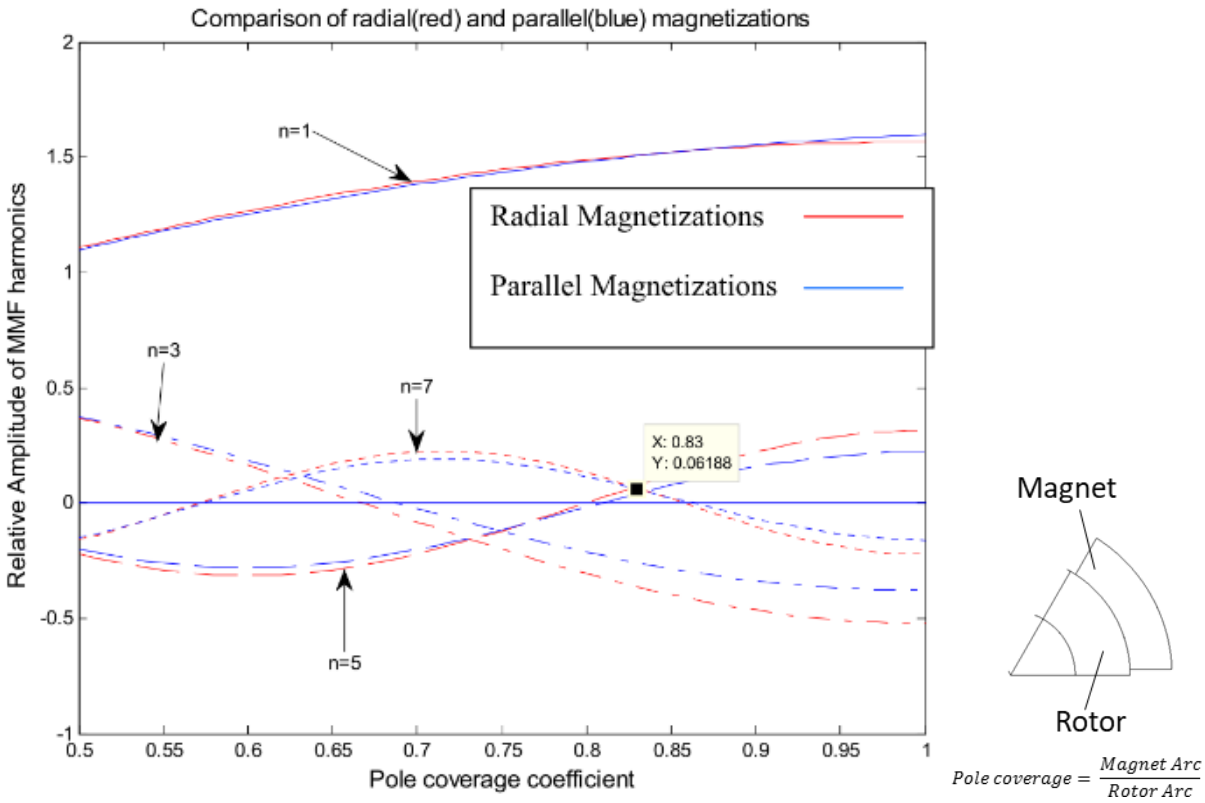

(b) Due to geometrical magnet arc shaping [100]

Fig. 2-24. Frequency spectrum of magnetic flux density in airgap

2.6 Summary

In this chapter, the fundamental idea to manipulate magnetization patterns in permanent magnets has been discussed using a model to represent the spatial de/re-magnetization. It has been analytically shown that the dynamic magnetization pattern manipulation is possible in machines with either distributed windings or concentrated windings. The concept of the proposed magnetization pattern change method is verified using FEA indicating that the magnetization pattern shaping in low-coercive magnets in machines using large pulse current supplied by stator winding can bring substantially the same effect with the geometrical magnet's arc change.

Chapter 3 Design of VMP-PMSMs

3.1 Introduction

Chapter 3 discusses the design of VMP-PMSMs. The first section shows the overview of the design process for VMP-PMSMs. Two key components appeared in the overveiw, choice of the slot pole combination and material selection, are discussed in the following sections.

3.2 Overview of Design Process for VMP-PMSMs

Fundamental design framework of VMP-PMSMs is essentially the same with the conventional SPMSMs since VMP-PMSMs are a subset of SPMSMs in terms of topology. Siginificant differences in VMP-PMSM design from the conventional SPMSM design are slot pole combinations and material choices.

As seen in the previous chapter, proposed dynamic magnetization pattern change technique is deeply connected to the MMF distribution in airgap, which is a function of the slot and pole combination. Some specific slot-pole combinations are applicable for conventional SPMSM but not for VMP-PMSMs since they do not satisfy the assumption imposed in the active magnetization change technique.

In a similar manner, magnet material is essentially an important key factor in machines with dynamic magnetization pattern change. In the case of the conventional PMSMs, a constraint regarding a magnet is simply not to be demagnetized in the normal operation. From that, high coercive magnets such as NdFeB are often used in the conventional PMSMs. In the case of machines with active magnetization change techicnique, low coercive magnets need to be used due to the intentional de/re-magnetization. Therefore, in addition to the constraint about normal

operation, two additional constraints about no-load operation and remagnetizing operation are imposed in magnet selection for VMP-PMSMS.

Figure 3-1 shows an example of a design flow of VMP-PMSMs. Starting from a required specification, a volume and dimensions of a machine are roughly estimated. Then, a slot pole combination is selected considering the geometrically available area in a stator and a rotor as well as the requirement to the torque ripple and losses. In the case of the VMP-PMSMs, some specific slot-pole combinations need to be eliminated from the consideration at this step due to their incapability of controlling spatial magnetization distribution. After picking up a slot pole combination, magnet material and design details around airgap are chosen considering the required torque. In this process, a number of turns that enables the required torque along with the selected geometry and magnets need to be considered. If the selected number of turns fill slots more than expected, the design step needs to go back to a selection of a slot pole combination.

Two key components appeared in this oveveiw, choice of the slot pole combination and material selection are discussed in the following sections respectively.

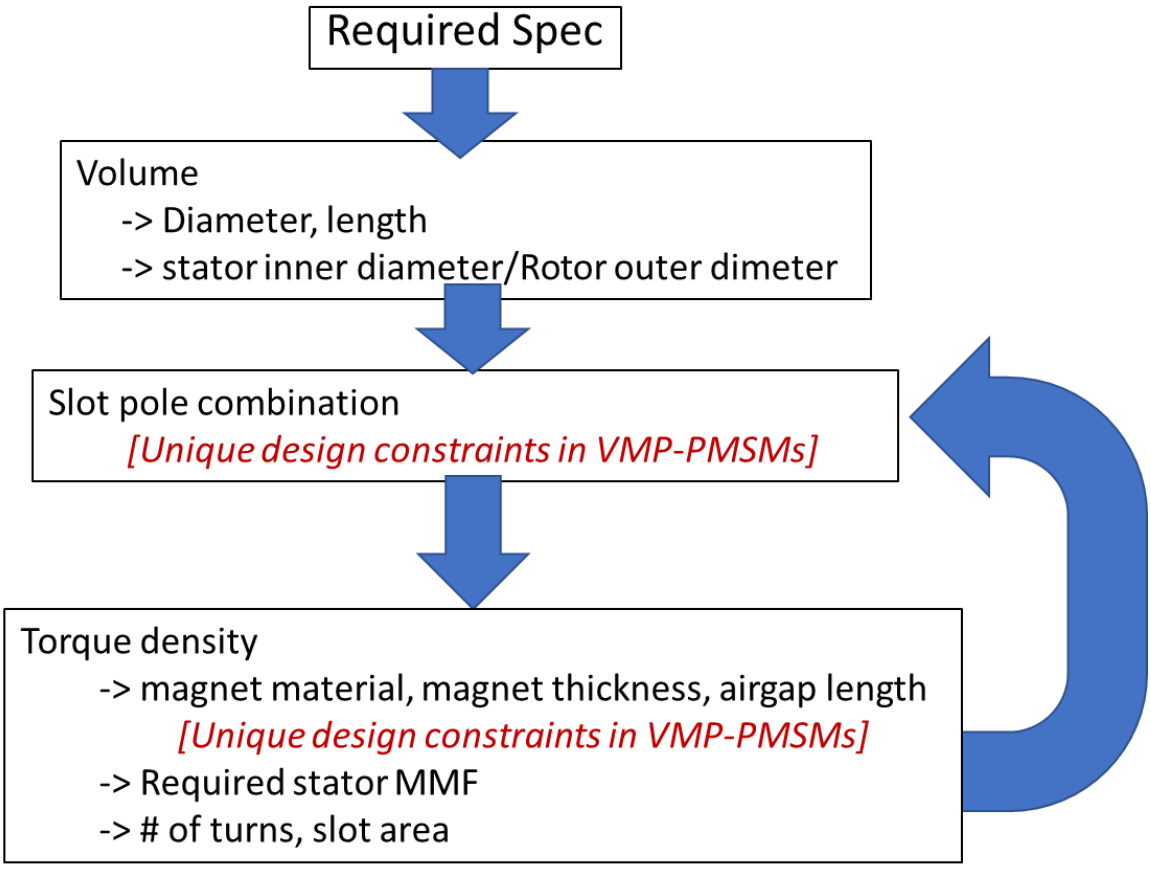

Fig. 3-1 Overview of design process of VMP-PMSMs

3.3 Slot Pole Combinations for Active Magnetization Change

In this section, the stator MMF is analyzed to identify the general guideline of the slot pole combination. Through this analysis, it is found that the sub-harmonic components in the stator MMF are a key to defining the applicable slot pole combinations for VMP-PMSMs.

3.3.1 MMF harmonic spectrum analysis

In the existing study of the spatial MMF[106]-[108], the fundamental component is defined as the harmonic component of the lowest order, and its wavelength is equal to the air-gap circumference. The harmonic which has a wavelength equal to the pole pair pitch is called the

main harmonic. It has an order h = P/2 [106]. The harmonics that have a lower order than the main harmonic are called subharmonics [106][107]. The wavelengths of the subharmonics are essentially longer than the pole pair pitch.

Figure 3-2 shows the relationship between the stator MMF and magnet pole pair. By definition, a cycle of the main harmonic and components higher than the main harmonic can fit within one pole pair. Hence the magnetization change by the stator winding MMF can happen equally on all pole pairs. Meanwhile, in the case of the subharmonics, its cycle is beyond one pole pair. Therefore, it is infeasible to achieve the same magnetization in every pole pair if the stator MMF contains a subharmonic.

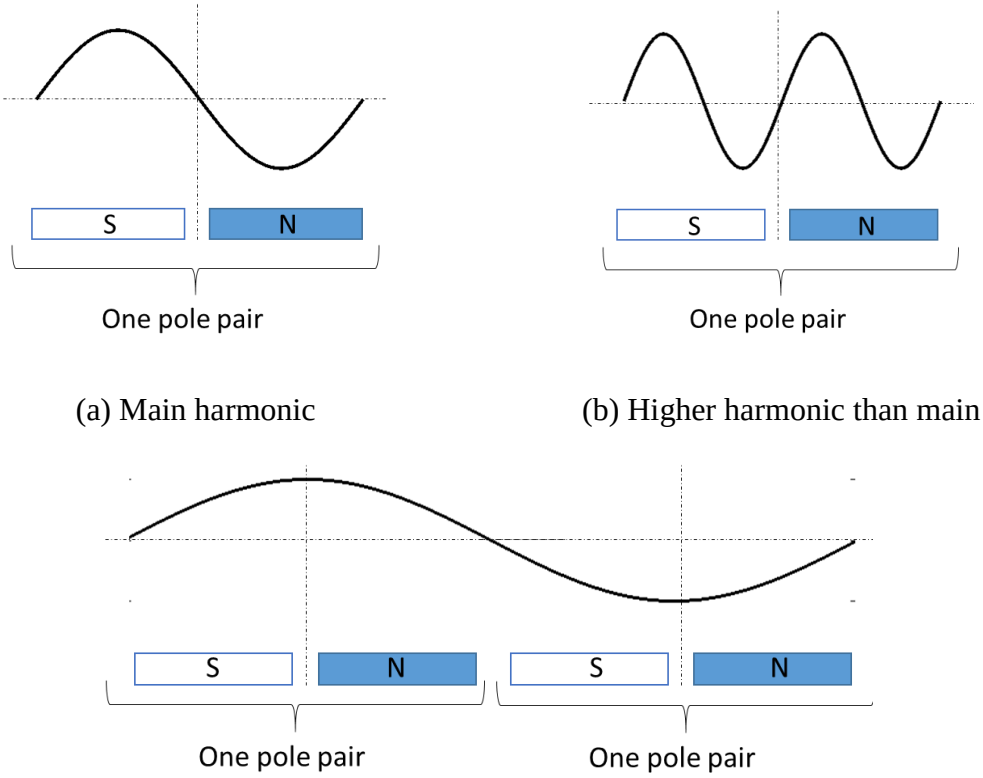

(a) Main harmonic (b) Higher harmonic than main

(c) Subharmonic

Fig. 3-2 Relationship of stator MMF harmonic and pole pair

Figure 3-3 shows the winding configuration, flux line at $\omega_e t=0$ and MMF harmonic spectra for a 6-pole 18-slot machine. This is the most classical distributed winding machine with q=1. Since the number of pole pairs is three, the order of the main harmonic is defined as the third. The spatial MMF spectra have the harmonic components of 3rd, 6th, 12th, 15th … No subharmonics exist. Hence, this topology is suitable for active magnetization change.

Figure 3-4 shows the profile of a 6-pole 9-slot machine. This machine has a concentrated winding and is often used as a brushless DC motor (BLDC) [109]. Since the number of pole pairs is three, the main harmonic is found at the third order. The spatial MMF spectra have the harmonic components of 3rd, 6th, 12th, 15th…. Subharmonics do not exist. Hence, this topology is also a candidate as a machine using the active magnetization change technique.

Figure 3-5 shows the profile of 8-pole 9-slot machine. This machine also has a concentrated winding but has relatively low torque ripple due to low harmonic winding factors. The main harmonic is found at the fourth order in this case. The MMF spectra contain harmonics of 1st, 2nd, 4th, 5th…. The harmonic components lower than fourth order correspond to subharmonics. Due to the existence of these subharmonics, an 8-pole 9-slot topology cannot be used for the application of the active magnetization change technique.

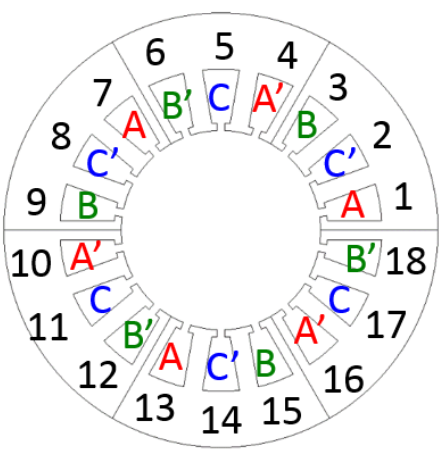

(a) Winding configuration

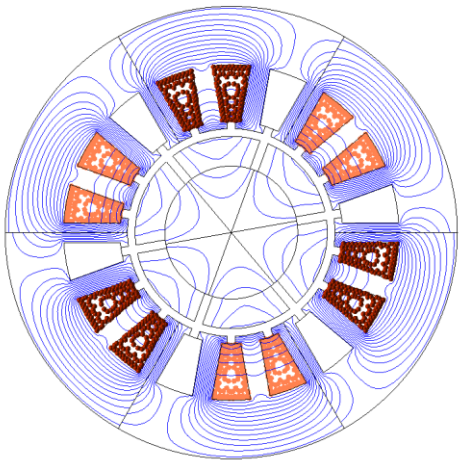

(b) Flux line and current density

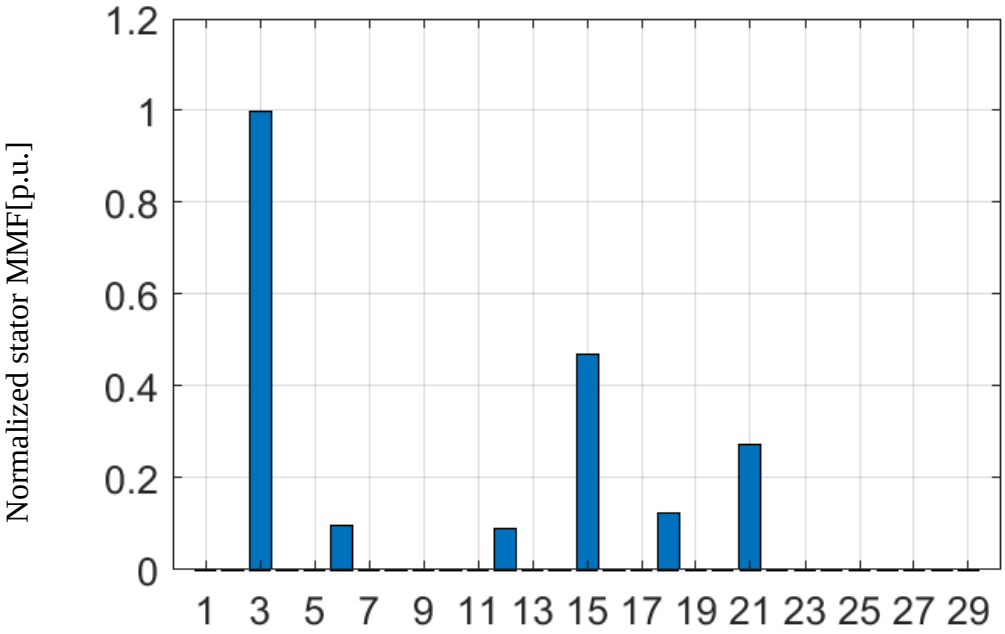

(c) Harmonic spectra of stator MMF

Fig. 3-3 Profile of 6-pole 18-slot machine

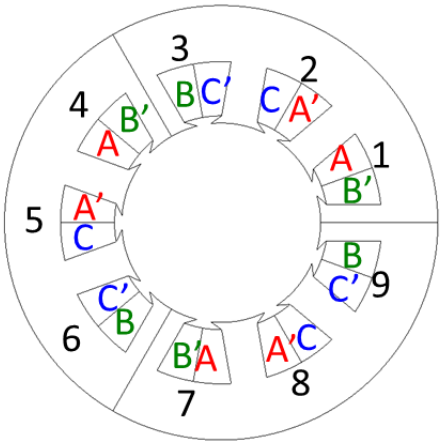

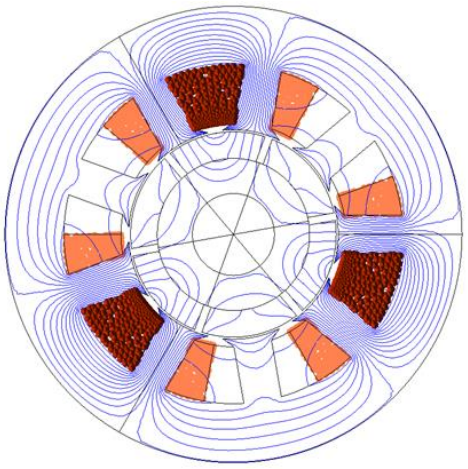

(a) Winding configuration (b) Flux line and current density

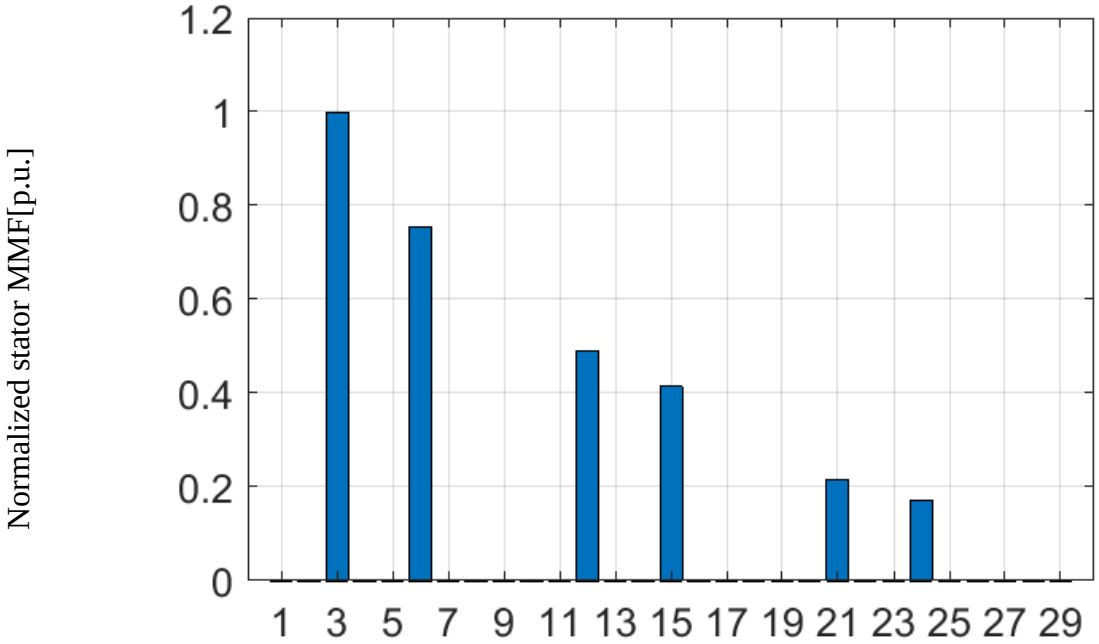

(c) Harmonic spectra of stator MMF

Fig. 3-4 Profile of 6-pole 9-slot machine

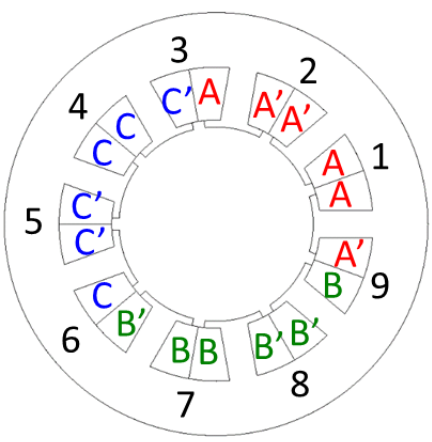

(a) Winding configuration

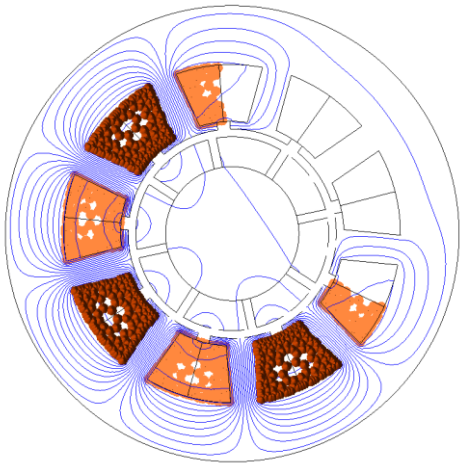

(b) Flux line and current density

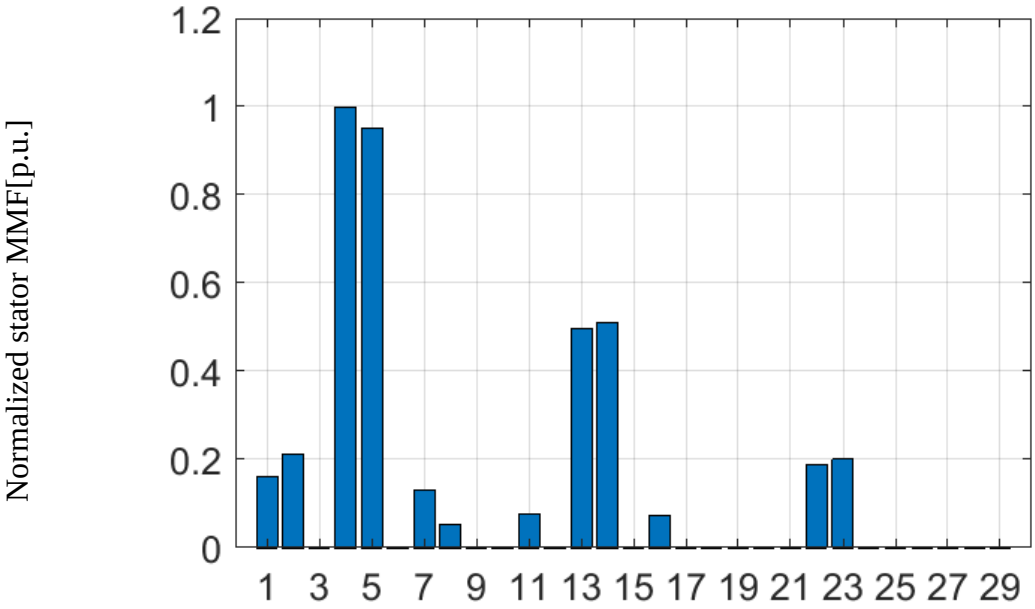

(c) Harmonic spectra of stator MMF

Fig. 3-5 Profile of 8-pole 9-slot machine

3.3.2 General guideline of slot pole combination for VMP-PMSMs

Based on the analysis of the nature of spatial MMF, this section develops an indicator of slot pole combination for VMP-PMSMs. The greatest common divisor (G.C.D) between the number of slots N_S and the number of poles P is defined as the electrical periodicity of machines as follows [106]:

$$g = \text{G.C.D.}\ \{N_s, \frac{P}{2}\} \tag{3-1}$$

If the electrical periodicity of a machine is equal to a number of pole pairs $\frac{P}{2}$, the spectrum does not contain subharmonics [108]. Therefore, the condition of the zero-subharmonics can be derived as:

$$g \equiv \frac{P}{2} \tag{3-2}$$

Hence the number of slots that satisfy the zero-subharmonics condition is,

$$N_S = j \cdot g = j \cdot \frac{P}{2} \tag{3-3}$$

where: j = an arbitrary positive integer.

Consequently, SPP under the zero-subharmonics condition is,

$$q = \frac{Ns}{P \cdot m} = \frac{j}{2 \cdot m} \tag{3-4}$$

where: m = number of phases.

As shown in the last section, when the subharmonics exist in the stator current spatial MMF, each pole pair is subjected to a different magnetic field from the adjacent pole pairs. Hence, the

magnetization of each pole pair cannot change homogeneously. It means that the zero-subharmonics condition represented in (3-4) can also be used as a criterion of machine topologies that can fit the active magnetization change technique. A list of SPP for a three-phase machine that satisfies (3-4) is summarized in Table 3-1.

Based on the identified criterion, an SPP chart to find the possible slot pole combination for machines using active magnetization change is built as Table 3-2. In this table, cells highlighted by yellow color indicates the SPP numbers applicable for active magnetization change. Cells colored as dark gray are infeasible combination due to the unbalanced winding [110]. For instance, among the examples shown in the previous section, combinations of 6 pole 18-slot and 6-pole 9-slot have q=1 and q=0.5 respectively. These SPPs are in Table 3-1 and highlighted with yellow in Table 3-2. Hence, they are feasible as an application of the active magnetization change technique. Meanwhile, one remaining example, a combination of 8-pole 9-slot, has q=0.375, which does not satisfy (3-4) and is not highlighted in Table 3-2. Hence, the active magnetization technique cannot be applied to this topology.

Table 3-3 shows a list of SPPs of existing VF-PMSMs from the published literature from various research institutions. These examples have SPPs that match with the analytically obtained SPP guideline for three-phase VF-PMSMs in Table 3-2. Note: Only VF-PMSMs that change the magnetization using the armature current while spinning rotor are summarized here.

Table 3-1. SPP FOR ACTIVE MAGNETIZATION CHANGE IN THREE-PHASE MACHINE

j	Q	J	q	j	q
1	0.167	11	1.833	21	3.5
2	0.333	12	2.0	22	3.667
3	0.5	13	2.2	23	3.8
4	0.667	14	2.333	24	4.0
5	0.833	15	2.5	25	4.167
6	1.0	16	2.7	26	4.3
7	1.167	17	2.833	27	4.500
8	1.333	18	3.0	28	4.667
9	1.5	19	3.2	29	4.8
10	1.667	20	3.333	30	5.0

Table 3-2. SPP FOR SEVERAL SLOT POLE COMBINATIONS

	p								
Ns	4	6	8	10	12	14	16	18	20
6	0.5	0.333	0.25	0.2	0.167	0.143	0.125	0.111	0.1
9	0.75	0.5	0.375	0.3	0.25	0.214	0.188	0.167	0.15
12	1.0	0.667	0.5	0.4	0.333	0.286	0.25	0.222	0.2
15	1.25	0.833	0.625	0.5	0.417	0.357	0.313	0.278	0.25
18	1.5	1.0	0.75	0.6	0.5	0.429	0.375	0.333	0.3
21	1.75	1.167	0.875	0.7	0.583	0.5	0.438	0.389	0.35
24	2.0	1.333	1.0	0.8	0.667	0.571	0.5	0.444	0.4
27	2.25	1.5	1.125	0.9	0.75	0.643	0.563	0.5	0.45
30	2.5	1.667	1.25	1.0	0.833	0.714	0.625	0.556	0.5
33	2.75	1.833	1.375	1.1	0.917	0.786	0.688	0.611	0.55
36	3.0	2.0	1.5	1.2	1.0	0.857	0.750	0.667	0.6
39	3.25	2.167	1.625	1.3	1.083	0.929	0.813	0.722	0.65
42	3.50	2.333	1.75	1.4	1.167	1.0	0.875	0.778	0.7
45	3.75	2.5	1.875	1.5	1.25	1.071	0.938	0.833	0.75
48	4.0	2.667	2.0	1.6	1.333	1.143	1.0	0.889	0.8
51	4.25	2.833	2.125	1.7	1.417	1.214	1.063	0.944	0.85
54	4.5	3.0	2.25	1.8	1.5	1.286	1.125	1.0	0.9
57	4.75	3.167	2.375	1.9	1.583	1.357	1.188	1.056	0.95
60	5.0	3.333	2.5	2.0	1.667	1.429	1.25	1.111	1.0

Infeasible combination

Possible combination

Active magnetization change is applicable

Table 3-3. SPP OF EXISTING VF-PMSM/VMP-PMSM

ID	Ref.	Machine Type	Slot	Pole	Winding	SPP
#1	A.Athavale, WEMPEC [74]	VF-PMSM	60	8	FSDW	2.5
#2	C.Yu, WEMPEC [46]	VF-PMSM	45	6	FSDW	2.5
#3	C.Yu, WEMPEC [46]	VF-PMSM	36	6	ISDW	2
#4	M.Ibrahim, Concordia Univ. [77]	VF-PMSM	18	6	ISDW	1
#5	M.Ibrahim, Concordia Univ. [77]	VF-PMSM	36	6	ISDW	2
#6	M.Ibrahim, Concordia Univ. [77]	VF-PMSM	54	6	ISDW	3
#7	M.Ibrahim, Concordia Univ. [77]	VF-PMSM	9	6	FSCW	0.5
#8	M.Ibrahim, Concordia Univ. [77]	VF-PMSM	27	6	ISDW	1.5
#9	H.Liu, Univ of Sheffield [113]	VF-PMSM	24	4	ISDW	2
#10	H.Hua, Univ of Sheffield [112]	VF-PMSM	48	8	ISDW	2

ISDW: Integer Slot Distributed Winding

FSDW: Fractional Slot Distributed Winding

FSCW: Fractional Slot Concentrated Winding

3.4 Selection of Low-H_c Magnet and Rotor Design for Active Magnetization Change

Unlike conventional PMSMs that use high coercive magnets, such as NdFeB (H_{ic} > 1000kA/m), low coercive magnets are required in VF-PMSMs and VMP-PMSMs in order to intentionally demagnetize the magnet within the current limit that a drive system can allow. SmCo ($H_{ic} \approx 600$kA/m) and AlNiCo (50kA/m<H_{ic}<150kA/m) are magnets most commonly used in this type of machines. Magnet material characteristics are essentially one of the most critical factors in VF-PMSMs and VMP-PMSMs since they predominantly determine the performance

of the machines. Nevertheless, besides the magnitude of the coercivity, comprehensive design guideline for the material selection has not been discussed in this field.

In this section, first, design trade-offs in geometrical constraints of VF-PMSMs and VMP-PMSMs dependent on the B-H curve of the permanent magnet are described. Afterword, possible combinations of geometrical parameters for three sample magnet materials, AlNiCo9, SmCo R26, and SmCo R30, are compared using the proposed metrics.

3.4.1 Design constraints to have active magnetization change characteristic

In this section, three key design constraints for machines using the active magnetization change technique are discussed. In order to simplify the discussion, an assumption that area of the airgap and the surface area of the magnet are the same is applied in all analysis in this section and the following sections.

No-load condition

A permanent magnet can be naturally demagnetized without additional magnetic field if the operating point for no-load condition locates at below the knee point. In order to fully utilize the energy density of the magnet, avoiding demagnetization in the no-load status is one of the most basic practices in the machine design with magnets. Equation (3-5) is an equation for the load line at the no-load condition.

$$B = -\mu_0 \frac{l_m}{l_g} H \tag{3-5}$$

Demagnetizing operation

The current that the demagnetization starts essentially needs to be larger than the maximum load current. Compared to the case of the conventional PMSM with high coercive NdFeB, this concern is more severe in VF-PMSMs and VMP-PMSMs since the low coercive force magnets

are predominantly used in these machines. Equation (3-6) represents a load line of the magnet at the load operation.

$$B = \mu_0 \frac{l_m}{l_g}(H - \frac{NI_{demag}}{l_m}) \quad (3\text{-}6)$$

Remagnetizing operation

VF-PMSMs and VMP-PMSMs need to be designed so that they can push the operating point of magnets to the saturated point in the B-H curve within the inverter capacity to recover the magnetism. Smaller remagnetizing current is required in order to reduce the required inverter capacity. Equation (3-7) shows load line of the magnet at remagnetizing operation.

$$B = -\mu_0 \frac{l_m}{l_g}(H - \frac{NI_{remag}}{l_m}) \quad (3\text{-}7)$$

Trade-off of the geometrical parameter in de/re-magnetization operation

Figure 3-6 shows the difference between the required MMF for de/re-magnetization depending on the permeance coefficient. Smaller permeance coefficient needs larger MMF for the demagnetization and smaller MMF for the remagnetization. The magnet thickness and the airgap length directly affect the de/re-magnetization capability since the permeance coefficient is a function of these geometrical parameters. As summarized in Table 3-4, either thicker magnet or thinner airgap make the full remagnetizing current smaller. However, in general, the possible airgap length is limited to above 0.5 mm from the manufacturing point of view. Also, the allowable maximum magnet thickness depends on machine size. Geometrical parameters for VF-PMSMs and VMP-PMSMs need to be selected considering these trade-offs.

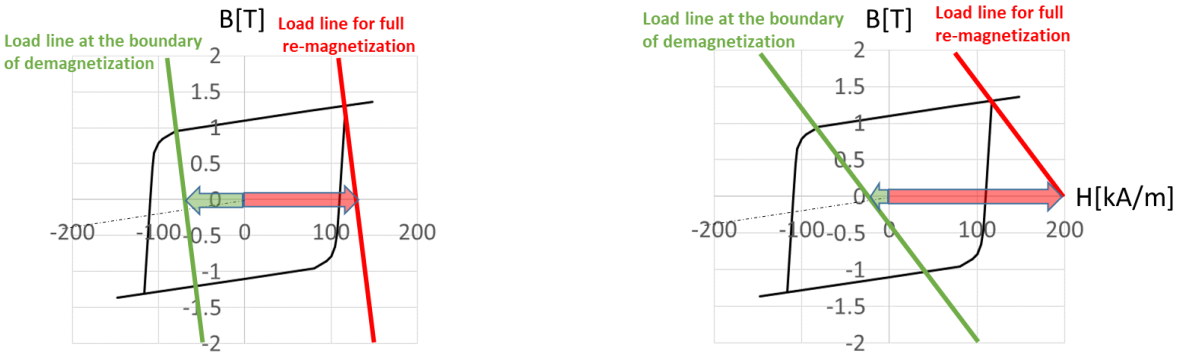

(a) small permeance coefficient (b) large permeance coefficient

Fig. 3-6 Required MMF for de/re-magnetization depending on the permeance coefficient

TABLE 3-4.. MAGNETIZATION CAPABILITY AND GEOMETRY

	Thicker magnet	**Thicker airgap**
Permeance Coefficient	Smaller	Larger
Demagnetization	Harder (required current is larger)	Easier (required current is smaller)
Full re-magnetization	Easier (required current is smaller)	Harder (required current is larger)

3.4.2 Rotor parameter design with different magnet material

In this section, three sample magnet materials are compared in terms of the remagnetizing capability and the torque density using the multiple combinations of the magnet thickness and the airgap length. A few hundred-watt servo machine is assumed as a design goal in this example. Only SPMSMs are considered here because they are closest to the ideal model of demagnetization mechanism.

Test Materials

Three materials, AlNiCo9 (Arnold Magnetic Technologies Corp.), SmCo R26 (Shin-Etsu Chemical Co., Ltd.) and SmCo R30 (Shin-Etsu Chemical Co., Ltd.) are picked up for the

investigation from a commercial FEA software database [111]. In general, only the second and the third quadrant information are disclosed from material companies to the public. Therefore, estimated saturated points from the original data are used in this investigation assuming the rotational symmetricity of the B-H curve. The linearized material curves including the first and the fourth quadrant are shown in Fig.4. As shown in Fig. 4, AlNiCo has the smallest coercive force and SmCoR26 has the largest stored energy.

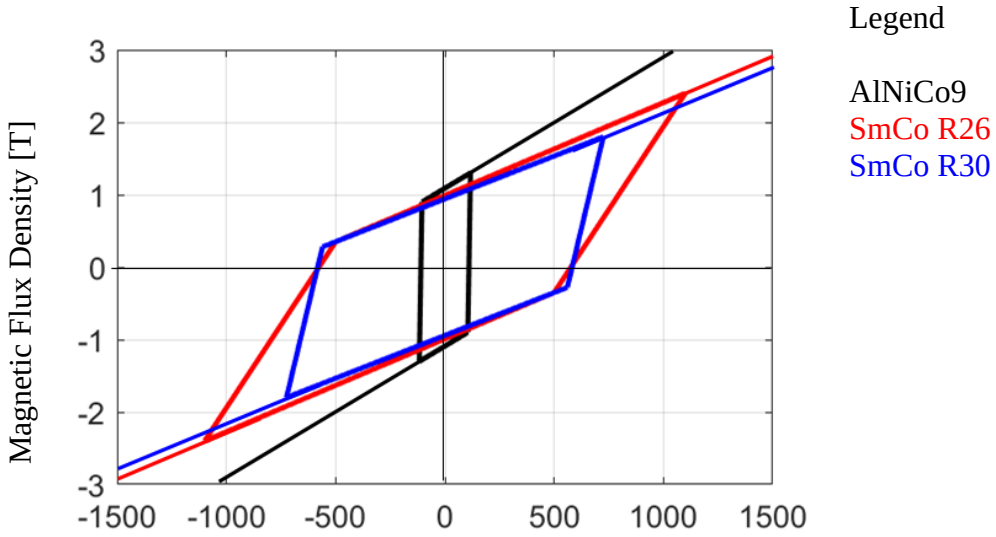

Fig. 3-7 Modified linearized material curve

Metrics

Following indicators are employed in this investigation to evaluate the selected magnets,

Remagnetizing current in per unit

Efforts to reduce the ratio of the remagnetizing current per the load current need to be taken in the design process of machines using the active magnetization change to reduce the total drive system cost including the inverter. The remagnetizing current in per unit in a machine is defined using the MMF for the remagnetizing operation and the maximum load operation as follows

assuming the winding function for the remagnetizing operation and the maximum load operation do not change.

$$I_{remag,p.u.} = \frac{I_{remag}}{I_{max\ load}} = \frac{MMF_{remag}}{MMF_{max\ load}} = \frac{\mu_0 H_{remag} l_m + B_{remag} l_g}{\mu_0 H_{max\ load} l_m + B_{max\ load} l_g} \quad (3\text{-}8)$$

$$\text{Where } I_{max\ load} = \frac{MMF_{max\ load}}{N},\ I_{remag} = \frac{MMF_{remag}}{N}$$

Torque density turn per pole in MMF base

Torque density is a function of the permanent magnet, the winding current, number of poles and the machine volume. In order to narrow down the discussion to the material characteristics, the torque density per pole in MMF base is used here to evaluate the torque capability assuming that the stator geometries of the machines used in the comparison are same. The torque density per pole in MMF base is defined as follows.

$$\tau_{density\ per\ pole\ in\ MMF\ base} = \frac{3}{4} \lambda_{PM\ per\ volume}\, MMF_{max\ load} \quad (3\text{-}9)$$

$$\text{Where } \lambda_{per\ volume} = \frac{\pi}{4} B_{no\text{-}load}$$

Permanent magnet geometrical dimension calculation to meet the design constraints

Figure.3-8 shows remagnetizing current in per unit calculated while changing the magnet thickness (lm) and the airgap length (lg). In Fig.3-8, it is shown that 2.5 p.u. is the minimum remagnetizing current for AlNiCo and SmCo R26, whereas SmCo R30 just needs 2.0 p.u. remagnetizing current. Smaller remagnetizing current than 2.5 p.u. is theoretically possible even for AlNiCo 9 and SmCo R26 if the magnet can be thicker than 12 mm or the airgap can be shorter than 0.5 mm. However, these numbers are not practical for the fabrication. Therefore, their remagnetizing current is limited to 2.5 p.u. The reason that AlNiCo9 tends to be thicker is that it is easily get demagnetized in the load operation due to the small coercivity. Meanwhile,

SmCo R26 tends to be thicker because its B-H curve has a large area and its saturated point is located far from the origin. In order to reach such saturated point with relatively small remagnetizing current, the slope of the load line needs to be shallower, so the magnet needs to be thicker.

Figure 3-9 shows that the possible torque density in MMF base of AlNiCo 9 is quite low compared to the other two materials at any magnet thickness. SmCo R26 with 2.5 p.u. remagnetizing current achieves the highest torque density around 600 -800 Nm/m^2. However, when the design target is a few hundred-watt small machines as assumed in this discussion, 8 mm of magnet's thickness is not acceptable. Since SmCo R26 has the largest B-H curve area, technically it can take the highest torque density, however, to minimize the remagnetizing current to reach the saturated point, which is corresponding to the vertex of the B-H curve area, SmCo R26 tends to be thicker. Meanwhile, SmCo R30 in Fig.6 shows that it achieves the same level of the torque density with SmCo R26 using much lower remagnetizing current than SmCo R26 within reasonable magnet thickness.

In summary, when three design constraints for active magnetization change capability are considered, it is found that a magnet material that has the lowest coercive force is not necessarily an ideal candidae. Likewise, a magnet with the largest energy density does not necessarily achieve the highest torque density with the realistic dimension. By evaluating magnets using the proposed metrics, a suitable magnet material for VMP-PMSMs and VF-PMSMs that meets the design goal can be identified.

Legend: 2.0 p.u Remag current., 2.5 p.u Remag current., 3.0 p.u. Remag current, 3.5 p.u. Remag current, 4.0 p.u Remag curent .

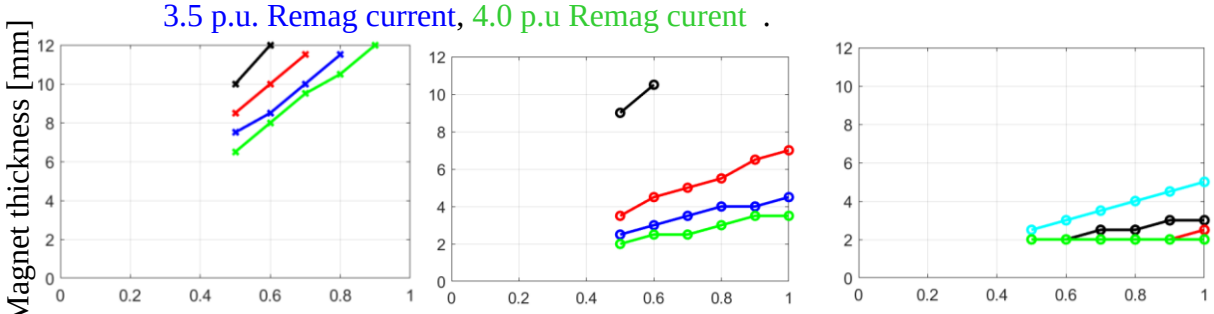

(a) AlNiCo9 (b) SmCo R26 (c) SmCo R30

Fig. 3-8 Required magnetizing current for various geometrical parameters

Legend: 2.0 p.u. Remag current, 2.5 p.u. Remag current, 3.0 p.u. Remag current, 3.5 p.u. Remag current, 4.0 p.u Remag curent .

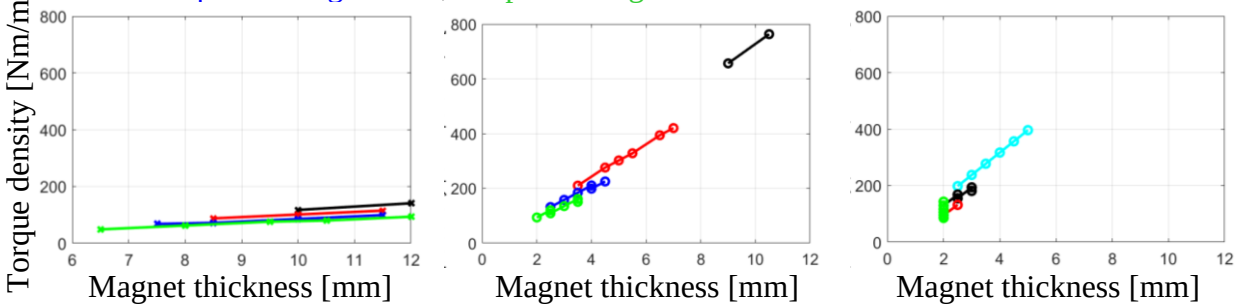

(a) AlNiCo9 (b) SmCo R26 (c) SmCo R30

Fig. 3-9 Achievable torque density with different magnet thickness

3.5 Summary

In this chapter, the design of VMP-PMSMs is discussed. Two key components, choice of the slot pole combination and material selection, differentiate VMP-PMSM design process from the conventional SPMSM design process. Design guidelines regarding the applicable slot pole combinations of active magnetization change are analytically identified and validated using ten examples taken from existing publications. A methodology to identify a permanent magnet material for VF-PMSMs and VMP-PMSMs considering the remagnetizing current capability and the torque density is analytically developed.

Chapter 4 Control of VMP-PMSMs

4.1 Introduction

Chapter 4 investigates the current characteristics and some potential factors in VMP-PMSM control systems that affect the quality of the resultant magnetization pattern. In the first two sections, the relationship of the magnetizing current and the resultant magnetization pattern is investigated assuming the ideal pulse current with infinitely small rise time. From the third section, the assumption is removed and the impact of the design of the commanded pulse width on the resultant magnetization pattern is investigated. Pulsating torque caused during the magnetization pattern shaping process is also discussed here. Lastly, the effect of harmonic current caused by PWM is investigated. All investigations in this chapter are assumed a 6-pole 9-slot concentrated winding machine.

4.2 Current Vectors for Uniform Magnetization State Change

As the first example of the magnetization pattern change with various magnetizing current, the uniform magnetization change is shown in this section. The uniform magnetization change corresponds to the global magnetization state change in conventional VF-PMSMs. Here, a similarity in VMP-PMSMs and VF-PMSMs are shown from the viewpoint of the controllability of the magnet flux.

Consider the sequential magnetizing current injection of positive and negative q-axis pulse with different magnitudes, 5 A, 7 A, 8 A and 9 A as shown in Fig. 4-1. This corresponds to two magnetizing current vector injections with $ß_1$= 0 deg. and $ß_2$= 180 deg..

Figure 4-2 shows a trajectory of operating points at the center of the permanent magnet during the magnetization change operation with different magnetizing currents. As the

magnitude of the magnetizing current pulse increases, the operating point drops further on the major loop after it passes the knee point.

The resultant no-load back-EMFs obtained after injecting these magnetizing current vectors are shown in the spatial domain in Fig.4-3(a). The magnitude and THD of these no-load back-EMFs along with the change of the magnitude of the magnetizing current is shown in Fig. 4-3(b). It can be observed in Fig. 4-3(b) that the decrease of the no-load back-EMF magnitude is proportional to the increase of the magnetizing current. Meanwhile, THD of no-load back-EMF is nearly stable regardless of the magnitude of the magnetizing current, meaning the ratio of the harmonic components are always same regardless of the magnitude of the magnetizing current. This set of two magnetizing current vectors achieves the global uniform magnetization state change in the permanent magnet in a similar manner with VF-PMSMs.

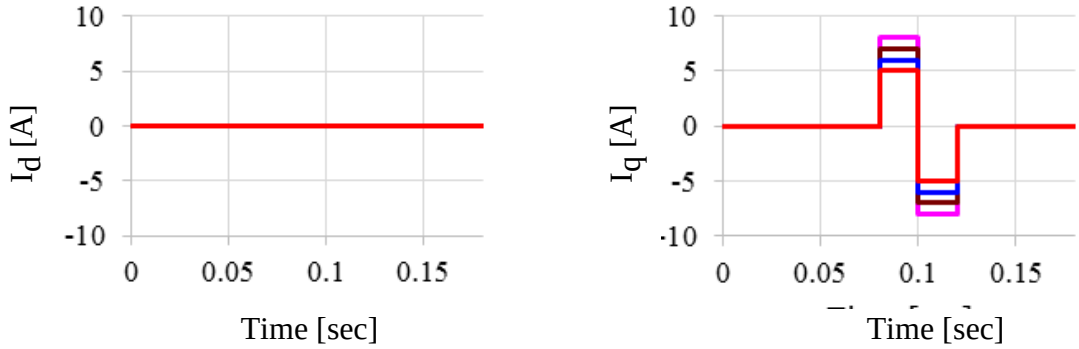

Fig. 4-1 Magnetizing current trajectory for uniform magnetization state change (FEA)

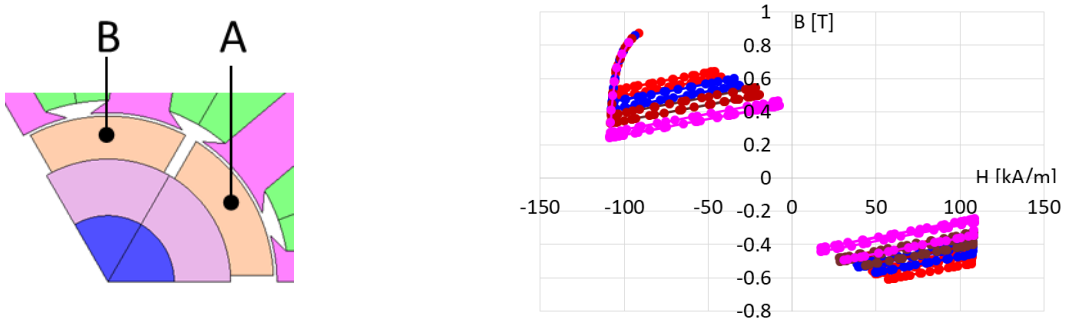

(a) Sampling points in permanent magnet (b) Operating points history

Fig. 4-2 Operating points history in permanent magnets(FEA)

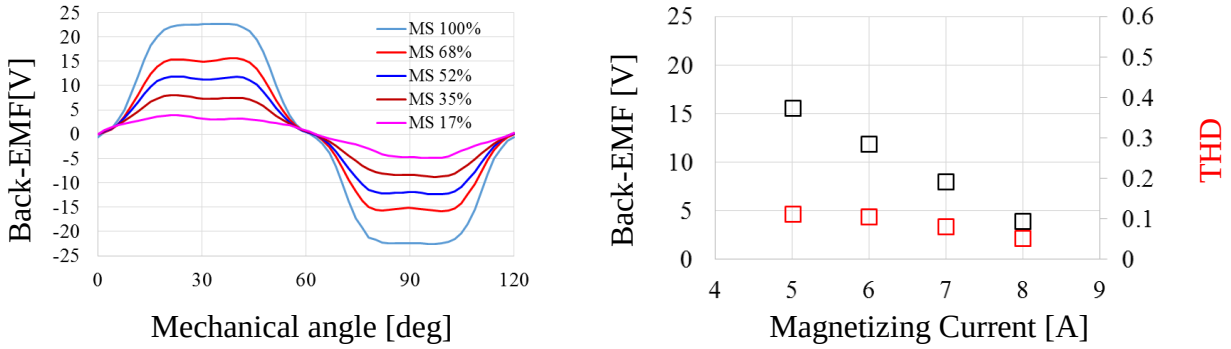

(a) Back-EMF in time domain (b) Magnetizing current characteristics

Fig. 4-3 Resultant back-EMF by uniform magnetization state change

4.3 Current Vectors for the Least back-EMF THD

The second example is non-uniform magnetization pattern change with a sequential injection of two magnetizing current pulses aiming a back-EMF waveform with the least THD. The VF-PMSMs, in which only the global magnetization state is a target to control, inherently cannot manipulate spatial harmonic components in the magnetization pattern. Hence, non-uniform magnetization pattern theoretically cannot be created in VF-PMSMs. Here, the fundamental difference between VMP-PMSMs and VF-PMSMs will be shown in terms of the manipulation of the spatial attributes.

In the discussion in Chapter 2-6, it has been shown that two magnetizing current vectors defined in (4-1) can locally demagnetize the permanent magnets from the edges of magnets.

$$\begin{cases} I_1 = I \angle ß_1 & ß_1 = 270° - \varepsilon \\ I_2 = I \angle ß_2 & ß_2 = 270° + \varepsilon \end{cases} \qquad (4\text{-}1)$$

Command current trajectories corresponding to (4-1) with 7A magnitude of ε =27 deg., 60 deg., and 80 deg. are shown in Fig. 4-4 in dq format. A set of the double magnetizing current vectors substantially results in the same effect with the geometrical change of the magnet's arc. Hence, the local optimum current phase angle to achieve the minimum harmonics is found in the resultant no-load back-EMF (Fig. 4-5) in a similar manner with the optimization of the magnet arc shape.

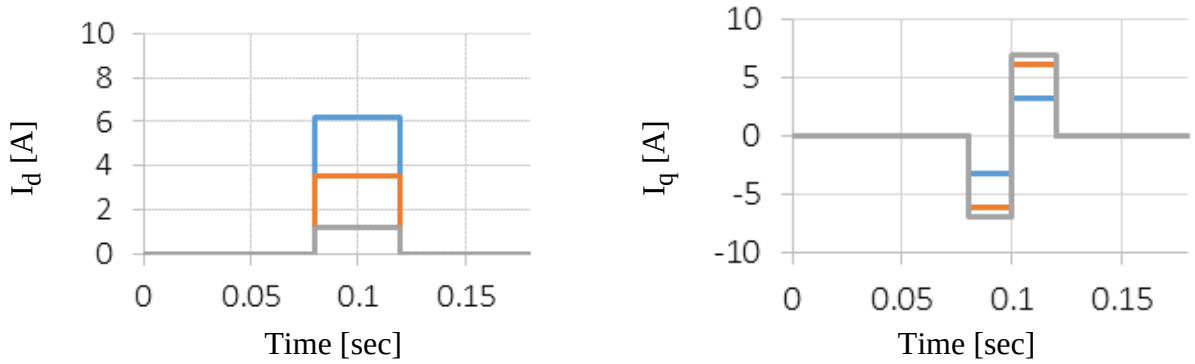

Fig. 4-4 Magnetizing current for symmetrical non-uniform magnetization pattern

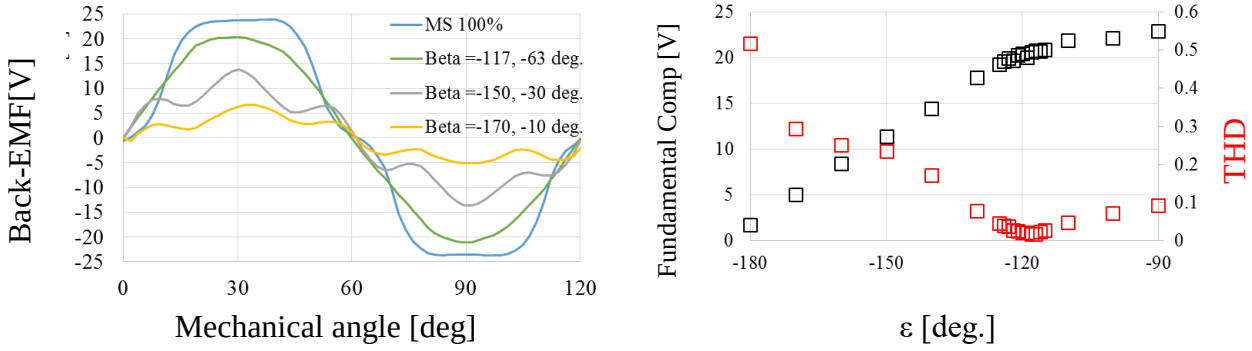

(a) Back-EMF in time domain (b) Fundamental Comp and THD

Fig. 4-5 Resultant back-EMF by symmetrical non-uniform magnetization state change

Following that, the analysis of the two-sequential magnetizing current pulses with different current magnitudes and different current angles is conducted to investigate the effect of the

magnitude of the magnetizing current in the spatial distribution of magnetization. Figure 4-6 illustrates the fundamental component and THD of the no-load back-EMF obtained after injecting two-sequential magnetizing current pulses.

In the case of I = 5 A, the change of the back-EMF along ε is not significant compared to 7 A and 9 A, because an area in the magnet demagnetized by the envelope of the magnetic field profile of 5 A is quite small. Meanwhile, the resultant peak magnetic fields due to 7 A and 9 A are large enough so that it has significant effect even when ε is small.

The minimum back-EMF THD is found at I = 7 A, ε = 30 deg. and I = 9 A, ε = 20 deg. as shown in Fig.4-6. A current vector with lower magnitude is a better choice to reduce the unwanted torque during the magnetization pattern change, thus, I = 7A, ε = 30 deg. is selected as the best magnetizing current in these test cases.

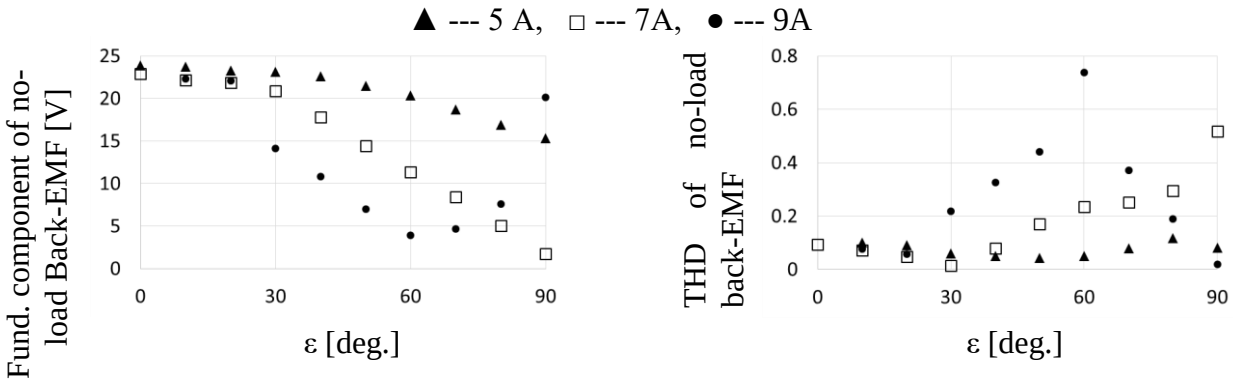

(a) Fundamental Component (b) THD

Fig. 4-6 Correlation of magnetizing current phase and resultant no-load back-EMF (FEA result)

4.4 Magnetizing Current Pulse Width and Pulsating Torque during Magnetization Pattern Change

The dynamic spatial magnetization change method uses the magnetic field for one electrical cycle as a basic unit of the magnetization pattern control. As identified in Chapter 2, the magnetizing current pulse width is theoretically determined as a function of the operation speed based on that principle as shown in Fig. 4-7.

However, to make the method more robust and feasible, other practical concerns such as pulsating torque, overheating and eddy current during the magnetization shaping process, also need to be considered in the design decision regarding the pulse width. For instance, in order to suppress the overheating in the winding, shorter pulse width is better. Meanwhile, from the consideration of the eddy current in magnets, longer pulse width is better. In this section, the vital minimum current pulse width is investigated in order to lay a foundation for those practical discussions.

In this simulation, a set of two magnetizing current vectors, 7 A∠ -60°, 7 A∠ -120°, are sequentially injected to a machine to change the no-load back-EMF from a trapezoidal shape to a sinusoidal shape. Through the calculation, various pulse width ratio, *k* defined in (4-2) and Fig. 4-8 are tested.

$$T_{inject} = kT = k\frac{60P}{N_{rpm}} \qquad (4\text{-}2)$$

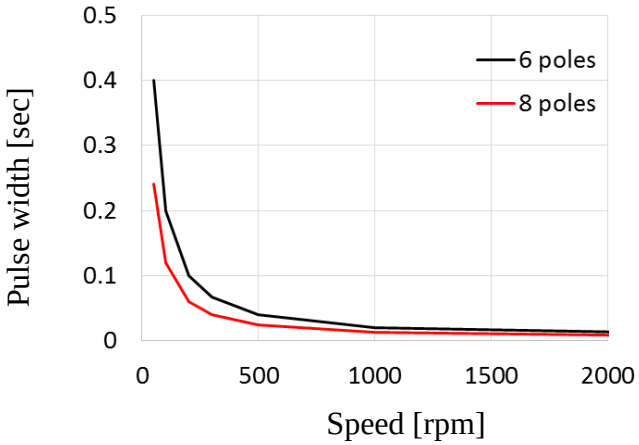

Fig. 4-7 Definition of pulse width ratio

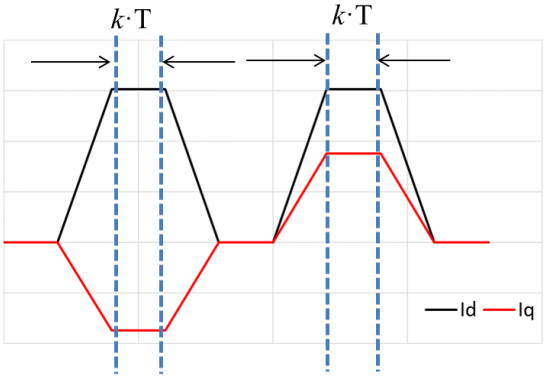

k: Pulse width ratio
T: Time period for one electrical cycle

Fig. 4-8 Definition of pulse width ratio

Figure 4-9 shows resultant no-load back-EMFs obtained from the sequential magnetizing current pulse injection with different pulse width. At k = 0.1 and k = 0.25, back-EMFs still have a corner and are far from the desired sinusoidal back-EMF. In contrast, all back-EMFs after k =0.5 are close to sinusoidal and lines are overlapped. As seen in Fig. 4-10, which is calculated using finer resolution interms of k, the fundamental component and THD of these resultant back-EMFs before k =0.33 is decreased as k is increased. Meanwhile the fundamental component and THD do not show any change after k = 0.33.

Figure 4-11 shows the magnetic field profile in the rotor reference frame at an arbitrary point during this magnetization shaping process in the time domain. As seen in Fig 4-11, the third-

harmonic component dominates the profile for one electrical cycle. As seen in Fig. 4-12 (b), the external magnetic field generated by the sinusoidal three-phase stator winding current does not contain time harmonics in the stator reference frame. However, in the rotor reference frame, the magnetic field is affected by the permeance distribution due to the slot openings. Since the tested machine has a 6-pole 9-slot configuration, the external magnetic field has third time harmonics in the rotor refrerence frame (Fig. 4-12(c)).

Figure 4-13 shows a magnetic field vector with harmonic components rotating in the rotor reference frame. Due to the existence of the rotating harmonic component, the magnitude of the instantaneous total magnetic field in the rotor reference frame varies depending on time. The maximum magnitude of the total magnetic field vector is derived when the fundamental component vector, and the harmonic component vector are aligned. For instance, when the third harmonic component is the most dominant component besides the fundamental component, the fundamental component vector and the third component vector aligns every one- third of the electrical cycle (corresponding to $k = 0.33$)

From this simulation, it has been found that minimum pulse duration required for the dynamic spatial magnetization shaping method is an inverse of the minimum time-harmonic frequency contained in the airgap magnetic field in the rotational reference frame. If the current pulse is shorter than an inverse of the minimum time harmonics frequency in the airgap magnetic field in the rotational reference frame, the quality of the magnetization pattern, defined using the fundamental component and THD of the resultant back-EMF, is deteriorated. If the current pulse is longer than or equal to an inverse of minimum time harmonics frequency in the airgap magnetic field in the rotational reference frame, the quality of the magnetization pattern can be same as when the current pulse is hold for one electrical cycle.

A generalized minimum required pulse period for active magnetization change can be represented in the following equation:

$$T' = \frac{2\pi}{\omega_e \cdot HO} \qquad (21)$$

Where: HO = the order of the lowest among harmonics above h=P/2

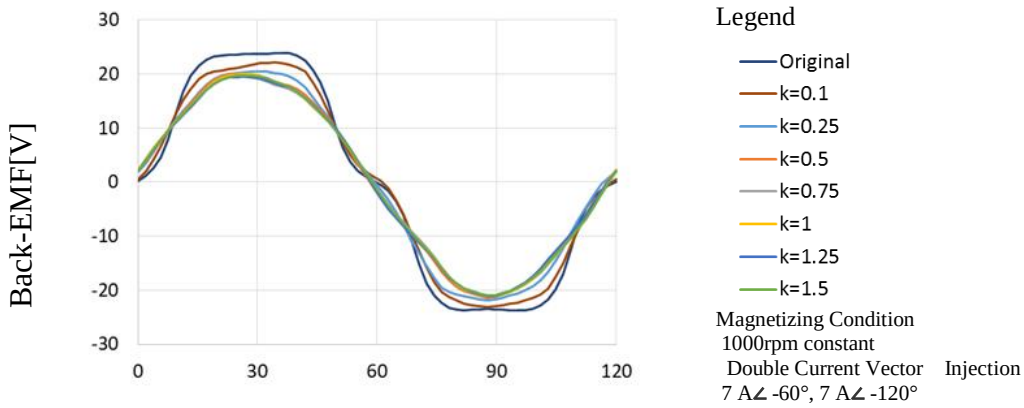

Fig. 4-9 Resultant back-EMF with different pulse width

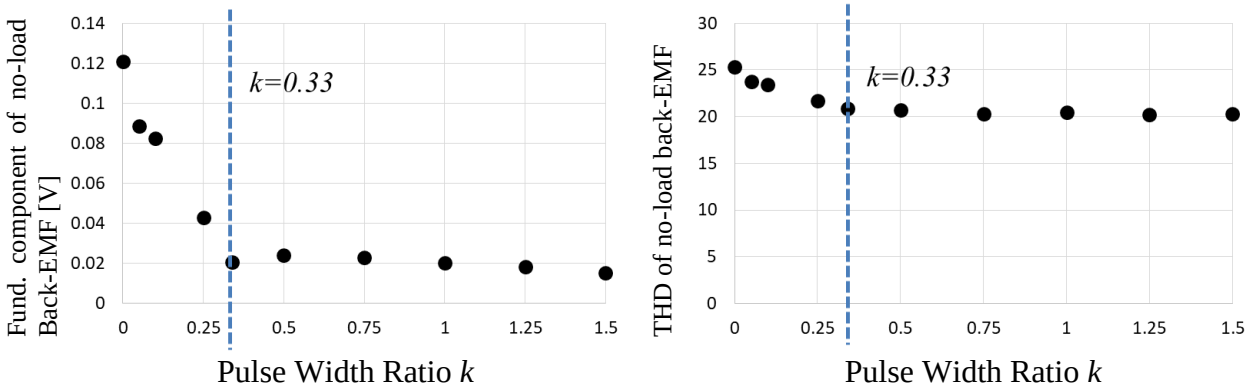

Fig. 4-10 Correlation of magnetizing current pulse width and resultant no-load back-EMF

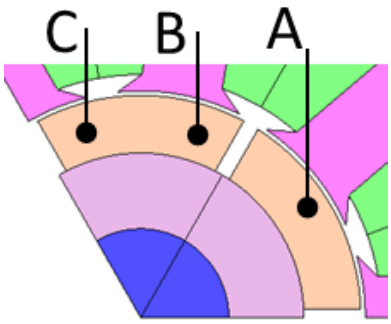

(a) Sampling Points

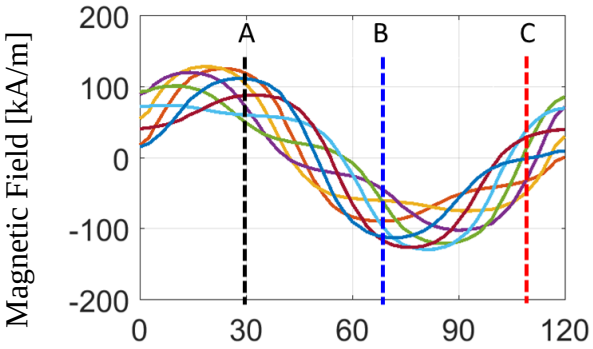

(b) Magnetic field profile in spatial domain in rotor reference frame

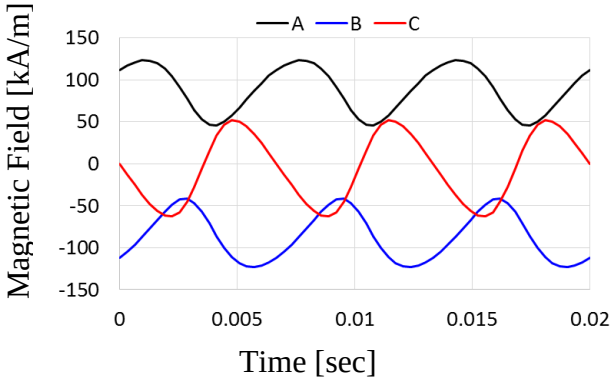

(c) Magnetic field profile in temporal domain

Fig. 4-11 Magnetic Field Profile in spatial and temporal domain (FEA result)

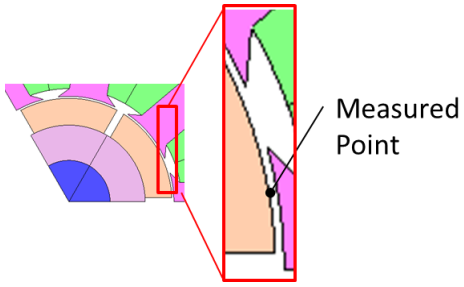

(a) Sampling Points

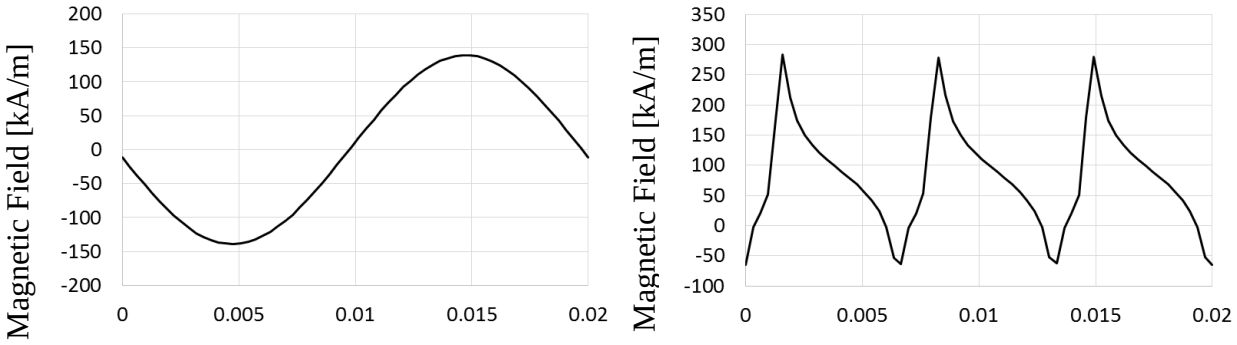

(b) Stationary Reference Frame (c) Rotor Reference Frame

Fig. 4-12 Magnetic Field Profile in spatial and time domain (FEA result)

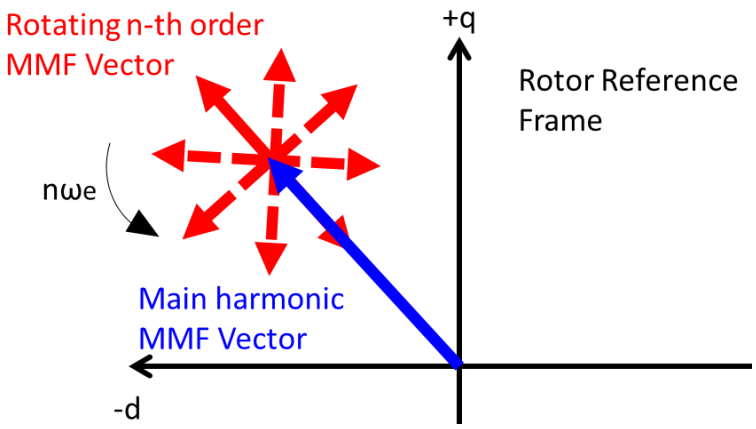

Fig. 4-13 Rotating MMF vector in rotor reference frame

The calculation results of torque during the magnetization pattern shaping process applied different pulse width (k = 1 and k = 0.333) are shown in Fig. 4-14 and Fig. 4-15. Before the magnetization pattern is shaped, this machine has a trapezoidal back-EMF. Hence, the torque ripple before shaping pattern is as high as 0.19 Nm while the average torque of 0.943 Nm. Two magnetizing current vectors are sequentially injected to shape the back-EMF into a sinusoidal waveform. The first vector contains a negative q-axis component, causing harsh negative pulsating torque (from 0.02-0.06sec in Fig.4-14 and from 0.02-0.04 in Fig. 4-15). In the second pulse, the q-axis component changes to the positive and it is close to the desired load current,

hence the pulsating torque due to the second pulse is less obvious (from 0.1-0.16sec in Fig.4-14 and from 0.05-0.07 in Fig. 4-15). After the two magnetizing current injections, the back-EMF becomes a sinusoidal shape, hence, the pulsating load torque is significantly reduced compared to the initial state (From 0.16-0.18sec in Fig.4-14 and from 0.08-0.18 in Fig. 4-15). Almost same torque performance is achieved in both cases because the current pulse width in both cases is longer than or equal to required minimum pulse, which is the inverse of the minimum harmonic frequency in this machine.

Figure 4-16 shows a case that uses the same pulse width with Fig.4-15 but operated half speed of Fig.4-15. Although the pulse time duration is exactly same, the case of Fig.4-16 actually corresponds to k = 0.1666 because the speed is half so the one electrical cycle is double of the case of Fig.4-15. k = 0.1666 does not satisfy the required minimum pulse width, hence, the incomplete magnetization change happens. In this case, the torque after shaping pattern in Fig.4-16 has a pulsating torque of 0.054Nm, which is 150% higher than the case of Fig. 4-15, in which the intended magnetization change has been achieved.

Note: There is a harsh negative pulse torque observed in all examples shown here. This torque is generated by the negative q-axis component in the magnetizing current vector. The pulsating torque during the magnetization change is one of the unavoidable inherent challenges in magnetization pattern change techniques. Some of the approaches to mitigate the pulsating torque in VF-PMSMs, such as a magnetization state feedback control system using DB-DTFC needs to be implemented on VMP-PMSMs in the future.

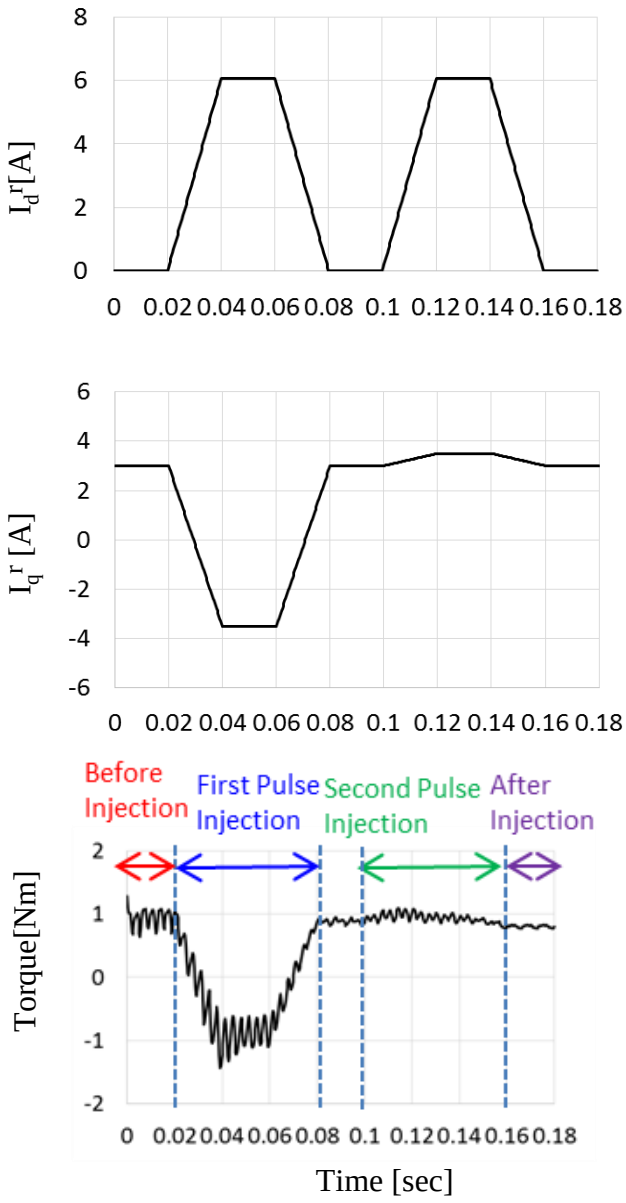

Before Shaping Pattern:
Avg Trq 0.943 Nm
Trq Ripple 0.19Nm

After Shaping Pattern:
Case #1 k=1
Avg Trq 0.829 Nm
Trq Ripple 0.036 Nm

Case #2 k=0.33
Avg Trq 0.828 Nm
Trq Ripple 0.037 Nm

1000rpm constant

Fig. 4-14 Magnetization pattern shaping process with *k=1* value @ 1000rpm

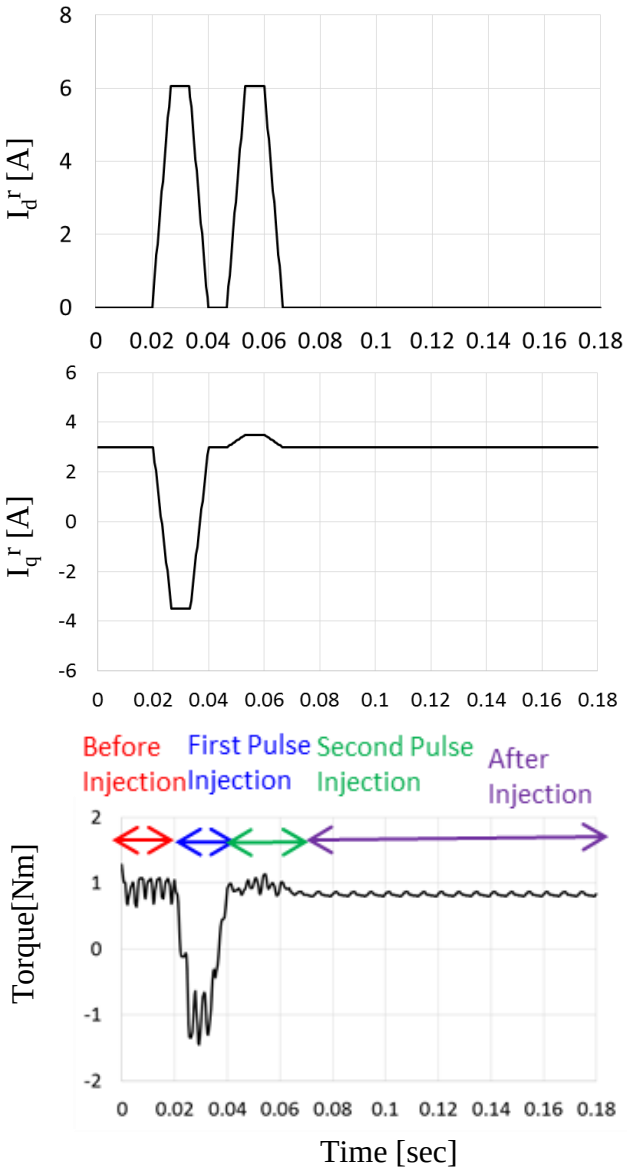

Before Shaping Pattern:
Avg Trq 0.943 Nm
Trq Ripple 0.19Nm

After Shaping Pattern:
Case #2 k=0.33
Avg Trq 0.828 Nm
Trq Ripple 0.037 Nm

1000rpm constant

Fig. 4-15 Magnetization pattern shaping process witht *k=0.33* value @ 1000rpm

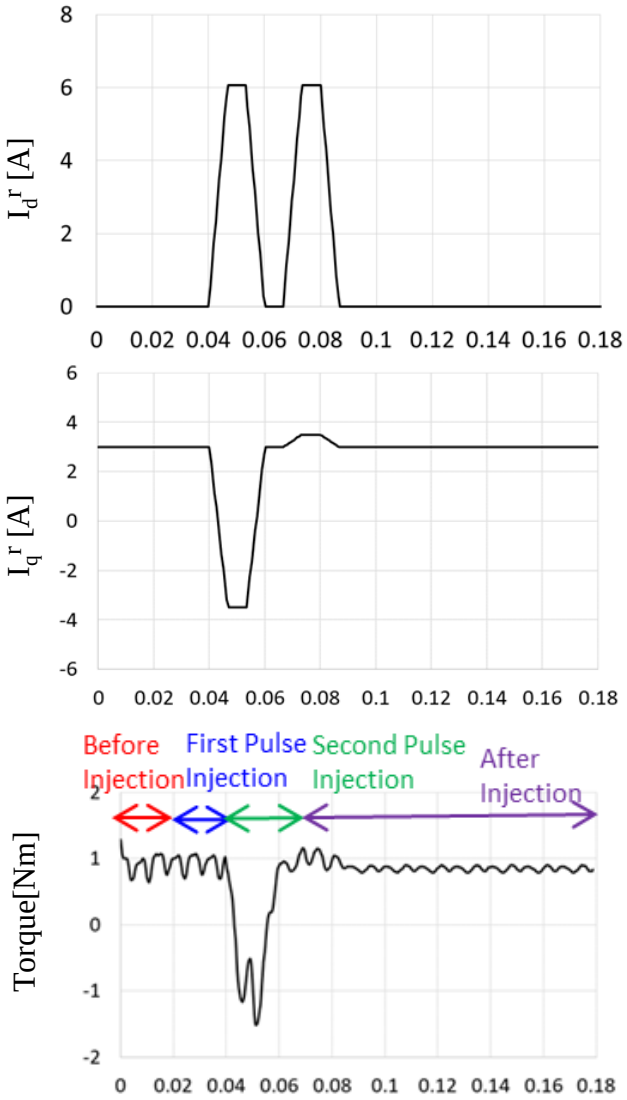

Before Shaping Pattern:
Avg Trq 0.943 Nm
Trq Ripple 0.19Nm

After Shaping Pattern:
Right Avg Trq 0.85 Nm
Trq Ripple 0.054Nm

500rpm constant

Fig. 4-16 Magnetization pattern shaping process with k = 0.166@ 500 rpm

4.5 Impact of Harmonic Magnetizing Current caused by PWM

4.5.1 Significance of the PWM harmonics in VMP-PMSMs

The analysis so far is discussed based on 2-D FEA analysis without considering PWM inverters on purpose to simplify the analysis and focus on each discussion subject. However, the harmonic current caused by pulse width modulation would affect magnetization pattern shaping from two aspects. First, ripples in the magnetic field due to the current ripples caused by modulation has a potential risk to deteriorate the resultant magnetization pattern. Second, the eddy current in permanent magnets caused by PWM excitation results in the reaction field, which has the opposite direction to the external magnetic field imposed by the stator winding current

Particularly, the reaction filed due to the eddy current in the permanent magnet can be a critical concern in the magnetization pattern shaping of AlNiCo and SmCo. The electrical resistivity of AlNiCo and SmCo is quite low as shown in Table 4-1 compared to NdFeB. Lower resistivity materials cause higher eddy current than higher resistive materials. Even NdFeB, which has much higher resistivity compared to AlNiCo as shown in Table 4-1, the eddy current is a non-negligible common concern in the machine design [43][44][45]. Therefore, it can be said that the reaction field by the eddy current is a potential key issue of VMP-PMSMs with AlNiCo and SmCo.

Figure 4-17 (a) shows an example of the 3-D FEA model including the end winding. Figure 4-17(b) is the eddy current distribution and (c) is the magnetic flux density in the permanent magnets in the VMP-PMSM operated with 10 kHz of PWM carrier frequency. The magnetic

flux density is inhomogeneous in the axial direction due to the reaction field caused by the eddy current.

Table 4-1. Electrical Resistivity of Magnet Materials

Note	Resistivity ρ [μΩ-m]	Skin depth δ [mm]	Percentage to magnet length [%] =2 δ /L *100
NdFeB	180	67.52	265
SmCo	1	5.03	19.73
AlNiCo	0.5	3.56	13.96

$\delta = \sqrt{\frac{2\rho}{\omega\mu}}$, ω=2πf, f=10k[Hz], L=51[mm], Source of material property : [104]

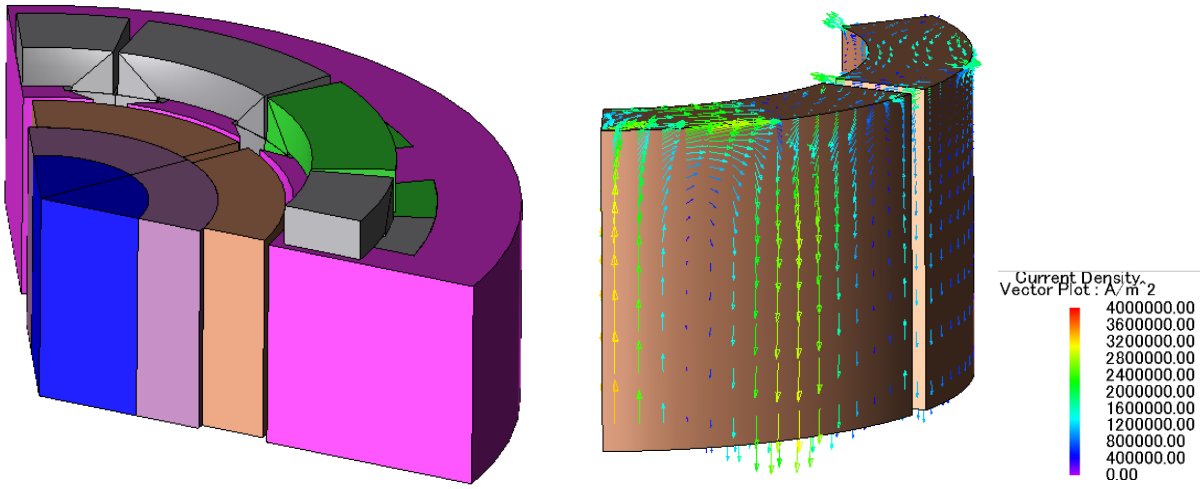

(a) 3-D FEA Model (b) Eddy current distribution in magnets

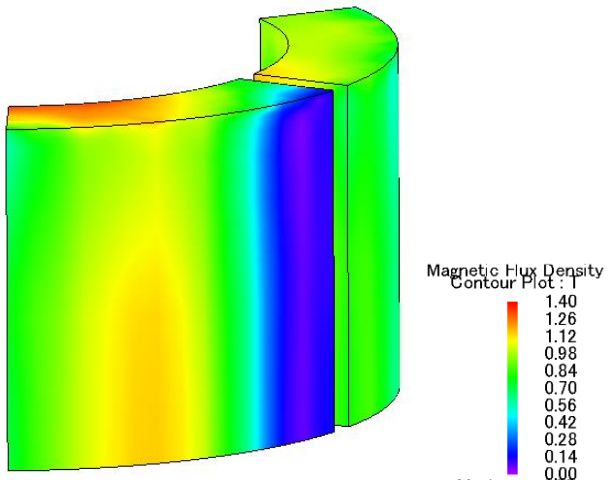

(c) Magnetic flux density distribution

Fig 4-17 Magnetic analysis considering eddy current in permanent magnets

4.5.2 Simulation of PWM harmonic current in VMP-PMSMs with AlNiCo

FEA analysis considering the magnet eddy current essentially needs 3-D geometry model with fine time resolution to capture the harmonic components in PWM current. Although the computational speed of numerical simulation has been remarkably improved in the last decade, the calculation cost of such models is still expensive. Hence, in this work, the following simplified calculation procedure is taken as combining 2-D and 3-D models, assuming that error between the 2-D analysis and the 3-D analysis due to the leakage inductance is negligible.

#1. Calculate 2-D FEA model driven by the voltage from PWM inverter.

#2. Run 3-D Analysis using the current from the 2-D analysis for a few switching cycles

Using this simulation procedure, the following three cases are tested.

1) A Fundamental component of current from 2D + with eddy current on PMs

2) Current including PWM harmonic from 2D + without eddy current on PMs

3) Current including PWM harmonic from 2D + With eddy current on PMs

Case 3) is a situation most close to the actual phenomenon. Case 1) and 2) are test cases to segregate the cause of deviations in the magnetic field. Case 1) replicates a situation when both

the current ripple due to PWM and the reaction field is not captured. Case 2) captures only the current ripple due to PWM and does not capture the reaction field. Case 3) captures both the ripple due to PWM and the reaction field.

Current waveform calculated with several PWM frequencies from the 2-D simulation is shown in Fig. 4-18. This calculation is executed by coupling an FEA motor model and an ideal inverter model on MATLAB/Simulink. As expected from the approximated equation of the carrier current in (4-3) [69][45], the current ripple is decreased as the frequency is increased.

$$i_c = \frac{1}{2}\frac{V_{dc}\text{-}e}{f_c L}\frac{\omega\phi}{V_{dc}\varepsilon} \qquad (4\text{-}3)$$

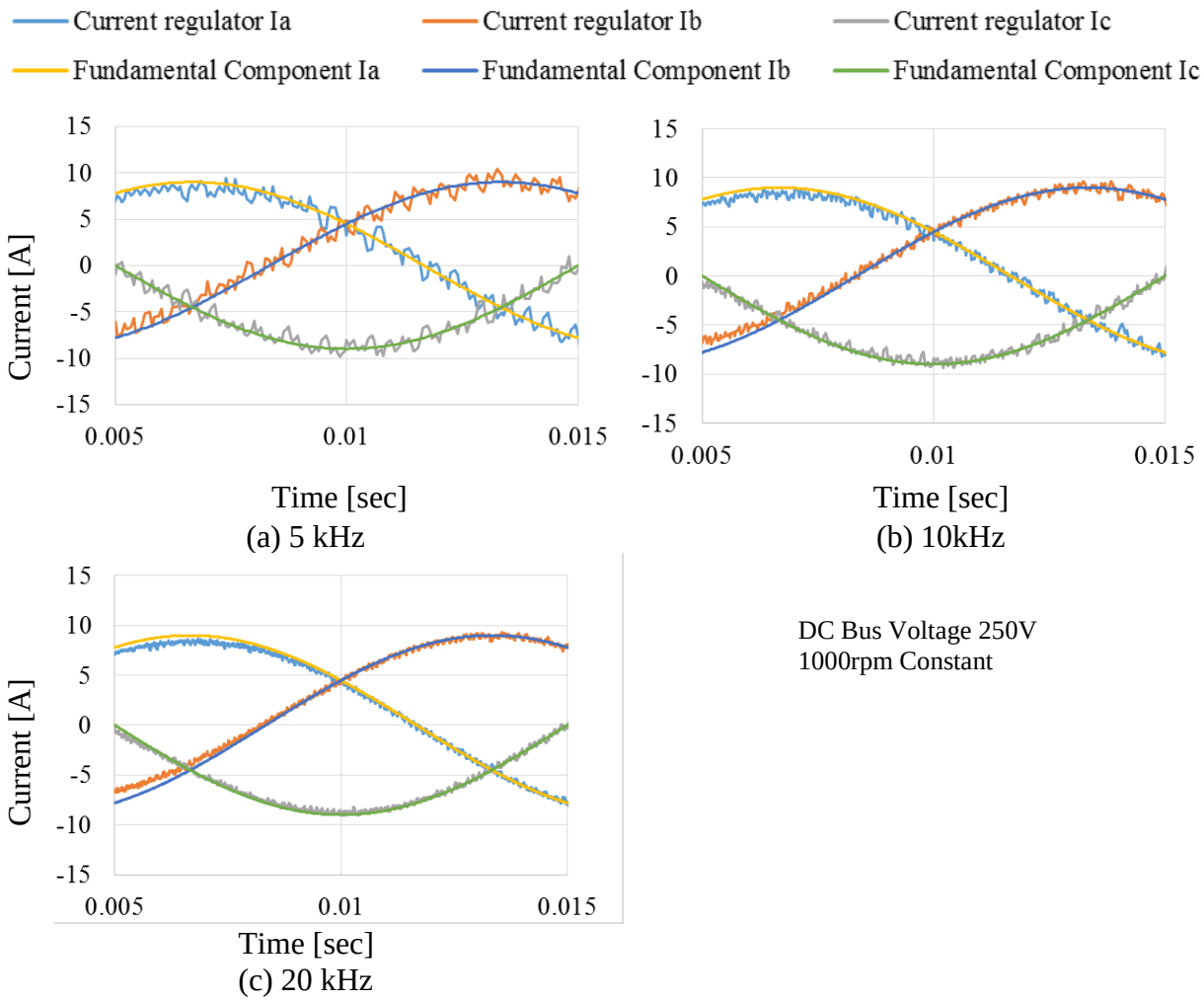

Fig 4-18 Current trajectory from analysis considering PWM inverter

After obtaining the current waveforms, 3-D analysis using the current from the 2-D analysis is executed. The magnetic field at the points near the edge in the surface of permanent magnets shown in Fig. 4-19 are picked up to evaluate the external magnetic field strength. In this simulation, it is assumed that the peak magnetic field is located near the right edge of the magnet as shown in Fig. 4-19. The resultant operating points of three sampling points in B-H plane at 5k Hz is shown in Fig. 4-20. As expected from the location of the injected magnetic field, the operating points at the left of the magnet are located on the major loop, meaning these points are not demagnetized. The operating points at the center are located slightly lower position than the operating points at the left but still are on the major loop, indicating they are not demagnetized as well. The operating points at the right are located under the knee and some points are on the minor loop.

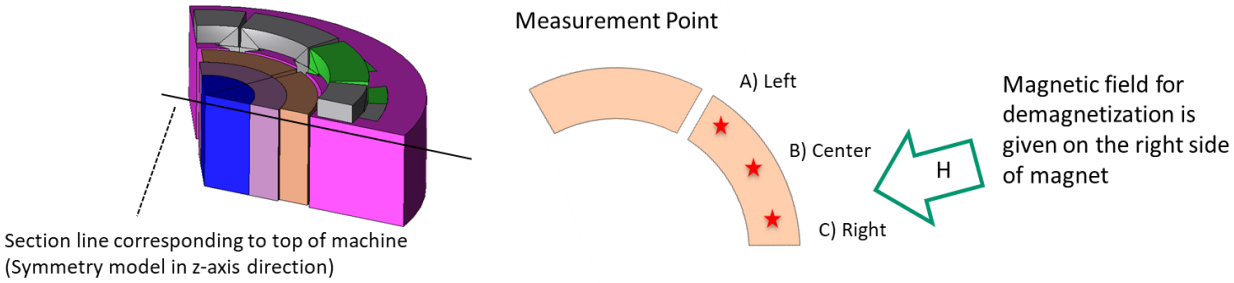

Fig 4-19 Measurement points in machines

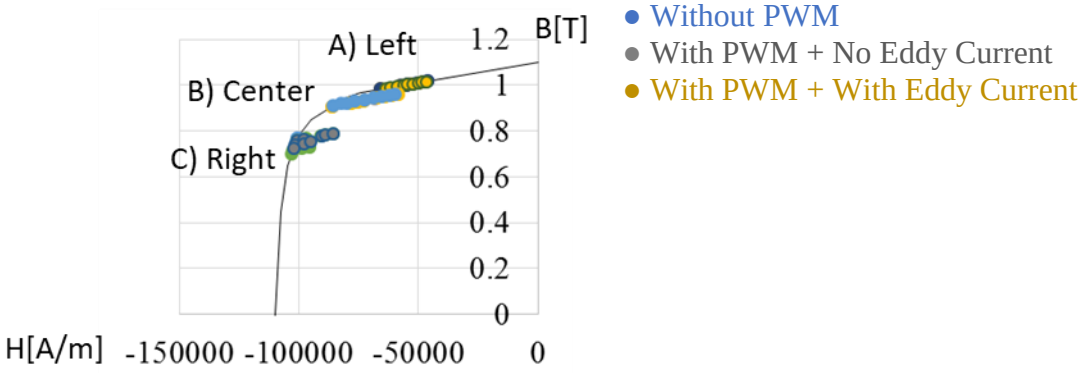

Fig 4-20 Operating points in B-H curves from analysis considering PWM inverter

Figure 4-21 is an enlarged figure of Fig. 4-20. At the left edge of the magnet, where the demagnetizing magnetic field is not subjected to, the condition of three test cases are substantially same. Hence all operating points from three cases are aligned on the one single. At the center (Fig. 4-21 (b)), the effect of PMW current slightly appears, so the calculation results not considering the PWM harmonic and considering PMW harmonics show a discrepancy. At the right edge of the permanent magnet (Fig. 4-21 (c)), the gray dots, representing the effect of the ripple in the external magnetic field due to PWM harmonic, reaches the lower location than 'without PWM'. A test case 'with PWM ripple and with Eddy Current' locates even lower position. From this observation, it is expected that the local magnetization state achieved by the PWM current in experiments becomes always lower than the local magnetization state assumed from a simulation using the fundamental current.

Figure 4-22 shows the operating points migration at the center and at the right of the magnets with different frequencies. The error between 'without PWM' and other dots becomes smaller along with the increase of the frequency. It is because the carrier harmonic current ripple becomes smaller as the frequency is increased. From (d) to (f) in Fig. 4-22, a similar trend can be observed. The right edge of the magnet is most affected by the reaction field due to the eddy current in the permanent magnets, hence the operating points scattered in (d) to (f) more than (a) to (c).

Figure 4-23 shows the error of the archived remanence at different locations with different PWM frequencies. The analysis of 'without PWM' is defined as the baseline and the errors are defined as the absolute difference from the baseline. In the case of the left of the magnet, which

is the farthest from the external magnetic field peak, the error stays at almost zero regardless of the PWM frequency and regardless of the existence of the eddy current.

At the center of the magnet, a small error is observed, and the error is decreased as PWM frequency is increased. This error is considered as a result of the current ripple due to PWM. As the PWM frequency is increased, the ripples in the current are decreased. Hence, the error is decreased when PWM frequency is increased. There is no observed difference between the case with and without consideration of the eddy current.

At the right of the magnet, the error becomes quite obvious compared to the other locations and the difference between with and without eddy current becomes also significant because this location is subjected to the high external magnetic field. Since the eddy current becomes larger as PWM frequency goes higher, the reaction field caused by the eddy current also becomes larger along with the increase of PWM frequency. Meanwhile, the deviation in the external magnetic field supplied from the stator winding is decreased as PWM frequency is increased as observed in the result at the center. Because of this trade-off, the error at the right edge of the magnet does not monotonically decrease when the eddy current is considered in the simulation. From 5 kHz to 10 kHz, the error is decreased, while, from 10 kHz to 20 kHz, the error is slightly increased. It is assumed that, from 5 kHz to 10 kHz, the reduction of the deviation in the magnetic field due to the increase of PWM frequency contributes to reducing error, whereas from 10 kHz to 20 kHz, the increased reaction field due to the eddy current contributes to increasing the error.

Key observations from this simulation are summalized as follows.

- The current ripple and the reaction field generated by pulse width modulation cause non-negligible errors between the desired magnetization pattern and the resultant magnetization pattern.
- The location exposed to the higher magnetic field has a higher error.
- The error due to the harmonic ripple becomes smaller as the PWM frequency increases.
- The error due to the reaction filed caused by the eddy current becomes larger as the PWM frequency increases.

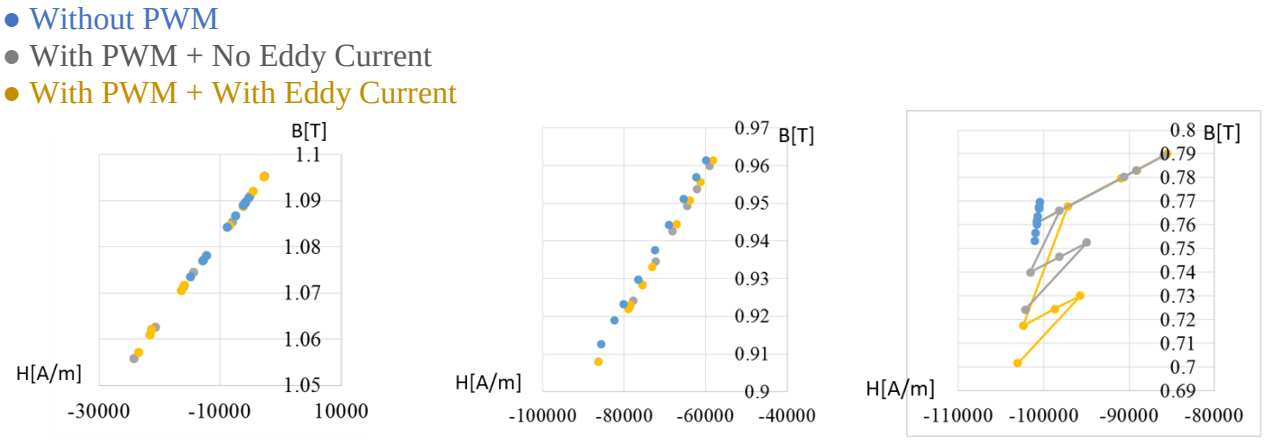

(a) Left @ 5kHz (b) Center @ 5kHz (c) Right @ 5kHz

Fig 4-21 Operating points behavior at different location in magnets at 5kHz PWM frequency

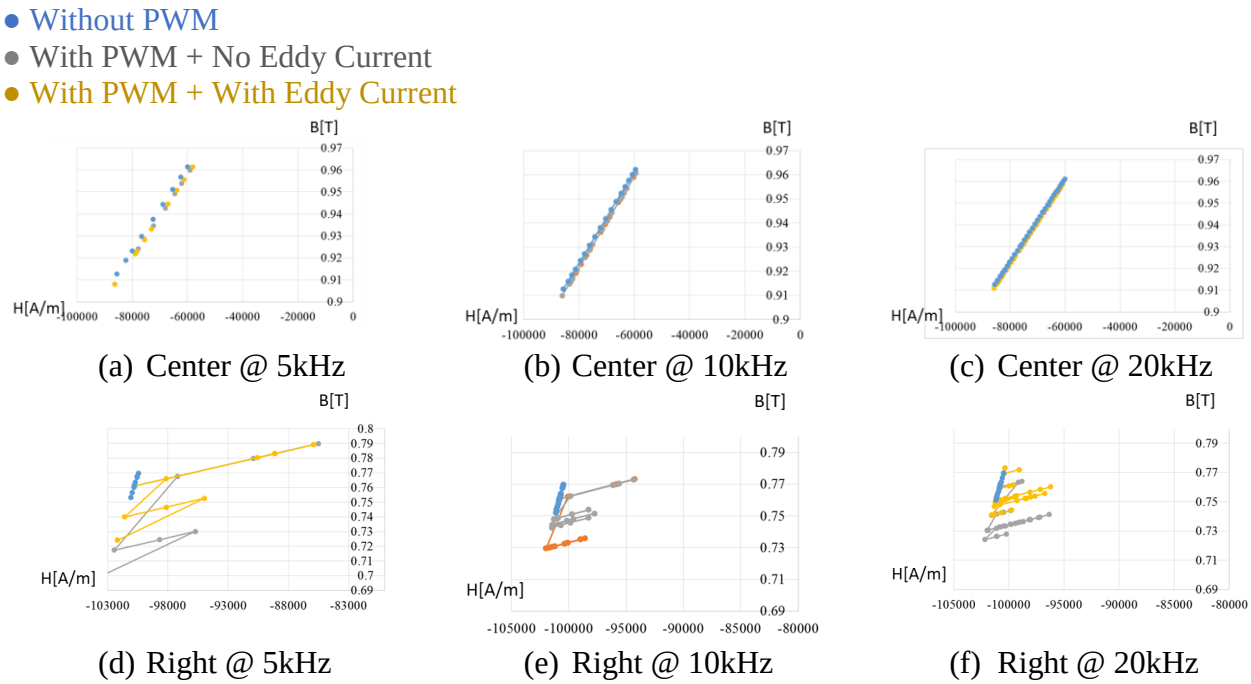

(a) Center @ 5kHz (b) Center @ 10kHz (c) Center @ 20kHz

(d) Right @ 5kHz (e) Right @ 10kHz (f) Right @ 20kHz

Fig 4-22 Operating points behavior at different PWM frequency (5, 10, 20 kHz)

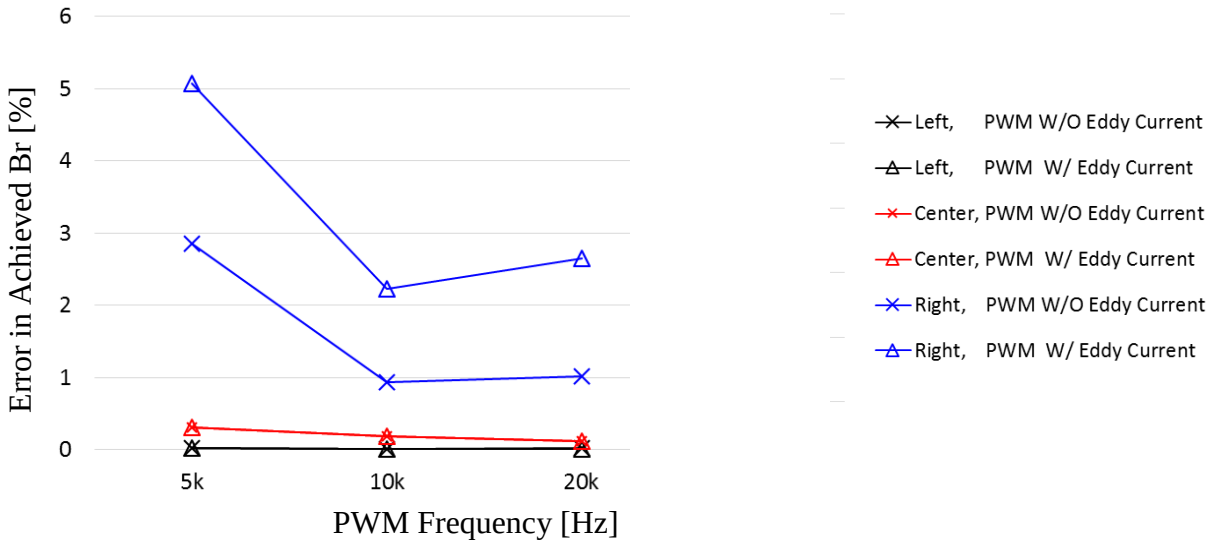

Fig 4-23 Error in Achieved remanence

4.6 Summary

Current characteristics and some potential factors in VMP-PMSM drive systems that affect the quality of the resultant magnetization patterns are investigated in this chapter. VMP-PMSMs can have either uniform magnetization patterns or non-uniform symmetric magnetization patterns by changing the phase angle of the magnetizing current vectors. It has been found that the minimum magnetizing current pulse width is constrained by the minimum harmonic order contained in the magnetic field in the rotational reference frame. The period of the severe pulse torque happening during magnetization change can be reduced by setting appropriate current pulse width using the identified methodology. The current ripple and the magnetic field caused by the eddy current due to the pulse width modulation generates non-negligible errors between the desired magnetization pattern and the resultant magnetization pattern.

Chapter 5 Experimental Evaluation of a Prototype VMP-PMSM

5.1 Introduction

In this chapter, experiment results of a prototype VMP-PMSM are reported. First, the prototype machine is designed using parametric FEA. The optimum magnet shape and airgap geometry that show the desired magnetization change capability are picked up from the simulated models then a prototype machine is fabricated. Measured results of the no-load back-EMF before and after magnetization pattern change are documented.

5.2 Design of Prototype

In this section, a prototype machine to validate the concept is designed using FEA. A goal of the design is to have a capability in changing back-EMF waveform from a square shape to a sinusoidal shape. A model shown in Fig. 5-1 is parepared as a baseline model. The baseline model has been obtained using the sizing equation [99], aiming the rated torque of 1.27 Nm at $4A_{pk}$. These specifications are determined based on an existing commercial 400W SPMSM with NdFeB [105]. In this design process, only AlNiCo9 was considered due to the availability from a material company.

5.2.1 Performance of the baseline model

The no-load back-EMF of the baseline model in time-domain and FFT are shown in Fig. 5-2. Since the details around the airgap are not designed yet, the back-EMF before magnetization pattern change is far from the intended square waveform. Similarly, the back-EMF after magnetization pattern change is also not the intended sinusoidal waveform. In the next section, this design is modified considering the performance in changing the back-EMF waveform.

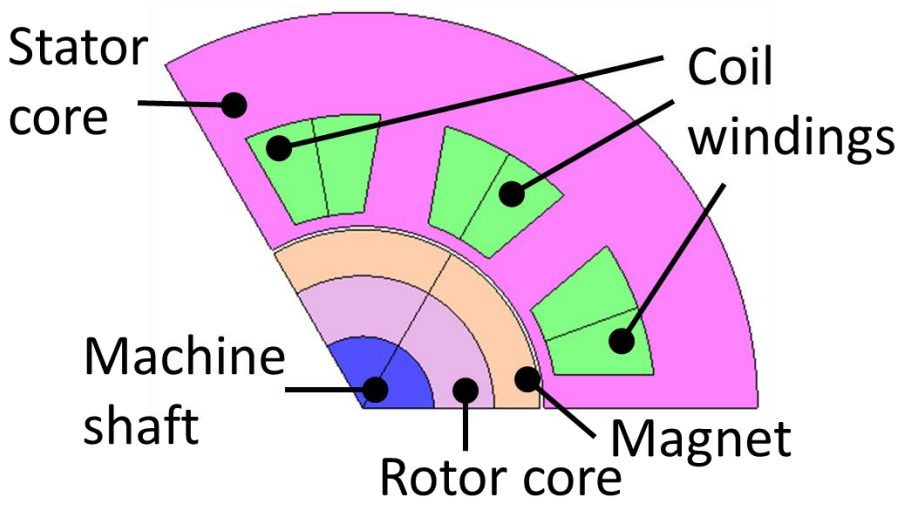

Fig. 5-1 Baseline VMP-PMSM (6-pole 9-slot concentrated winding)

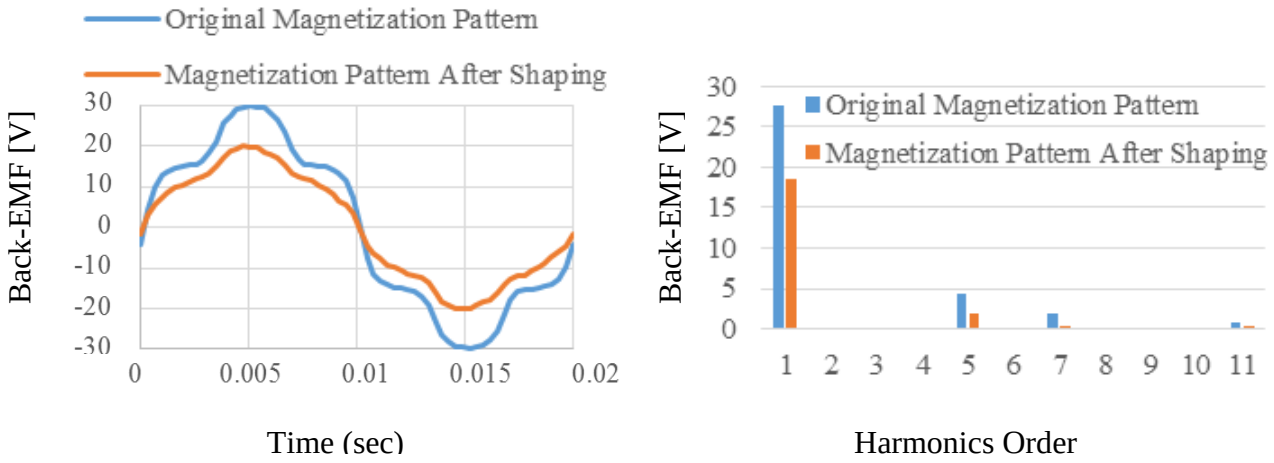

Fig. 5-2 Back-EMF of baseline model

5.2.2 Parametric design evaluation

The magnetizing current and geometric parameters are studied to achieve a back-EMF with a nearly square shape (before shaping) and a better sinusoidal shape (after shaping). Three magnetizing current magnitudes (7 A, 9 A, 11 A) and seven magnetizing current angles (270º to 330º, every 10º) are tested as changing the geometric parameters shown in Fig. 5-3. The tested geometric parameters are shown in Table 5-1. THD defined (5-1) and the fundamental component of back-EMF are evaluated.

$$THD = \sqrt{\frac{1}{V_1}\sum_{i=2}^{N} V_i^2} \tag{5-1}$$

The ratio of THD and the fundamental component before and after shaping defined as (5-2) are introduced as β_{THD} and β_{fund} to quantify the shaping performance.

$$\beta_{THD} = \frac{THD_{Before}}{THD_{After}}, \ \beta_{fund} = \frac{V1_{After}}{V1_{Before}} \tag{5-2}$$

In the context of this parametric analysis, smaller β_{THD} is better because it suggests that the parameter set can achieve a higher THD before changing the pattern and a lower THD after changing pattern. Also, β_{fund} close to one is regarded as better because it means the fundamental component after pattern shaping is the same level as before pattern shaping.

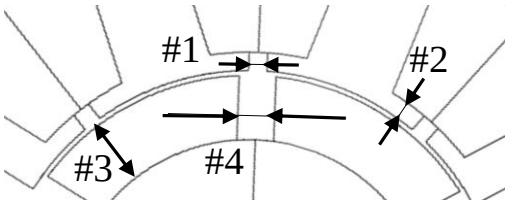

Fig. 5-3 Geometry parameters for parametric studies

Table 5-1. Parametric Geometry Test List

ID	Marker	Case Name	Slot Open (mm)	Mag. Thickness (mm)	Gap between Mag. (mm)
1	■	Baseline	0	3.5	0
2	▲	Slot Open 1mm	1	3.5	0
3	●	Slot Open 2mm	2	3.5	0
4	■	Square Tip	2	3.5	0
5	▲	Triangle Tip	2	3.5	0
6	■	Mag. Thickness 4.5mm	1	4.5	0
7	▲	Mag. Thickness 3.5mm	1	3.5	0
8	●	Mag. Thickness 3mm	1	3	0
9	■	Gap b/w magnets 1mm	1	3.5	1
10	▲	Gap b/w magnets 2mm	1	3.5	2

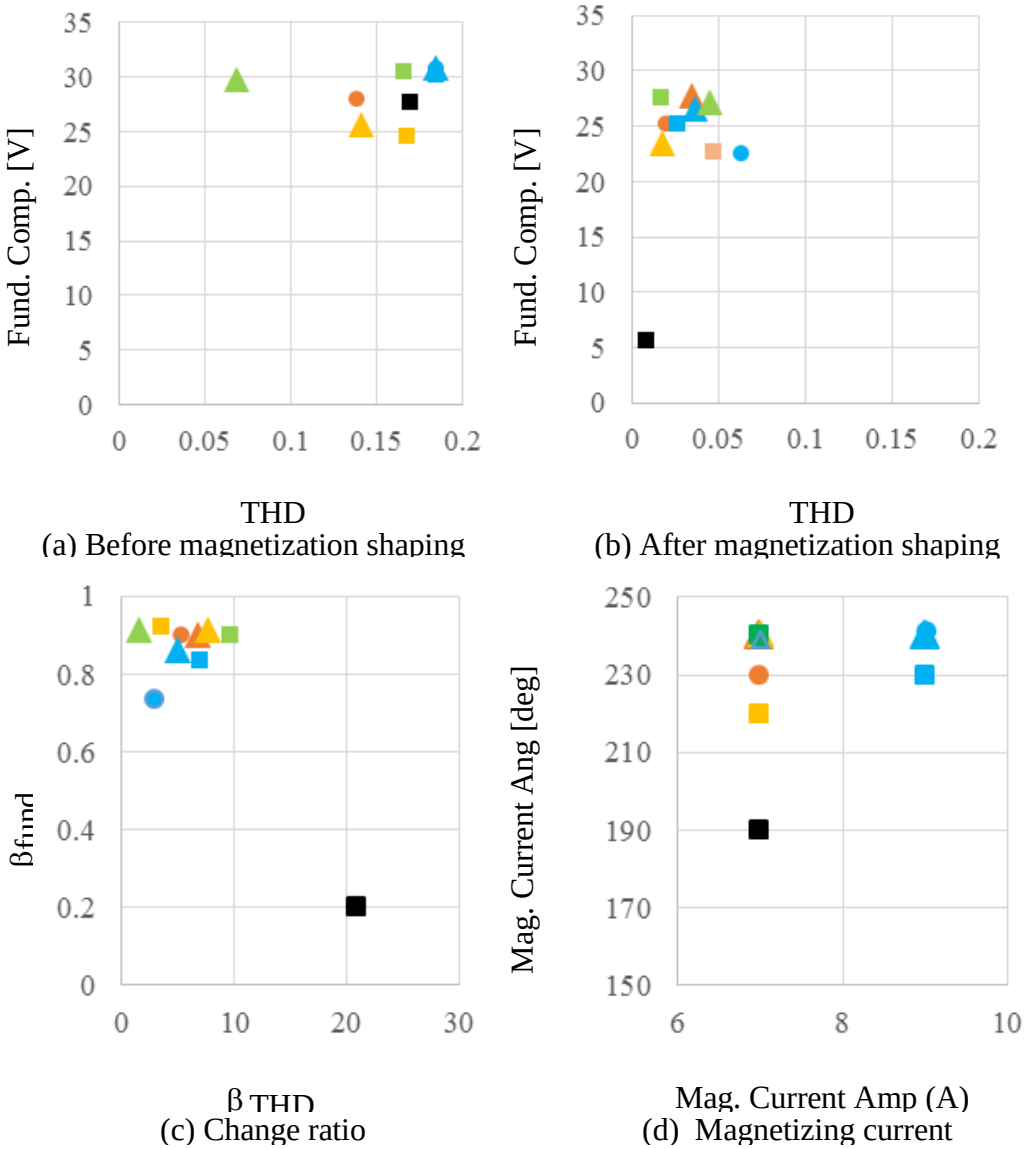

Fig. 5-4 Evaluation charts of parametric study

Figure 5-4 are the evaluation charts of these test cases. The legend of markers in this evaluation chart is shown in the second column of Table 5-1. The best parameter combination is picked up by examining the score of each candidate on the charts. For instance, in the case of 'Before magnetization shaping' shown in Fig.5-4(a), higher THD and higher fundamental component are better, thus, the candidates near the right top corner are treated as a better choice. Meanwhile, in the case of 'After magnetization shaping', lower THD and higher fundamental

component are better, hence, the candidates near the left corner are regarded as better. The effect of each design parameter on magnetization shaping capability is summarized as follows based on Fig. 5-4.

#1 Slot opening width:

Narrower slot opening achieves lower THD after magnetization pattern shaping while sacrificing the magnitude of the fundamental component. It is because the harmonics due to the slot opening is decreased but the leakage flux is increased.

#2 Teeth tip shape:

The triangle tip is slightly harder to maintain square back-EMF but easier to shape sinusoidal back-EMF compared to the square tip. It is assumed that the triangle tip can transfer the magnetic field from the stator to the rotor more efficiently without losing flux as leakage.

#3 Magnet's thickness:

Quality of the initial square back-EMF does not depend on a magnet's thickness. Thinner magnet has lower fundamental component after magnetization shaping because the thinner magnet is easy to demagnetize.

#4 Gap between magnets:

Wider gap makes the initial back-EMF far from the square shape. Sinusoidal pattern shaping is harder on zero-gap magnets than the 1mm- or 2mm-gap because the magnet cannot be demagnetized as intended due to the leakage magnet flux path across the adjacent magnets (fringe effect).

Based on the trend observed in the evaluation chart, a parameter set, "2mm slot open, triangle tip, 3.5mm magnet thickness and 1mm gap between magnets" is selected as a new design. Figure 5-5 and Table 5-2 show the new design and the specifications, respectively.

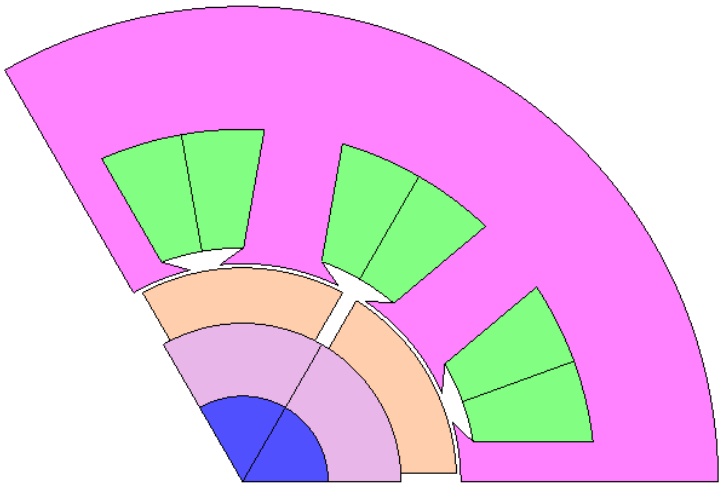

Fig. 5-5 Modified VMP-PMSM (6-pole 9-slot concentrated winding)

Table 5-2. Specification of new design

Parameters	
Diameter (mm)	60
Stack length (mm)	51
Magnet Thickness (mm)	3.5
Airgap Thickness (mm)	0.4
Number of Turns	70
Phase Resistance (Ohm)	2.23
Number of poles	6
Number of slots	9
Magnet Material	AlNiCo9
Magnetization Orientation	Radial

5.3 Performance of Prototype Machine (FEA)

The machine designed in the previous section is evaluated from the viewpoint of the performance regarding the magnetization pattern change using simulation.

The magnetizing current injection trajectory to change the magnetization pattern from the square to the sinusoidal is shown in Fig.5-6. In this example, magnetizing current vectors 9 A ∠ -60°is injected from 0.04 sec to 0.06 sec and 9 A ∠ -120°is injected from 0.06 sec to 0.08 sec. Before the magnetizing current vector is injected, the magnetization is uniformly distributed (Fig.5-7 (a)). After the first magnetizing current vector is injected, the right side of the magnet is demagnetized (Fig.5-7 (b)). Similar demagnetization happens at the opposite side of the magnet after the second magnetizing current vector is injected (Fig.5-7(c)). As seen in Fig.5-6(b), the back-EMF before injecting the currents close to trapezoidal whereas the back-EMF after injecting the current shows sinusoidal trajectory.

No-load back-EMFs in the time domain and frequency domain before and after the magnetization pattern change are shown in Fig. 5-8. Before injecting the magnetizing current, the back-EMF contains significant 5th and 7th harmonics. By changing the magnetization pattern to Fig.5-7 (c), the 5th and 7th harmonics are substantially eliminated. As a result, the back-EMF in the time-domain becomes almost pure sinusoidal waveform.

The magnetization pattern change process in the reverse direction from the sinusoidal to the uniform is shown in Fig.5-9 and 5-10. In this case, the opposite current vector angle and larger magnitude than the demagnetizing current are used to partially re-magnetize the permanent magnets.

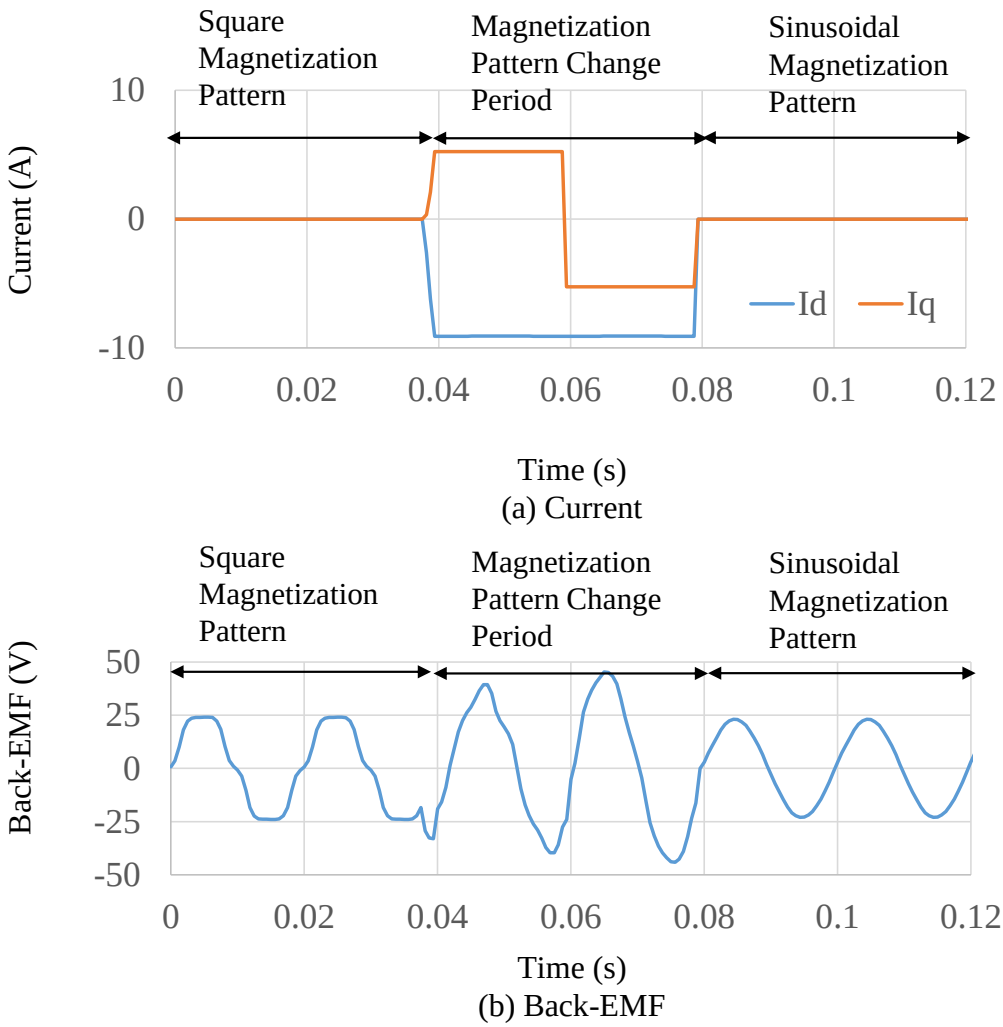

Fig. 5-6 Current and Back-EMF before, after and in the Middle of the Magnetization Shaping of the Concentrated Winding Machine (1000 rpm)

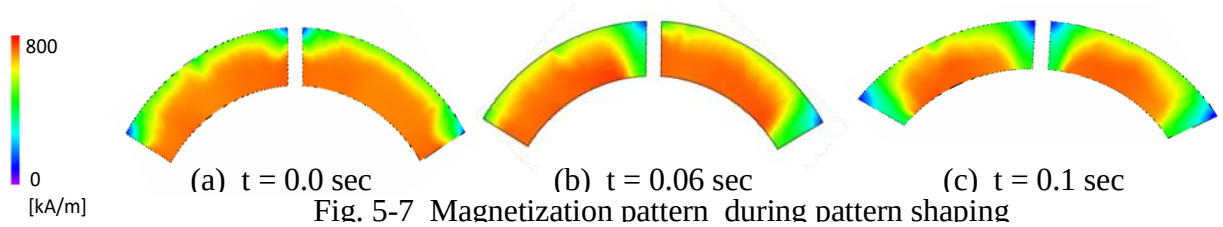

Fig. 5-7 Magnetization pattern during pattern shaping

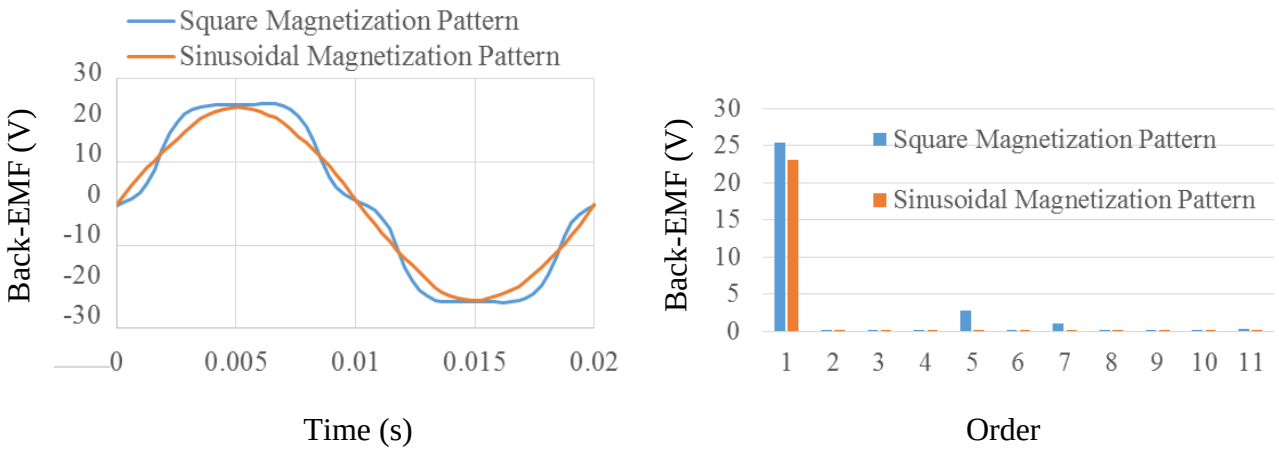

Fig. 5-8 Back-EMF before/after shaping magnetization pattern

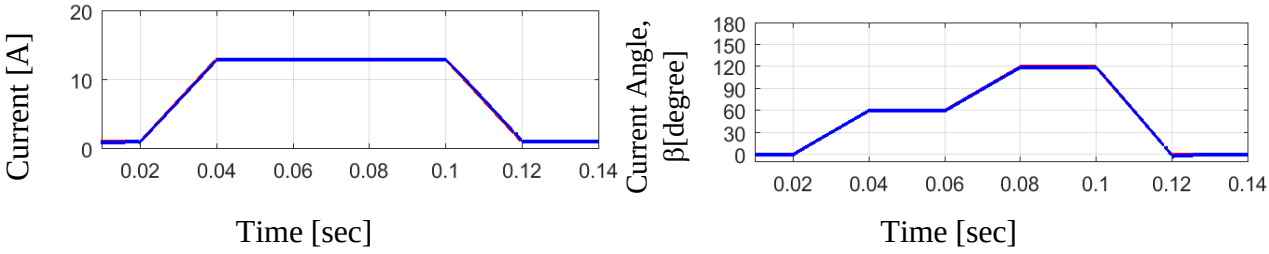

Fig. 5-9 Current trajectory to remagnetize the magnet

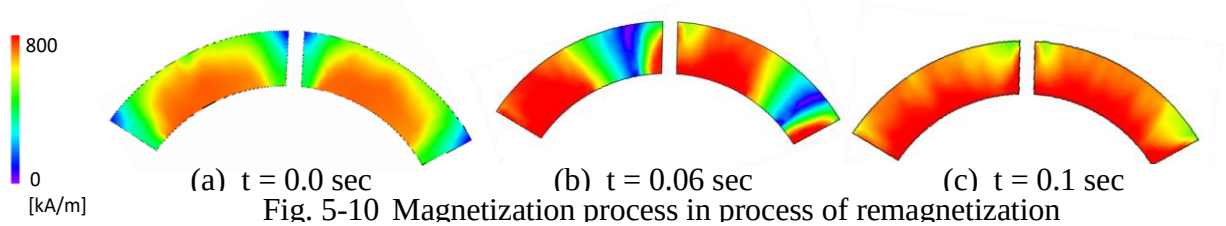

Fig. 5-10 Magnetization process in process of remagnetization

5.4 Performance of Prototype Machine (Experiment)

5.4.1 Magnetization pattern change operation

A prototype machine has been fabricated using the dimensions shown in Table 5-2. The stack length was modified to 51mm due to the manufacturing constraints. Figure 5-11 shows a setup of the prototype. The shaft of the prototype machine is mechanically coupled to a commercial SPMSM (ESTUN EMJ04-A) that provides constant speed. Figure 5-12 shows an overview of a VMP-PMSM drive system. A complex vector current regulator [114], which has an inherent capability to decouple the cross coupling between d- and q- axis, is employed in this drive system. The drive system is implemented on AIX XCS 2000 DSP with an inverter of 10kHz sampling PWM frequency.

Figure 5-13 shows a measured result of the magnetizing current to change the no-load back-EMF from the trapezoidal shape to the sinusoidal shape. Two current pulses, 6A ∠ -160º and 6A ∠ -20º are injected in the machine spinning at 600 rpm. Fig 5-14 shows no-load back-EMF before and after injecting magnetizing current with three sets of different current angles; (6A ∠ -180º, 6A ∠ -0º), (6A ∠ -165º, 6A ∠ -15º), and (6A ∠ -160º, 6A ∠ -20º). It has been observed that a current set of (6A ∠ -180º, 6A ∠ -0º) does not change the shape of the back-EMF but change the scale of the back-EMF. Meanwhile a current set of (6A ∠ -160º, 6A ∠ -20º) change the back-EMF waveform from a trapezoidal shape to a sinusoidal shape. These experiment results show that this prototype concentrated winding machine has a capability to change the no-load back-EMF depending on the angle of the magnetizing current vectors.

Figure 5-15 shows that the harmonic spectrum of these no-load back-EMFs. After injecting the current set of (6A ∠ -160º, 6A ∠ -20º), the 7th and 11th harmonics become nearly 0. This

result suggests that this prototype machine with a concentrated winding can have nearly sinusoidal no-load back-EMF by intentional partial demagnetization.

The magnet's minor loop is one of the possible reasons for the discrepancy between the simulation and the experiment in terms of the magnitude and the angle of the magnetizing current vecor set that achieves nearly sinusoidal back-EMF. It is expected that the reliable material B-H curve information and the material modeling method considering the demagnetizing curve improve the simulation accuracy. PWM harmonics investigated in Chapter 4 also can be considered as a reason of the discrepancy.

(a) Machine configuration

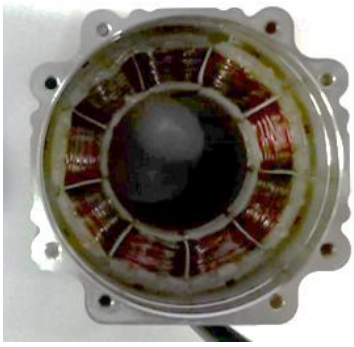

(b) Stator

(c) Rotor

Fig. 5-11 Prototype machine

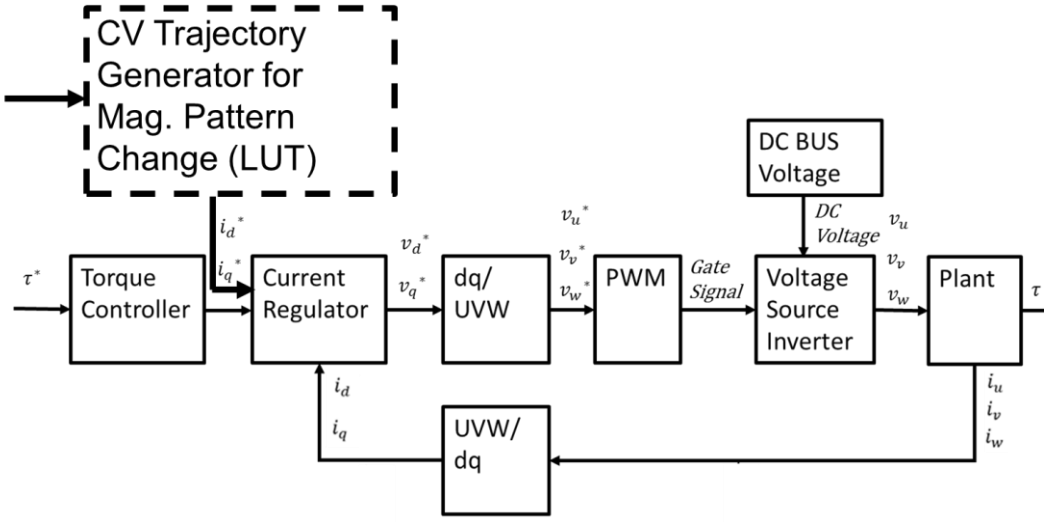

Fig. 5-12 VMP-PMSM drive system

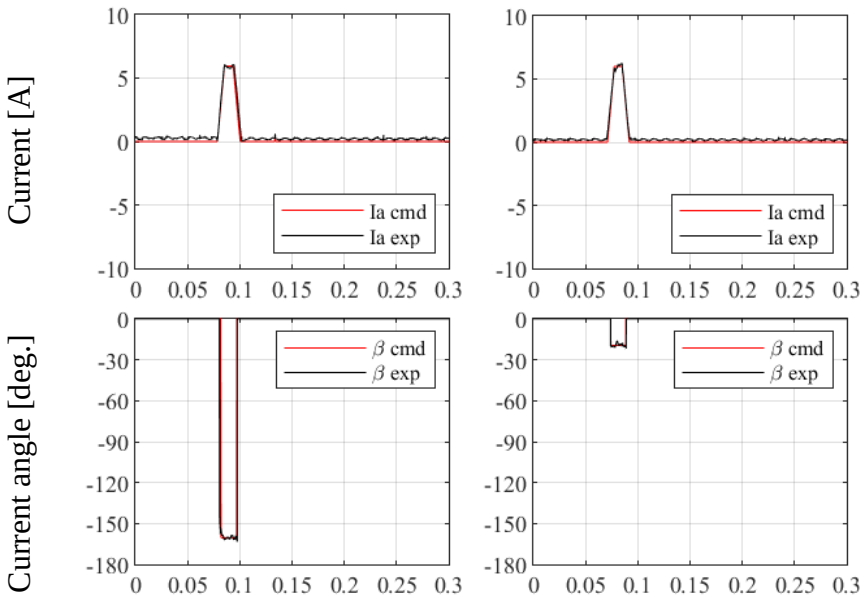

Fig. 5-13 14. Magnetizing current history (Experiment)

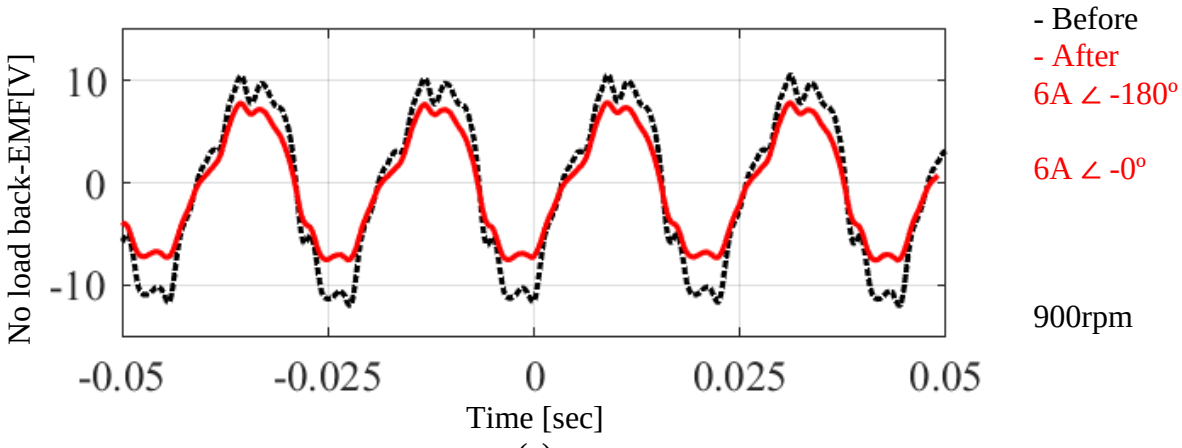

(a)

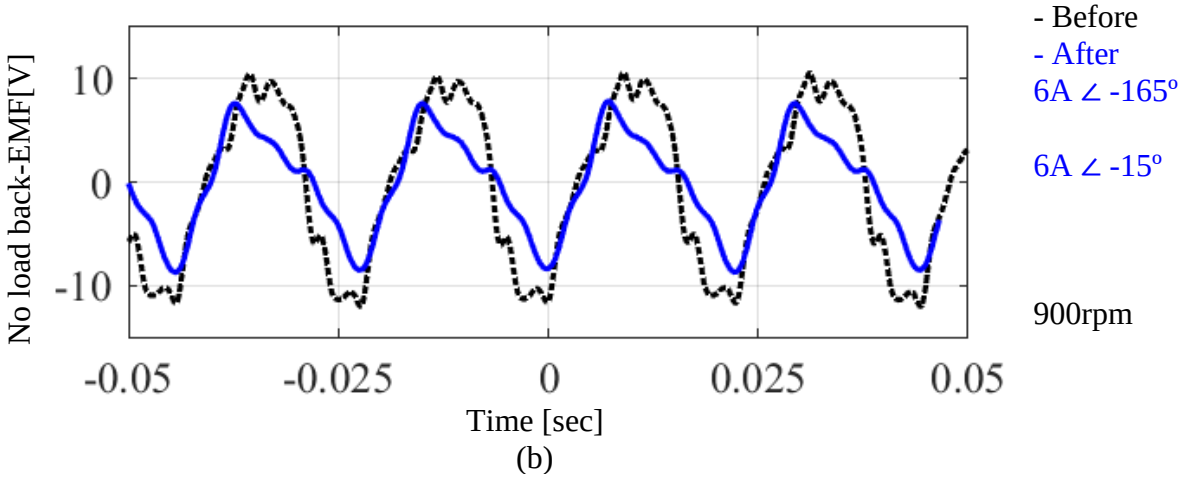

(b)

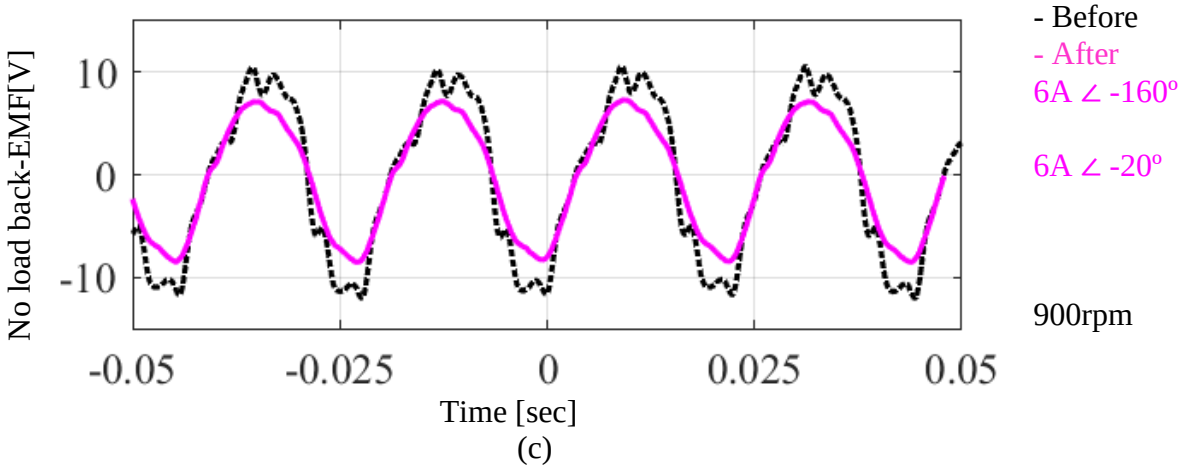

(c)

Fig. 5-15 Original and resultant No-load back-EMF (Experiment)

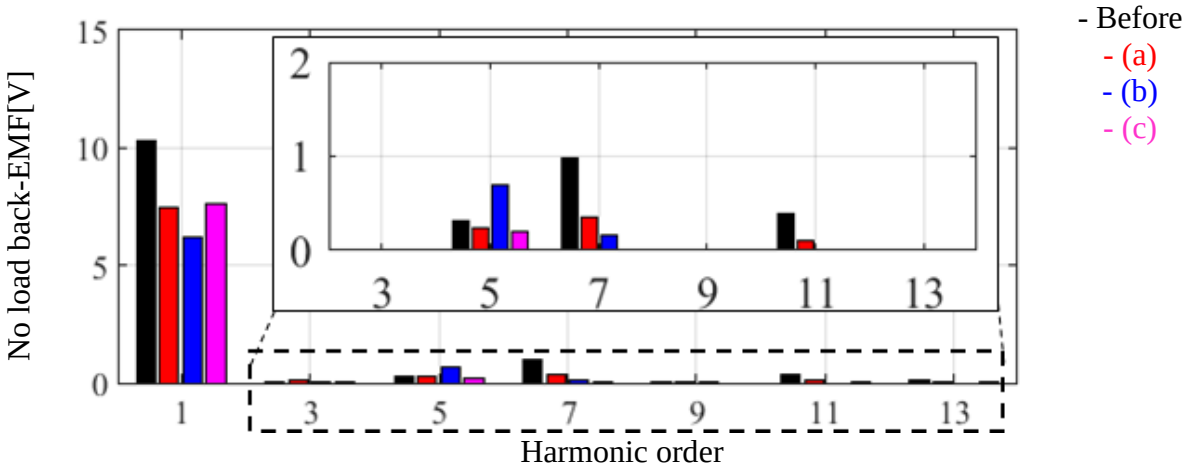

Fig. 5-16 Harmonic spectra of No-load back-EMF (Experiment)

5.4.2 Normal operation

Figure 5-17 shows the speed control result using the magnets after injecting the magnetizing current set of (6A ∠ -160º , 6A ∠ -20º). The machine was capable to sustain the speed following the command without experiencing the uncontrolled demagnetization during the normal operation. It is assumed that the achieved magnetization distribution in each piece of magnets is not completely identical because three-phase current in Fig. 5-17 (a) is slightly unbalanced. Uniform quality among every piece of magnets are remaining changes for this technique.

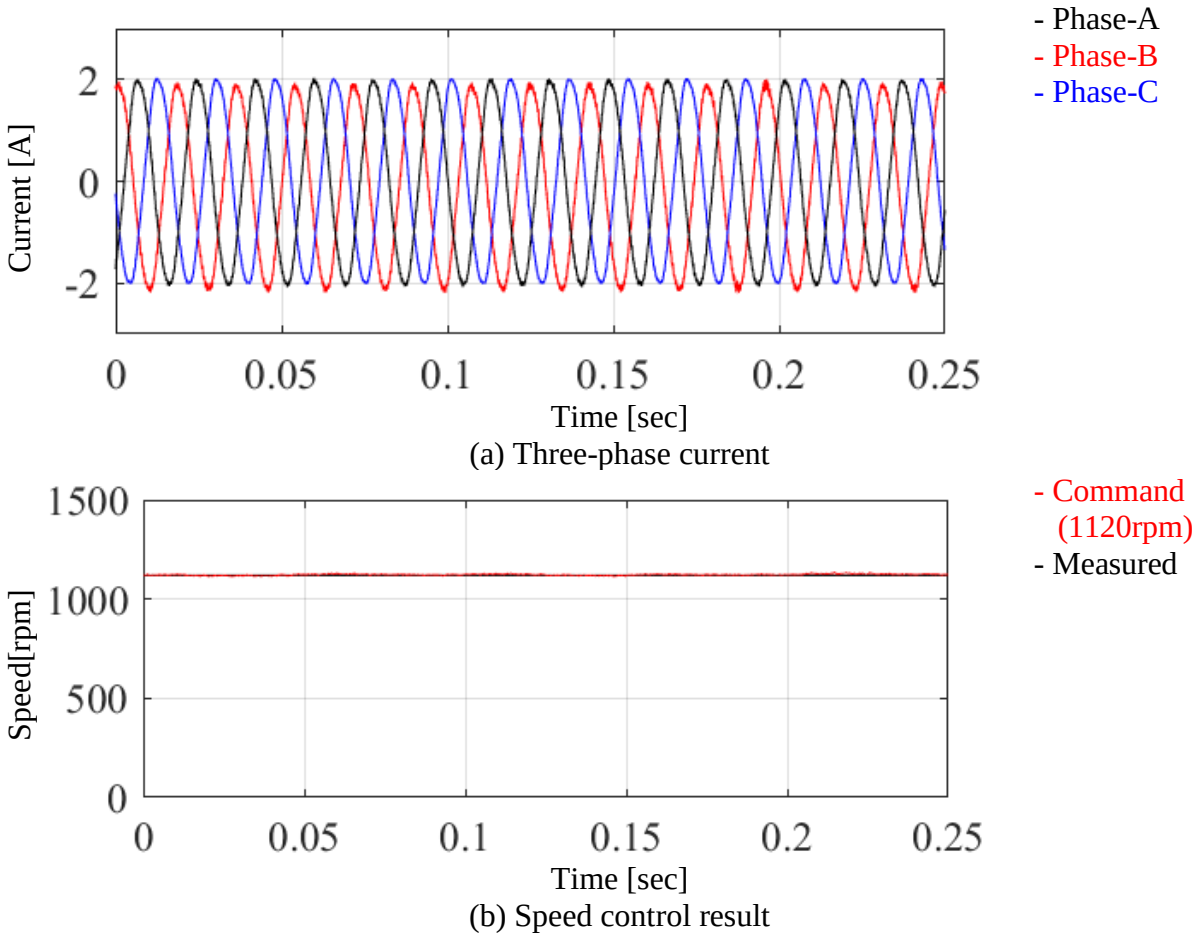

Fig. 5-17 . Speed operation after changing magnetization pattern (Experiment)

5.5 Summary

In this chapter, experiment results of a prototype VMP-PMSM have been documented. It has been shown that the performance of the magnetization pattern shaping capability is quantitatively evaluated in design process by using back-EMF as an indicator. It enables the parametric design analysis as well as the systematic design improvement of VMP-PMSMs. It is verified by experiment results using a fabricated prototype VMP-PMSM that the magnetization pattern can be manipulated by changing the angle of the magnetizing current vector even in the concentrated winding machine. In addition, the experiment result shows that the sinusoidal back-EMF can be created even in the concentrated winding machine.

Chapter 6 Torque and Loss Characteristics of VMP-PMSMs

6.1 Introduction

Chapter 6 investigates the performance of VMP-PMSMs using the machine designed in Chapter 5. Pulsating torque in normal operation, N-T characteristics and loss characteristics in VMP-PMSMs with sinusoidal magnetization patterns are calculated and compared with the case when the machine is operated as VF-PMSM with uniform magnetization pattern. The calculation results of the VMP-PMSM with a six-step operation and sinusoidal PWM are also shown in this chapter.

6.2 Pulsating Torque in Normal Operation

Concentrated winding machines have advantages in terms of size and lower copper losses compared to distributed winding machines. However, concentrated winding machines have larger torque ripples due to their rich harmonics components in the back-EMF. VMP-PMSMs can generate the sinusoidal back-EMF even in the concentrated winding configuration, thus it is expected that it can achieve lower torque ripple without sacrificing the other advantages of the concentrated winding. In this section, the pulsating torque during the normal operation, not during the magnetization pattern change operation, is calculated.

The torque quality achieved by two magnetization patterns is compared using the average torque per ampere of RMS phase current and the standard torque ripple represented in (6-1).

$$\bar{T}_e = \sqrt{\frac{1}{N}\sum_{i=1}^{N}(T_i - \bar{T})^2} \qquad (6\text{-}1)$$

The calculated result is shown in Fig.6-1 and Table 6-1. By changing the back-EMF from the uniform (ID 1) to the sinusoidal (ID 2), the torque ripple drops significantly to 16% of ID 1 while sacrificing 6% of the average torque. Torque ripple is caused by the harmonic component of the back-EMF which does not contribute to the torque production when the sinusoidal current is applied. These harmonics can be eliminated by changing back-EMF to a sinusoidal shape using the magnetization pattern shaping technique, thus, significantly torque ripple is significantly decreased. The average torque of the sinusoidal back-EMF is slightly lower than the uniform because the fundamental component of a sinusoidal waveform is intrinsically lower than a square waveform when both have a same magnitude.

As Table 6-1 shows, the uniform back-EMF is advantageous in terms of the achievable maximum torque, whereas the sinusoidal back-EMF is advantageous in terms of the lower torque ripple. Conventionally, the design decision regarding the desired back-EMF waveform has to be made in the machine design phase considering the applications. The variable magnetization pattern permanent synchronous machines can have both features so that the most appropriate magnetization pattern can be chosen according to the situation in which the machine actually operates even after the machine fabrication.

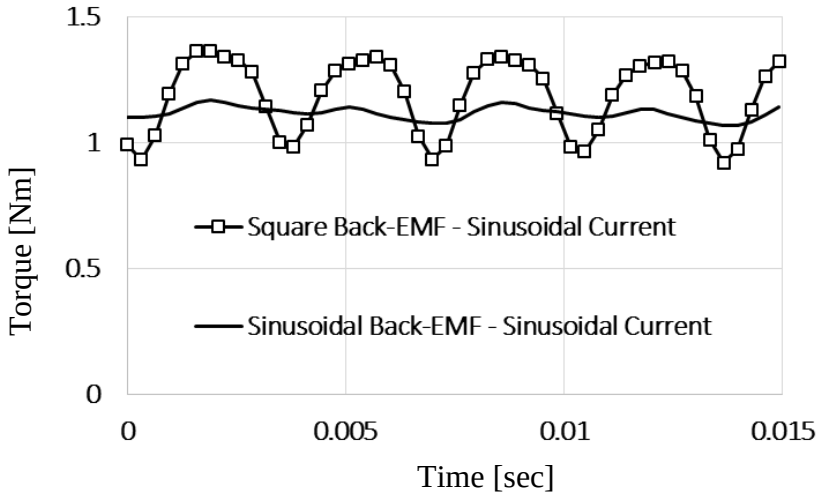

Fig. 6-1 Copper loss from machines with different magnetization state/pattern

Table 6-1. Torque Performance

Magnetization Pattern	Source	Avg.Torque Per Phase Current (Nm/Arms)	Avg. Torque Ratio (%)	Standard Torque Ripple (Nm)	Torque Ripple Ratio (%)
Uniform	Sine	0.418	100	0.135	100
Sine	Sine	0.392	94	0.022	16

6.3 Losses

Loss maps of the designed VMP-PMSM are calculated using parameters in Table 6-2 with three different magnetization patterns; 1) uniform pattern with 100% MS, 2) uniform pattern with 87% MS, and 3) sinusoidal pattern. These patterns are selected to compare the performance of a conventional fixed magnetization pattern machine, a VF-PMSM and a VMP-PMSM. Magnetization change from the 100% MS to 87% MS corresponds to the behavior of a VF-PMSM. Similarly, magnetization change from the 100% MS to the sinusoidal pattern corresponds to the behavior of VMP-PMSMs. The MS level of uniform 87% MS has been adjusted so that it has the same magnet flux fundamental component with the sinusoidal pattern. In this simulation, losses from the PWM inverter carrier frequency are not considered.

Table 6-2. Loss Map Calculation Settings

DC Bus Voltage (V)	250
Rated Current (Apk)	4
Control Method	Max Power
Current Waveform	Sinusoidal

6.3.1 Copper losses

The copper loss maps for each magnetization pattern are shown in Fig. 6-2. In high torque-low to medium speed region (zone A), the 100% MS shows lower copper losses than the other two magnetization patterns. This is because the fundamental component in the magnet flux of 100% MS is higher than the others, thus, the required load current to achieve the same level torque is essentially the least among the three magnetization patterns. Meanwhile, in low to medium torque-low to medium speed (zone B), the copper losses of the three magnetization patterns show

an almost similar trend since the load current to achieve the specified torque is not significantly different. Low to medium torque-medium to high speed (Zone C) in Fig. 6-2 corresponds to the deep flux weakening region of the 100% MS. Because of the higher fundamental component in the magnet flux, the 100% MS needs flux weakening current at lower speeds compared to the other two patterns. It results in higher copper losses in 100% MS compared to the other two magnetization patterns.

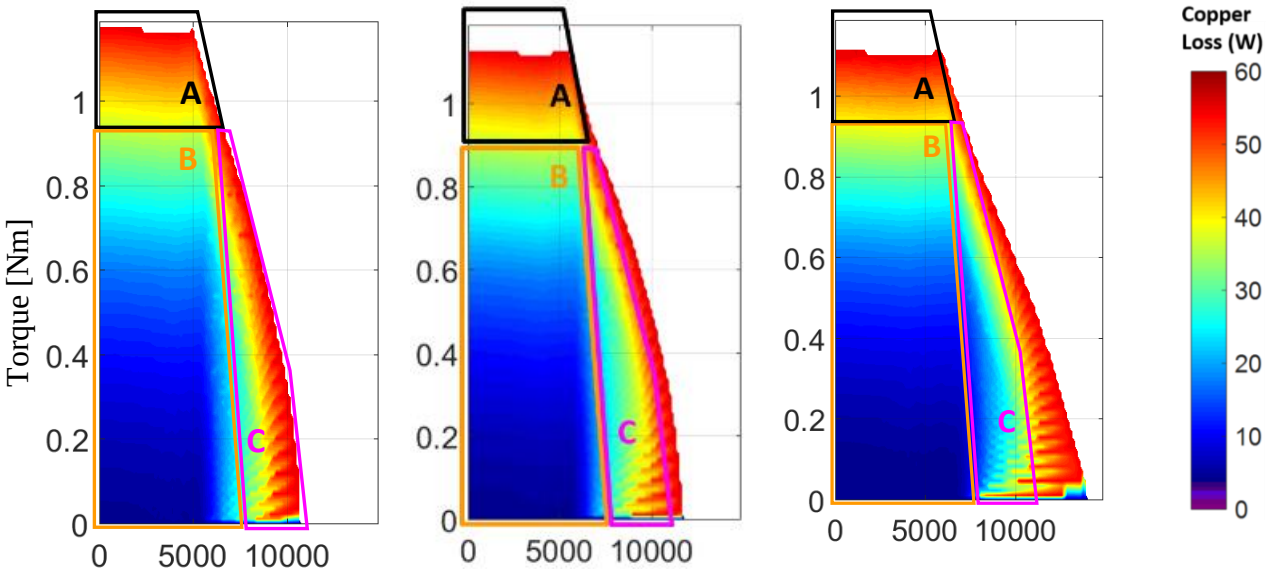

(a) 100% MS Uniform (b) 87% MS Uniform (c) Sinusoidal MS

Fig. 6-2 Copper loss from machines with different magnetization state/pattern

6.3.2 Iron losses

The iron loss maps for each magnetization pattern are shown in Fig. 6-3. In the low-speed region (zone a), no significant difference is observed among these three magnetization patterns. After medium speeds (zone b), the 100% MS uniform and the 87% MS uniform shows the highest and second highest iron loss, respectively. It is because the 100% MS uniform has higher fundamental and harmonic components than the other two patterns in terms of magnet flux.

Hence, the iron losses of 100% MS become the largest. In the case of 87% MS uniform, it has the same level of the fundamental component with the sinusoidal magnetization pattern, but the harmonics components are still higher than the sinusoidal magnetization pattern, hence, it has higher iron losses than the sinusoidal magnetization pattern.

Figure 6-4 shows the harmonic spectrum of the iron losses at 5000rpm, 0.25 Nm. Figure 6-5 is a per unit base version of Fig. 6-4. The fundamental component of each magnetization pattern is used as the base unit. By comparing Fig. 6-4 (a), (b) and Fig. 6-5 (a), (b), it is found that the uniform magnetization change effectively reduces the iron losses but the ratio of the harmonic losses to the fundamental loss does not change from the original 100% MS uniform. In contrast, in the case of the sinusoidal magnetization pattern, harmonic component becomes nearly zero.

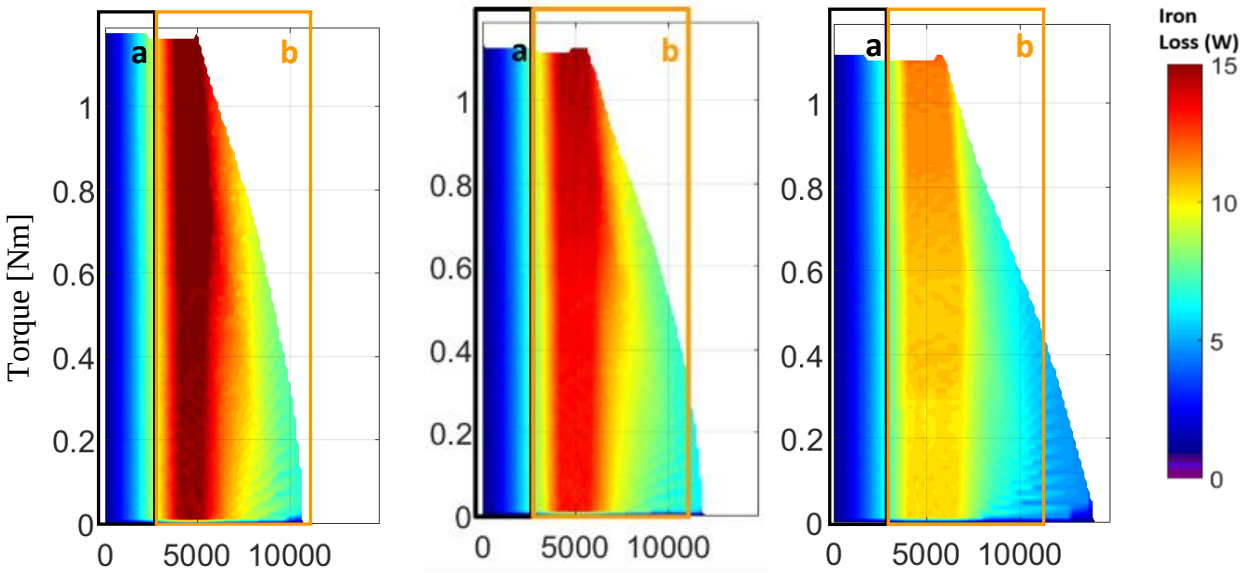

(a) 100% MS Uniform (b) 87% MS Uniform (c) Sinusoidal MS

Fig. 6-3 Iron loss from machines with different magnetization state/pattern

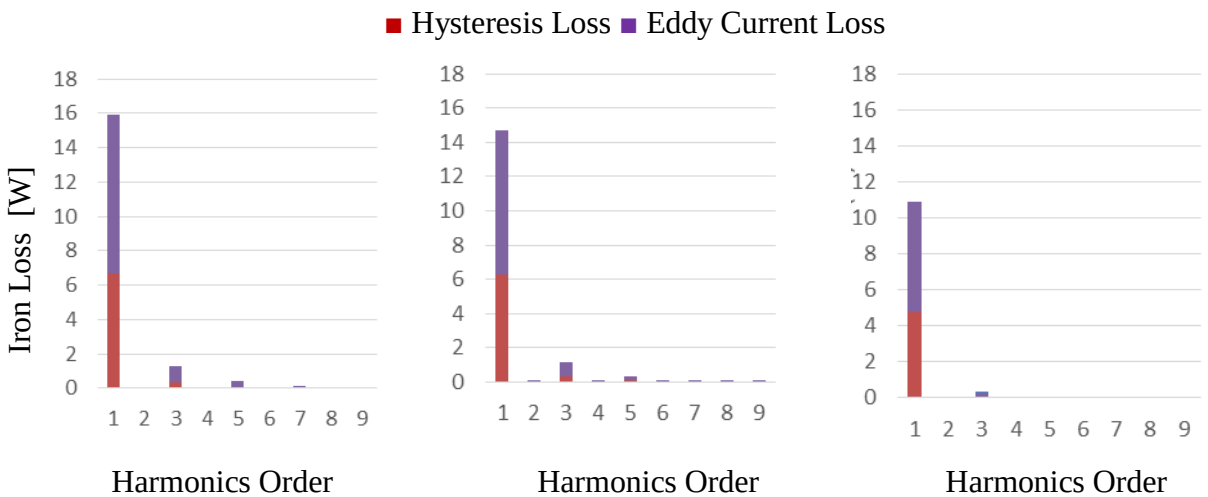

(a) 100% MS Uniform (b) 87% MS Uniform (c) Sinusoidal MS

Fig. 6-4 Iron loss at 5000rpm, 0.25Nm (Appx. 1A) with actual value

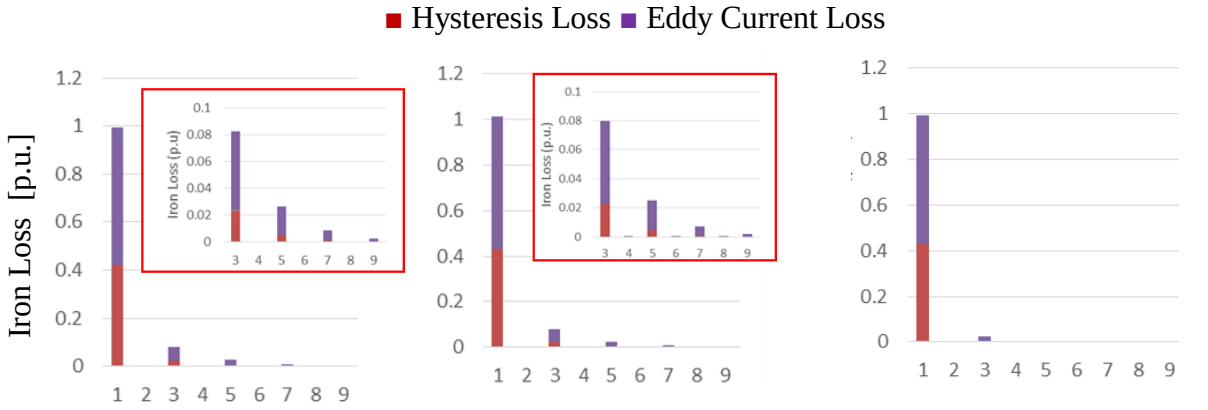

(a) 100% MS Uniform (b) 87% MS Uniform (c) Sinusoidal MS

Fig. 6-5 Iron loss at 5000rpm, 0.25Nm (Appx. 1A) in per unit

6.3.3 Total losses

The total loss maps are shown in Fig. 6-6. As expected from the discussion of copper losses and the iron losses, (a) uniform 100% MS achieves lowest losses in the high torque-low speed region and (c) sinusoidal MS shows lowest losses in the high-speed region. The advantage of the VMP-PMSM is that it can switch to both magnetization patterns depending on the operating point so that it can achieve the combined loss characteristics of both magnetization patterns.

In addition, it is found that VMP-PMSM can achieve even lower losses than VF-PMSM from the comparison of (b) uniform 87% MS (effectively, VF-PMSM) and (c) sinusoidal MS. For instance, the total loss from the sinusoidal magnetization pattern at 10000 rpm, 0.4Nm is around 40W, while the total loss from the 87%MS at the same operating point is 50W.

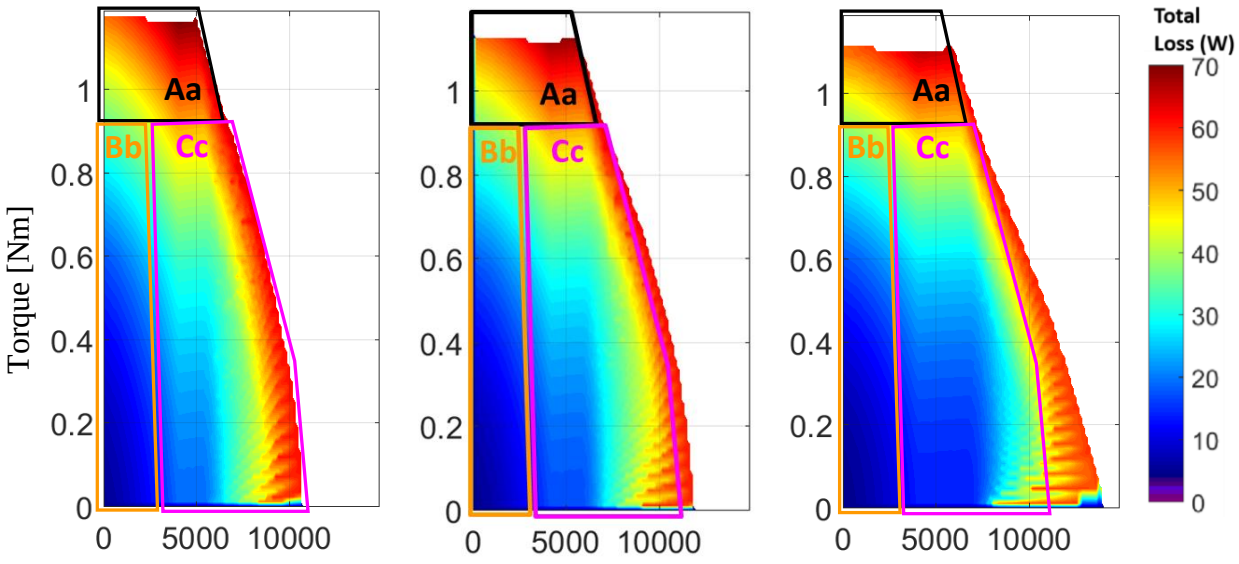

(a) 100% MS Uniform (b) 87% MS Uniform (c) Sinusoidal MS

Fig. 6-6. Total loss from machines with different magnetization state/pattern

6.4 VMP-PMSM Drive with Six-step operation and Sinusoidal PWM

The speed-torque characteristics and losses of VMP-PMSMs are calculated using six-step operation and sinusoidal PWM. Modulation techniques normally assume the back-EMF from the machine is static. In the case of the VMP-PMSMs, the back-EMF also can have a dynamic property. Assuming an ideal inverter modulation technique with the sinusoidal current generated by the sinusoidal PWM and the square current generated by the six-step operation, the possibility of the additional degree of freedom obtained by dynamic variable property in both current and back-EMF in a machine drive system are investigated here.

Consider the following four combinations of the back-EMF and current waveform.

#1. Square back-EMF + Square current waveform

#2. Sinusoidal back-EMF + Square current waveform

#3. Square back-EMF + Sinusoidal current waveform

#4. Sinusoidal back-EMF + Sinusoidal current waveform

Speed-torque characteristics of each combination are calculated as shown in Fig. 6-7. In the constant max torque region, the combination of the square back-EMF and square current waveform (#1) achieves the highest torque. It is because this combination has the highest fundamental components in the magnet flux and the current waveform. After the corner speed, the combination of the sinusoidal back-EMF and square current waveform (#2) shows the widest operating area among four combinations. When this combination is taken, the induced voltage due to the rotor spin has relatively lower peak value among the four combinations due to the sinusoidal back-EMF while the utilization of the terminal voltage is maximized due to the six-

step operation. Hence, this combination achieves the highest maximum speed among four combinations.

Four operating points, A, B, C, and D, are picked up from Fig. 6-7 and the losses at these points are calculated as shown in Fig. 6-8. At low torque, sinusoidal back-EMF and sinusoidal current (#4) is advantageous due to the lower iron losses based on the lower harmonics in magnet flux and the lower harmonics in the current. Meanwhile, at high torque, square back-EMF and the sinusoidal current (#3) is superior due to the lower copper losses achieved by higher fundamental component in magnet flux and lower harmonics in the current.

As shown here, every one of combinations has an advantage depending on the operating region. Hence, it can be said that the combination of VMP-PMSMs with the variable current waveform technique brings more choices to the control system in terms of the loss minimization and drive region expansion. Dynamic variable spatial magnetization manipulation technique changes the spatial magnetization distribution from the static property fixed in the geometry to the dynamic property manipulated by the control system during the machine operation.

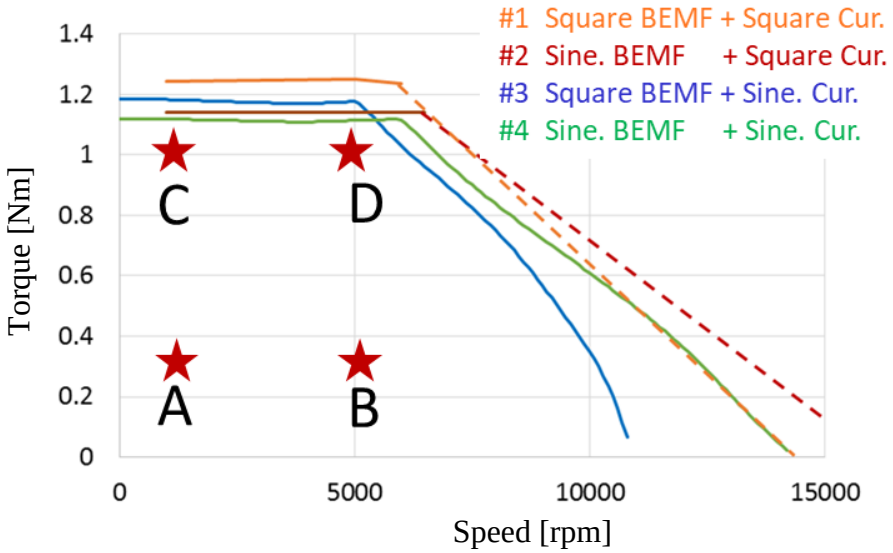

Fig. 6-7 N-T characteristics with four combinations of back-EMF and current

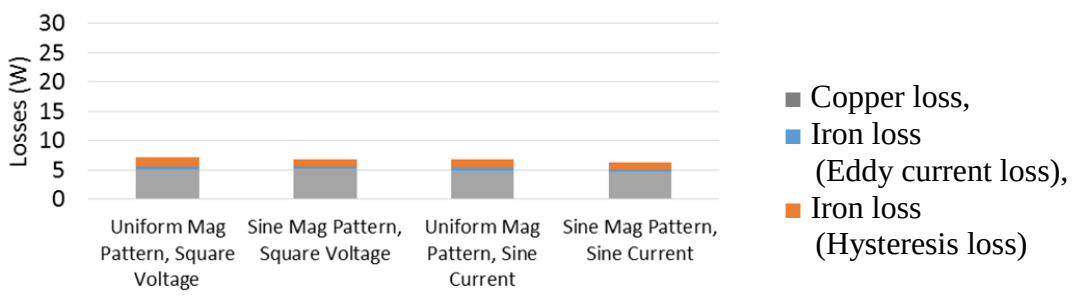

(a) A: Low torque, Low speed

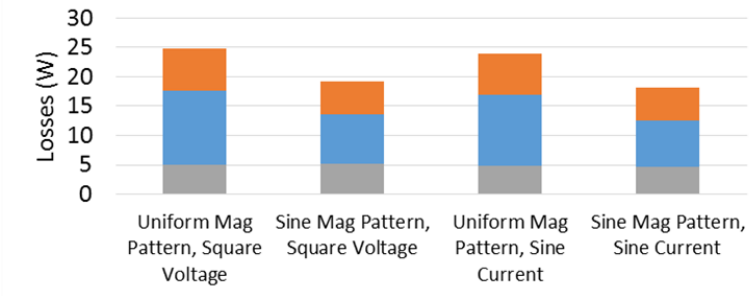

(b) B: Low torque, Med. Speed

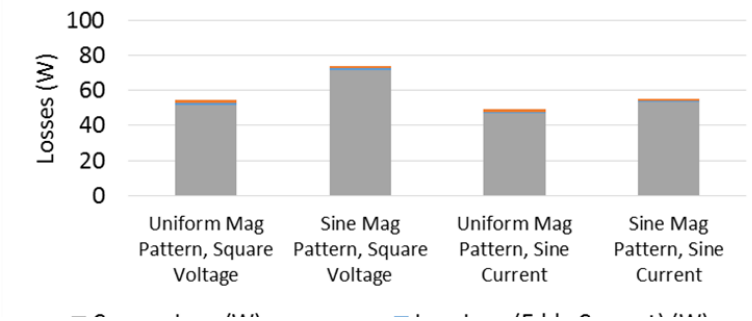

(c) C: High torque, Low speed

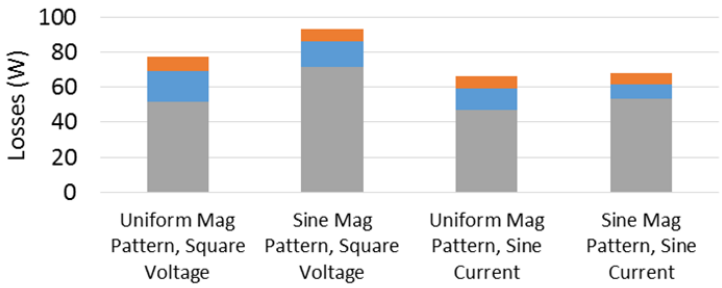

(d) D: High torque, Med. Speed

Fig. 6-8 Losses from different combinations of back-EMF and current at different operating points

6.5 Summary

VMP-PMSMs can achieve low torque ripple operation while maintaining the possible maximum torque capability. VMP-PMSMs can achieve lower losses than the conventional fixed magnetization pattern machine due to the capability to change the magnetization pattern according to the operating point. It is showed that a VMP-PMSM can achieve lower losses than a conventional VF-PMSM since the VMP-PMSM is able to effectively manipulate the harmonics components. Combination of a VMP-PMSM and techniques to switch modulation methods (from six-step to sinusoidal PWM or vice versa) brings more choices to the control system in terms of the loss minimization and drive region expansion.

Chapter 7 Conclusions, Contributions, and Recommended Future Work

In this chapter, the key conclusions and contributions are summarized and recommended future work are proposed.

7.1 Conclusions

The following list summarizes the key conclusions reached in this research.

State-of-the-Art Review

- The spatial magnetization distribution in SPMSMs has a dominant role in determining the shape of the back-EMF waveform since it is exposed to the airgap. Hence, it directly affects the pulsating torque and iron losses as well.
- In order to minimize the harmonic components in the spatial magnetization distribution, several static design approaches, such as the geometrical magnet shaping and magnet segmentation, have been explored.
- In the existing static machine design approach, the magnetization pattern cannot be changed once the machine is fabricated.
- Demagnetization has been predominantly researched in the context of machine topologies to prevent demagnetization faults.
- Numerical analysis is the most commonly used tool to replicate the spatial magnetization distribution. Analytical models to connect the spatial magnetization distribution and the conventional control scheme based on the lumped circuit parameter have not been studied.
- VF-PMSMs have achieved lower losses and wider control range of the magnet flux compared to the conventional machines since VF-PMSMs can directly reduce the magnet

flux by injecting negative d-axis current pulse instead of weakening it by the sustained negative d-axis current.

- Although VF-PMSMs have demonstrated significant loss reduction effect compared to the fixed magnetization state machines, they only focus on the change of the magnitude of the magnetization and do not address the manipulation of spatial harmonic components in the spatial magnetization distribution.
- Drive control techniques that change modulation methods from the six-step operation to sinusoidal PWM or vice versa have been shown to achieve reduced total loss and the increased speed capability.
- The mainstream of today's machine design approaches focus on static geometrical modifications and assume that machines are driven by a fixed modulation method.
- Further loss reduction and operating area expansion can be expected if the back-EMF waveform can change according to the modulation method change.

Dynamic Manipulation of Spatial Magnetization Distribution

- Spatial magnetization distribution in SPMSMs can be modeled by virtually subdividing magnets on a rotor surface and a stator MMF in the circumferential direction.
- A partial de/re-magnetized area in permanent magnets due to the magnetizing current injection is determined from the magnitude and the angle of the stator winding magnetizing current vector as well as the relative position of the magnet from the stator.
- By holding the magnetizing current vector for one electrical cycle, the overall magnetic field that the permanent magnet receives becomes independent of time.

- The spatial magnetization pattern can be shaped through the partial de/remagnetization by the magnetizing current vectors held for one electrical cycle.
- The magnetization pattern shaping using a set of two magnetizing current vectors can electromagnetically change the effective pole arc. Hence, benefits achieved by the geometrical magnet arc change in the conventional machine design, such as sinusoidal back-EMF, can be achieved by the magnetization pattern change method.

Design of VMP-PMSMs

- The active magnetization change technique is applicable to machines with specific slot-pole combinations that do not generate subharmonics in the stator winding MMF.
- The analytically identified design guideline regarding the applicable slot pole combinations of active magnetization change matches with ten examples taken from existing publications.
- The minimum remagnetizing current is constrained by manufacturing feasibility of magnet thickness and airgap length.
- The No-load condition, demagnetizing operation and remagnetizing operation need to be considered in a process to select a magnet material for VMP-PMSMs and VF-PMSMs.
- A suitable magnet material for VMP-PMSMs and VF-PMSMs are determined based on machine size, an available inverter capacity and required torque density.

Control of VMP-PMSMs

- When the current pulse is shorter than an inverse of the minimum time-harmonics frequency in the airgap magnetic field in the rotational reference frame, the quality of the

magnetization pattern, defined using the fundamental component and THD of the resultant back-EMF, is deteriorated.

- When the current pulse is longer than or equal to an inverse of minimum time harmonics frequency in the airgap magnetic field in the rotational reference frame, the quality of the magnetization pattern can be same as when the current pulse width is one electrical cycle.
- The minimum pulse period of the magnetizing current is determined as one cycle of the next lowest order component after the spatial main harmonic.
- Torque pulsation is generated during the magnetization pattern change process due to the q-axis component in the magnetizing current. The mitigation of this torque pulsation is a top priority challenge for VMP-PMSMs.
- The current ripple and the reaction field generated by the pulse width modulation cause non-negligible errors between the desired magnetization pattern and the resultant magnetization pattern.
- The error due to the harmonic ripple becomes smaller as the PWM frequency increases.
- The error due to the reaction field caused by the eddy current becomes larger as the PWM frequency increases.

Experimental Evaluation of a Prototype VMP-PMSM

- The performance of the magnetization pattern change is quantitatively evaluated by using no-load back-EMF waveform as an indicator. It enables parametric design analysis of magnetization pattern as well as a systematic design improvement of VMP-PMSMs.

- It is experimentally verified that a fabricated prototype concentrated winding machine has a capability to change the no-load back-EMF depending on the current angle of the magnetizing current vector.
- It is experimentally verified that the fabricated prototype machine with concentrated winding can have nearly sinusoidal no-load back-EMF by intentional partial demagnetization even with a concentrated winding configuration.

Performance of Variable Magnetization Pattern Permanent Synchronous Machines

- Unwanted properties in machines caused by the spatial harmonic component of the magnetic flux density, such as iron losses and torque ripple, are effectively reduced in VMP-PMSMs by controlling the spatial magnetization distribution.
- VMP-PMSMs can achieve lower losses than a conventional fixed magnetization pattern machine due to the capability to change the magnetization pattern depending on the operating point.
- Spatial magnetization pattern change can achieve lower losses than the global uniform magnetization state change operation since the spatial magnetization pattern change is able to effectively manipulate the harmonics components.
- The drive system using VMP-PMSMs provides more flexibility and choices than a conventional drive system in terms of the drive region expansion and the loss minimization due to the variable back-EMF property provided by VMP-PMSMs.

7.2 Contributions

Contributions of this research are listed in this section.

- **Proposed a concept of real-time variable spatial characteristics in machines using de/re-magnetization property of magnet material**

  This work proposes a concept of real-time variable spatial characteristics in machines using de/re-magnetization property of magnet material. Technical feasibility of the concept has been verified through theoretical analysis and experiments. Potential benefits of the proposed concepts that can not be achieved by conventional machines have been quantitatively exhibited.

- **Developed a simplified modeling method of demagnetization based on the conventional lumped circuit analogy**

  This work developed a virtually subdivided magnet model for the magnetization pattern change, which allows capturing the spatial demagnetization phenomena using the conventional lumped circuit analogy.

- **Developed a method to dynamically manipulate the spatial magnetization distribution in operating motors**

  This work developed a method to manipulate the spatial magnetization distribution based on the MMF analysis combined with the analytical demagnetization model.

- **Developed a procedure to design machines with a capability to dynamically change the spatial magnetization distribution**

  This work developed a design procedure for SPMSMs with real-time variable spatial characteristics to machines.

- **Developed a method to identify applicable slot-pole configurations for machines using active magnetization change techniques**

  By combining a generalized spatial MMF analysis and the fundamental idea of the demagnetization model, a method to find applicable slot-pole combinations for active magnetization pattern has been formulated.

- **Developed a method to identify suitable low-H_C magnet for active magnetization change techniques used in SPMSMs considering requirements in remagnetizing current and required torque density**

  This work recognized the absence of a systematic methodology to select suitable low-H_C magnets for active magnetization change method in existing researches. This work developed a general method to find a suitable magnet considering remagnetizing current and torque density assuming SPMSMs.

- **Identified an indicator to decide the minimum current pulse width for active magnetization change techniques**

  This work theoretically identified that the order of the harmonic components included in the stator winding MMF in the rotor reference frame determines the minimum current pulse width.

- **Investigated potential issues in a control system that affect the controllability of the spatial magnetization distribution**

  This work identified potential issues for dynamic magnetization change method in a control system, such as the magnetizing current pulse width, pulsating torque during the magnetization change and the reaction field due to the eddy current in the magnet.

7.3 Suggested future work

Based on the work presented in this document, the following is a list of the work identified as the suggested future work.

- Scalabilitty of VMP-PMSMs
- Develop a method to mitigate the pulsating torque during the magnetization pattern change
- Develop a modeling method to capture the minor loop behavior of low-H_c with low calculation cost including the distribution of magnetization
- Develop a feedback system incorporating the active magnetization pattern change technique with the magnetization pattern estimation method
- Investigate the possibility of active inductance manipulation using the magnetization pattern change technique
- Investigate the design space for IPMSMMs to apply the magnetization pattern change technique

References

[1] W. D. Callister and D. G. Rethwisch, *Materials Science and Engineering: An Introduction*, 7th ed., vol. 20024638. New Jersey, US, 2007.

[2] J. R. Reitz, F. J. Milford, and W. M. Schwarz, *Foundations of Electromagnetic Theory*, 2nd Editio. Addison-Wesley.

[3] G. W. Jewell, "The computer-aided design and analysis of impulse magnetizing fixtures.," no. August, 1992.

[4] C. Dinca, *Motor design for maximum material exploitation and magnetization procedure with in-line quality check for mass production*. .

[5] Donald W. Novotny and Thomas A. Lipo, "Vector Control and Dynamics of AC Drives." p. 440, 1996.

[6] M. S. Islam, S. Mir, and T. Sebastian, "Issues in reducing the cogging torque of mass-produced permanent-magnet brushless DC motor," *IEEE Trans. Ind. Appl.*, vol. 40, no. 3, pp. 813–820, 2004.

[7] T. M. Jahns and W. L. Soong, "Pulsating torque minimization techniques for permanent magnet AC motor drives - A review," *IEEE Trans. Ind. Electron.*, vol. 43, no. 2, pp. 321–330, 1996.

[8] L. Zhu, S. Z. Jiang, Z. Q. Zhu, and C. C. Chan, "Analytical methods for minimizing cogging torque in permanent-magnet machines," *IEEE Trans. Magn.*, vol. 45, no. 4, pp. 2023–2031, 2009.

[9] M. S. Islam, S. Mir, T. Sebastian, and S. Underwood, "Design considerations of sinusoidally excited permanent-magnet machines for low-torque-ripple applications," *IEEE Trans. Ind. Appl.*, vol. 41, no. 4, pp. 955–962, 2005.

[10] K. Yamazaki and M. Kumagai, "Rotor design of interior permanent magnet motors considering cross magnetization caused by magnetic saturation," in *2011 International Conference on Electrical Machines and Systems, ICEMS 2011*, 2011.

[11] L. Wu and Z. Zhu, "Analytical Modeling of Surface-Mounted PM Machines," *IEEE Trans. Magn.*, vol. 50, no. 7, 2014.

[12] Z. Q. Zhu and D. Howe, "Halbach permanent magnet machines and applications: a review," *IEE Proc. - Electr. Power Appl.*, vol. 148, no. 4, p. 299, 2001.

[13] E. Engineering, M. Street, S. Ruangsinchaiwanich, Z. Q. Zhu, and D. Howe, "Influence of Magnet Shape on Cogging Torque and Back-emf Waveform in Permanent Magnet Machines."

[14] A. Rahideh and T. Korakianitis, "Analytical open-circuit magnetic field distribution of slotless brushless permanent-magnet machines with rotor eccentricity," *IEEE Trans. Magn.*, vol. 47, no. 12, pp. 4791–4808, 2011.

[15] A. Rahideh and T. Korakianitis, "Analytical magnetic field calculation of slotted brushless permanent-magnet machines with surface inset magnets," *IEEE Trans. Magn.*, vol. 48, no. 10, pp. 2633–2649, 2012.

[16] L. Zhu, S. Z. Jiang, Z. Q. Zhu, and C. C. Chan, "Comparison of alternate analytical models for predicting cogging torque in surface-mounted permanent magnet machines," in *2008 IEEE Vehicle Power and Propulsion Conference, VPPC 2008*, 2008.

[17] N. Bianchi and S. Bolognani, "Design techniques for reducing the cogging torque in surface-mounted PM motors," *IEEE Trans. Ind. Appl.*, vol. 38, no. 5, pp. 1259–1265, 2002.

[18] K. Wang, Z. Q. Zhu, and G. Ombach, “Torque Enhancement of Surface-Mounted Permanent Magnet Machine Using Third-Order Harmonic,” *IEEE Trans. Magn.*, vol. 50, no. 3, pp. 104–113, Mar. 2014.
[19] D. Wang, X. Wang, and S. Y. Jung, “Cogging torque minimization and torque ripple suppression in surface-mounted permanent magnet synchronous machines using different magnet widths,” *IEEE Trans. Magn.*, vol. 49, no. 5, pp. 2295–2298, 2013.
[20] Y. Shen and Z. Q. Zhu, “Analysis of Electromagnetic Performance of Halbach PM Brushless Machines Having Mixed Grade and Unequal Height of Magnets,” *IEEE Trans. Magn.*, vol. 49, no. 4, pp. 1461–1469, Apr. 2013.
[21] W. Zhao, T. a. Lipo, and B. Il Kwon, “Material-efficient permanent-magnet shape for torque pulsation minimization in SPMSM motors for automotive applications,” *IEEE Trans. Ind. Electron.*, vol. 61, no. 10, pp. 5779–5787, 2014.
[22] K. I. Laskaris and A. G. Kladas, “Permanent-magnet shape optimization effects on synchronous motor performance,” *IEEE Trans. Ind. Electron.*, vol. 58, no. 9, pp. 3776–3783, 2011.
[23] S. M. Jang, H. W. Cho, S. H. Lee, H. S. Yang, and Y. H. Jeong, “The influence of magnetization pattern on the rotor losses of permanent magnet high-speed machines,” *IEEE Trans. Magn.*, vol. 40, no. 4, pp. 2062–2064, 2004.
[24] K. Yamazaki and A. Abe, “Loss Investigation of Interior Permanent-Magnet Motors Considering Carrier Harmonics and Magnet Eddy Currents,” *IEEE Trans. Ind. Appl.*, vol. 45, no. 2, pp. 659–665, 2009.
[25] Y. J. Zhou and Z. Q. Zhu, “Torque Density and Magnet Usage Ef fi ciency Enhancement of Sandwiched Switched Flux Permanent Magnet Machines Using V-Shaped Magnets,” vol. 49, no. 7, pp. 3834–3837, 2013.
[26] H. Lin, D. Wang, D. Liu, J. Chen, and A. S. P. M. Motor, “Influence of Magnet Shape on Torque Behavior in Surface-Mounted Permanent Magnet Motors,” no. 1, pp. 44–47, 2014.
[27] M. Ashabani and Y. A. R. I. Mohamed, “Multiobjective shape optimization of segmented pole permanent-magnet synchronous machines with improved torque characteristics,” *IEEE Trans. Magn.*, vol. 47, no. 4, pp. 795–804, 2011.
[28] a. H. Isfahani, S. Vaez-Zadeh, and M. a. Rahman, “Performance improvement of permanent magnet machines by modular poles,” *IET Electr. Power Appl.*, vol. 3, no. 4, p. 343, 2009.
[29] R. Lateb, N. Takorabet, and F. Meibody-Tabar, “Effect of magnet segmentation on the cogging torque in surface-mounted permanent-magnet motors,” *IEEE Trans. Magn.*, vol. 42, no. 3, pp. 442–445, 2006.
[30] Y. Li, J. Xing, T. Wang, and Y. Lu, “Programmable Design of Magnet Shape for Permanent-Magnet Synchronous Motors With Sinusoidal Back EMF Waveforms,” *IEEE Trans. Magn.*, vol. 44, no. 9, pp. 2163–2167, Sep. 2008.
[31] Z. Q. Zhu, “Investigation of Permanent Magnet Brushless Machines Having Unequal-Magnet Height Pole,” *IEEE Trans. Magn.*, vol. 48, no. 12, pp. 4815–4830, Dec. 2012.
[32] M. F. Hsieh, Y. M. Lien, and D. G. Dorrell, “Post-assembly magnetization of rare-earth fractional-slot surface permanent-magnet machines using a two-shot method,” *IEEE Trans. Ind. Appl.*, vol. 47, no. 6, pp. 2478–2486, 2011.
[33] C. Lo, “Magnetizing Method for the Post-Assembly Magnetization of a Hermetic DC Compressor,” 2006.
[34] M. F. Hsieh and Y. C. Hsu, “Characteristics regulation for manufacture of permanent-

magnet motors using post-assembly magnetization," *IEEE Trans. Magn.*, vol. 43, no. 6, pp. 2510–2512, 2007.

[35] D. G. Dorrell, M. F. Hsieh, and Y. C. Hsu, "Post assembly magnetization patterns in rare-earth permanent-magnet motors," *IEEE Trans. Magn.*, vol. 43, no. 6, pp. 2489–2491, 2007.

[36] S. L. Ho, H. L. Li, and W. N. Fu, "BU-11 A Post-assembly Magnetization method of Direct-start Interior Permanent Magnet Syn- chronous Motors and its Finite-element Analysis of Transient Magnetic Field. S. Ho, H. Li," vol. 43, no. 11, p. 2491, 2012.

[37] C. D. Riley, G. W. Jewell, and D. Howe, "Design of impulse magnetizing fixtures for the radial homopolar magnetization of isotropic NdFeB ring magnets," *IEEE Trans. Magn.*, vol. 36, no. 5, pp. 3846–3857, 2000.

[38] T. Wu, "Investigation of In-Motor Magnetization Pattern Shaping Methodology in SPMSMs using Anisotropic Magnets Investigation of In-Motor Magnetization Pattern Shaping Methodology in SPMSMs using Anisotropic Magnets," University of Wisconsin-Madison, 2016.

[39] G. Choi, "Analysis and Design Guidelines to Mitigate Demagnetization Vulnerability in PM Synchronous Machines," 2016.

[40] H.-K. Kim, D.-H. Kang, and J. Hur, "Fault Detection of Irreversible Demagnetization Based on Space Harmonics According to Equivalent Magnetizing Distribution," *IEEE Trans. Magn.*, vol. 9464, no. c, pp. 1–1, 2015.

[41] H. K. Kim and J. Hur, "Dynamic characteristic analysis of irreversible demagnetization in SPM- and IPMSMM- type BLDC motors," *IEEE Trans. Ind. Appl.*, vol. 53, no. 2, pp. 982–990, 2017.

[42] S. H. Won, W. H. Kim, and J. Lee, "Effect of the incomplete magnetization of permanent magnet in the characteristics of BLDC motor," *IEEE Trans. Magn.*, vol. 45, no. 6, pp. 2847–2850, 2009.

[43] K. Yamazaki, Y. Fukushima, and M. Sato, "Loss Analysis of Permanent-Magnet Motors With Concentrated Windings—Variation of Magnet Eddy-Current Loss Due to Stator and Rotor Shapes," *IEEE Trans. Ind. Appl.*, vol. 45, no. 4, pp. 1334–1342, Jul. 2009.

[44] K. Yamazaki, M. Shina, Y. Kanou, M. Miwa, and J. Hagiwara, "Effect of eddy current loss reduction by segmentation of magnets in synchronous motors: Difference between interior and surface types," *IEEE Trans. Magn.*, vol. 45, no. 10, pp. 4756–4759, 2009.

[45] S. H. Han, T. M. Jahns, and Z. Q. Zhu, "Analysis of rotor core eddy-current losses in interior permanent-magnet synchronous machines," *IEEE Trans. Ind. Appl.*, vol. 46, no. 1, pp. 196–205, 2010.

[46] C. Yu, T. Fukushige, A. Athavale, B. Gagas, K. Akatsu, D. Reigosa, and R. D. Lorenz, "Zero / Low Speed Magnet Magnetization State Estimation using High Frequency Injection for a Fractional Slot Variable Flux-Intensifying Interior Permanent Magnet Synchronous Machine," pp. 2495–2502, 2014.

[47] Y. Zhilichev, P. Campbell, and D. Miller, "In situ magnetization of isotropic permanent magnets," *IEEE Trans. Magn.*, vol. 38, no. 5, pp. 2988–2990, Sep. 2002.

[48] M. Mirzaei, a. Binder, and C. Deak, "3D analysis of circumferential and axial segmentation effect on magnet eddy current losses in permanent magnet synchronous machines with concentrated windings," *19th Int. Conf. Electr. Mach. ICEM 2010*, vol. 4, no. mm, pp. 0–5, 2010.

[49] G. W. Jewell, D. Howe, and C. D. Riley, "The design of radial-field multipole impulse magnetizing fixturesfor isotropic NdFeB magnets," *IEEE Trans. Magn.*, vol. 33, no. 1,

1997.

[50] J. K. Tangudu, T. M. Jahns, a. M. El-Refaie, and Z. Q. Zhu, “Segregation of torque components in fractional-slot concentrated-winding interior PM machines using frozen permeability,” *2009 IEEE Energy Convers. Congr. Expo.*, pp. 3814–3821, Sep. 2009.

[51] L. Zaixun, Z. Libing, G. Siyuan, and Z. Yi, “Equivalent Circuit Parameters Calculation of Induction Motor by Finite Element Analysis,” *Magn. IEEE Trans.*, vol. 50, no. 2, pp. 833–836, 2014.

[52] L. Alberti, N. Bianchi, and S. Bolognani, “High Frequency d - q Model of Synchronous Machines for Sensorless Control,” *Energy Convers. Congr. Expo. (ECCE), 2014 IEEE*, vol. 51, no. 5, pp. 4147–4153, 2014.

[53] A. Hemeida, P. Sergeant, and H. Vansompel, “Comparison of methods for permanent magnet eddy-current loss computations with and without reaction field considerations in axial flux PMSM,” *IEEE Trans. Magn.*, vol. 51, no. 9, 2015.

[54] J. R. Reitz, F. J. Milford, and W. M. Schwarz, *Foundations of Electromagnetic Theory*, 2nd Editio. Addison-Wesley.

[55] Magnetic Materials Producers Association, *Permanent Magnet Guidelines*. Chicago, IL, 1998.

[56] P. P. Silvester and R. L. Ferrari, *Finite Elements for Electrical Engineers*, 3rd editio. Cambridge University Press, 1983.

[57] S. J. Salon, *Finite Element Analysis of Electrical Machines*, 1995 editi. Springer, 1995.

[58] S. Ruoho, E. Dlala, and A. Arkkio, “Comparison of demagnetization models for finite-element analysis of permanent-magnet synchronous machines,” *IEEE Trans. Magn.*, vol. 43, no. 11, pp. 3964–3968, 2007.

[59] J. H. Lee and J. P. Hong, “Permanent Magnet Demagnetization Characteristic Analysis of a Variable Flux Memory Motor Using Coupled Preisach Modeling and FEM,” vol. 44, no. 6, pp. 1550–1553, 2008.

[60] S. Hamidizadeh, N. Alatawneh, R. R. Chromik, and D. A. Lowther, “Comparison of Different Demagnetization Models of Permanent Magnet in Machines for Electric Vehicle Application,” *IEEE Trans. Magn.*, vol. 52, no. 5, pp. 2–5, 2016.

[61] S. Ruoho, *Modeling Demagnetization of Sintered NdFeB Magnet Material in Time-Discretized Finite Element Analysis*. 2011.

[62] S. Hamidizadeh, “Study of Magnetic Properties and Demagnetization Models of Permanent Magnets for Electric Vehicles,” *MS Thesis, McGill Univ.*, no. April, 2016.

[63] S. Ruoho, “Demagnetisation of permanent magnets in electrical machines,” *OH Present. Helsinki Univ.*, pp. 181–185, 2006.

[64] S. Sjökvist and S. Eriksson, “Experimental Verification of a Simulation Model for Partial Demagnetization of Permanent Magnets,” *IEEE Trans. Magn.*, vol. 50, no. 12, pp. 1–5, 2014.

[65] Y. Gong, K. T. Chau, J. Z. Jiang, C. Yu, and W. Li, “Analysis of doubly salient memory motors using preisach theory,” *IEEE Trans. Magn.*, vol. 45, no. 10, pp. 4676–4679, 2009.

[66] C. Yu, S. Niu, S. L. Ho, W. Fu, and L. Li, “Hysteresis Modeling in Transient Analysis of Electric Motors With AlNiCo Magnets,” *IEEE Trans. Magn.*, vol. 51, no. 3, pp. 1–4, 2015.

[67] C. S. Koh and S. K. Hong, “Finite element analysis of magnetizer using Preisach model,” *Ieee Trans. Magn.*, vol. 35, no. 3, pp. 1227–1230, 1999.

[68] C. K. Lee, B. I. Kwon, B. T. Kim, K. I. Woo, and M. G. Han, “Analysis of magnetization of magnet in the rotor of line start permanent magnet motor,” *IEEE Trans. Magn.*, vol. 39,

no. 3, pp. 1499–1502, 2003.

[69] Y. Miyama, M. Hazeyama, S. Hanioka, N. Watanabe, A. Daikoku, and M. Inoue, “PWM Carrier Harmonic Iron Loss Reduction Technique of Permanent Magnet Motors for Electric Vehicles,” vol. 9994, no. c, pp. 475–481, 2015.

[70] J. Wang, X. Yuan, and K. Atallah, “Design optimization of a surface-mounted permanent-magnet motor with concentrated windings for electric vehicle applications,” *IEEE Trans. Veh. Technol.*, vol. 62, no. 3, pp. 1053–1064, 2013.

[71] S. Maekawa, K. Yuki, M. Matsushita, I. Nitta, Y. Hasegawa, T. Shiga, T. Hosoito, K. Nagai, and H. Kubota, “Study of the Magnetization Method Suitable for Magnetomotive-Force Memory Motor,” vol. 29, no. 9, pp. 4877–4887, 2014.

[72] T. M. Jahns, “Flux-Weakening Regime Operation of an Interior Permanent-Magnet Synchronous Motor Drive,” *IEEE Trans. Ind. Appl.*, vol. IA-23, no. 4, pp. 681–689, 1987.

[73] A. M. El-Refaie, T. M. Johns, P. J. McCleer, and J. W. McKeever, “Experimental verification of optimal flux weakening in surface PM machines using concentrated windings,” *Conf. Rec. - IAS Annu. Meet. (IEEE Ind. Appl. Soc.*, vol. 2, no. 2, pp. 1050–1057, 2005.

[74] A. Athavale, K. Sasaki, B. S. Gagas, T. Kato, and R. D. Lorenz, “Variable flux permanent magnet synchronous machine (VF-PMSM) design to meet electric vehicle traction requirements with reduced losses,” *IEEE Trans. Ind. Appl.*, vol. 53, no. 5, pp. 4318–4326, 2017.

[75] V. Ostovic, “Memory motors-a new class of controllable flux PM machines for a true wide speed operation,” in *Conference Record of the 2001 IEEE Industry Applications Conference. 36th IAS Annual Meeting (Cat. No.01CH37248)*, 2001, vol. 4, no. C, pp. 2577–2584.

[76] M. Ibrahim, L. Masisi, and P. Pillay, “Design of Variable-Flux Permanent-Magnet Machines Using Alnico Magnets,” *IEEE Trans. Ind. Appl.*, vol. 51, no. 6, pp. 4482–4491, 2015.

[77] M. Ibrahim, L. Masisi, and P. Pillay, “Design of Variable Flux Permanent-Magnet Machine for Reduced Inverter Rating,” *IEEE Trans. Ind. Appl.*, vol. 51, no. 5, pp. 3666–3674, 2015.

[78] L. Masisi, S. Member, M. Ibrahim, S. Member, and P. Pillay, “Control Strategy of A Variable Flux Machine Using AlNiCo Permanent Magnets,” pp. 5249–5255, 2015.

[79] N. Limsuwan, T. Kato, and R. D. Lorenz, “Concurrent design of interior-permanent-magnet machines for self-sensing and power conversion,” *IEEE Trans. Ind. Appl.*, vol. 48, no. 6, pp. 2157–2164, 2012.

[80] B. S. Gagas, K. Sasaki, T. Fukushige, A. Athavale, T. Kato, and R. D. Lorenz, “Analysis of Magnetizing Trajectories for Variable Time Duration,” vol. 52, no. 5, pp. 4029–4038, 2016.

[81] T. Kato, T. Fukushige, K. Akatsu, R. Lorenz, E. Hall, M. Wi, T. Kato, T. Fukushige, and R. Lorenz, “Variable Characteristic Permanent Magnet Motor for Automobile Application,” *SAE Tech. Pap.*, vol. 1, no. 1869, pp. 1–14, 2014.

[82] N. Limsuwan, T. Kato, K. Akatsu, and R. D. Lorenz, “Design and evaluation of a variable-flux flux-intensifying interior permanent magnet machine,” *2012 IEEE Energy Convers. Congr. Expo.*, pp. 3670–3677, Sep. 2012.

[83] C. Y. Yu, T. Fukushige, N. Limsuwan, T. Kato, D. Reigosa, and R. D. Lorenz, “Variable flux machine torque estimation and pulsating torque mitigation during magnetization state

manipulation," *2013 IEEE Energy Convers. Congr. Expo. ECCE 2013*, pp. 852–859, 2013.
[84] T. Kato and R. D. Lorenz, "Design Methodology for Variable Leakage Flux IPMSMM for Automobile Traction Drives," vol. 51, no. 5, pp. 3548–3555, 2014.
[85] A. Athavale, K. Sasaki, B. S. Gagas, T. Kato, and R. D. Lorenz, "Variable Flux Permanent Magnet Synchronous Machine (VF-PMSM) Design to Meet Electric Vehicle Traction Requirements with Reduced Losses," 2016.
[86] K. Sakai, H. Hashimoto, and S. Kuramochi, "Principle of hybrid variable-magnetic-force motors," *2011 IEEE Int. Electr. Mach. Drives Conf.*, pp. 53–58, May 2011.
[87] B. Gagas, T. Fukushige, T. Kato, and R. D. Lorenz, "Operating within dynamic voltage limits during magnetization state increases in variable flux PM synchronous machines," *2014 IEEE Energy Convers. Congr. Expo. ECCE 2014*, pp. 5206–5213, 2014.
[88] K. Sakai, K. Yuuki, and H. Mochikawa, "Variable-flux motor drive system," 8179068, 2012.
[89] A. Athavale, D. J. Erato, and R. D. Lorenz, "Enabling driving cycle loss reduction in variable flux PMSMs via closed-loop magnetization state control," *IEEE Trans. Ind. Appl.*, vol. 2017–Janua, no. c, 2017.
[90] J. S. Lee, C. Choi, J. Seok, S. Member, and R. D. Lorenz, "Deadbeat Direct Torque and Flux Control of Interior Permanent Magnet Machines with Discrete Time Stator Current and Stator Flux Linkage Observer," pp. 2504–2511, 2009.
[91] J. Holtz, W. Lotzkat, and A. M. Khambadkone, "On continuous control of PWM inverters in the overmodulation range including the six-step mode," *IEEE Trans. Power Electron.*, vol. 8, no. 4, pp. 546–552, 1993.
[92] T. M. Jahns, "Torque Production in Permanent-Magnet Synchronous Motor Drives with Rectangular Current Excitation," *IEEE Trans. Ind. Appl.*, vol. IA-20, no. 4, pp. 803–813, 1984.
[93] Y. C. Kwon, S. Kim, and S. K. Sul, "Six-step operation of PMSM with instantaneous current control," *IEEE Trans. Ind. Appl.*, vol. 50, no. 4, pp. 2614–2625, 2014.
[94] H. Nakai, H. Ohtani, E. Satoh, and Y. Inaguma, "Development and testing of the torque control for the permanent-magnet synchronous motor," *IEEE Trans. Ind. Electron.*, vol. 50, no. 3, pp. 288–295, 2003.
[95] K. W. Lee, S. Park, and S. Jeong, "A seamless transition control of sensorless PMSM compressor drives for improving efficiency based on a dual-mode operation," *IEEE Trans. Power Electron.*, vol. 30, no. 3, pp. 1446–1456, 2015.
[96] M. Miyamasu and K. Akatsu, "Efficiency comparison between Brushless dc motor and Brushless AC motor considering driving method and machine design," in *IECON 2011 - 37th Annual Conference of the IEEE Industrial Electronics Society*, 2011, pp. 1830–1835.
[97] S. Morimoto, Y. Takeda, T. Hirasa, and K. Taniguchi, "Expansion of operating limits for permanent magnet motor by current vector control considering inverter capacity," *IEEE Trans. Ind. Appl.*, vol. 26, no. 5, pp. 866–871, 1990.
[98] M. Farshadnia, R. Dutta, J. E. Fletcher, K. Ahsanullah, M. F. Rahman, and H. C. Lovatt, "Analysis of MMF and back-EMF waveforms for fractional-slot concentrated-wound permanent magnet machines," in *Proceedings - 2014 International Conference on Electrical Machines, ICEM 2014*, 2014, pp. 1976–1982.
[99] T. A. Lipo, *Introduction to AC Machine design*, Third Edit. University of Wisconsin, 2015.
[100] Y. Duan, "Method for Design and Optimization of Surface Mount Permanent Magnet Machines and Induction Machines," *Phd Thesis*, no. December, 2010.

[101] Z. Q. Zhu and D. Howe, “Instantaneous magnetic field distribution in brushless permanent magnet dc motors. Part I: Open-Circuit Field,” *IEEE Trans. Magn.*, vol. 29, no. 1, pp. 143–151, 1993.
[102] Alliance LLC// Magnetic as of 4/7/2018. Website:http://www.allianceorg.com/magneticproperties.html
[103] Arnold Magnetic Technologies, Cast-Alnico-Permanent-Magnet-Brochure-101117.pdf as of 4/7/2018. Website: http://www.arnoldmagnetics.com/products/alnico-magnets/
[104] Alnico Magnets (Red Magnets) - e-Magnets UK as of 4/7/2018. Website: https://e-magnetsuk.com/
[105] ESTUN Practitioner of China SMART Manufacturing as of 4/7/2018. http://en.estun.com/Download.aspx
[106] N.Bianchi, S.Bolognani, M.Dai Pré, and G.Grezzani, “Design considerations for fractional-slot winding configurations of synchronous machines,” IEEE Trans.Ind.Appl., vol.42, no.4, pp.997–1006, 2006.
[107] Z.Q.Zhu, Z.P.Xia, L.J.Wu, and G.W.Jewell, “Influence of slot and pole number combination on radial force and vibration modes in fractional slot PM brushless machines having single- and double-layer windings,” 2009 IEEE Energy Convers.Congr.Expo.ECCE 2009, pp.3443–3450, 2009.
[108] B.Aslan, E.Semail, J.Korecki, and J.Legranger, “Slot/pole combinations choice for concentrated multiphase machines dedicated to mild-hybrid applications,” IECON Proc.(Industrial Electron.Conf., no.1, pp.3698–3703, 2011.
[109] Z.Q.Zhu and D.Howe, “Influence of design parameters on cogging torque in permanent magnet machines,” IEEE Trans.Energy Convers., vol.15, no.4, pp.407–412, 2000.
[110] S.G.Min and B.Sarlioglu, “Modeling and Investigation on Electromagnetic Noise in PM Motors with Single and Double Layer Concentrated Winding for EV and HEV Application,” IEEE Trans.Transp.Electrif., vol.4, no.1, pp.1–1, 2017.
[111] JMAG-Designer V17.1 https://www.jmag-international.com/
[112] H.Hua, Z.Q.Zhu, A.Pride, R.Deodhar, and T.Sasaki, “Comparative study of variable flux memory machines with parallel and series hybrid magnets,” 2017 IEEE Energy Convers.Congr.Expo.ECCE 2017, vol.2017–Janua, pp.3942–3949, 2017.
[113] H.Liu, H.Lin, S.Fang, and Z.Q.Zhu, “Permanent Magnet Demagnetization Physics of a Variable Flux Memory Motor,” IEEE Trans.Energy Convers., vol.45, no.10, pp.4736–4739, 2009.
[114] F. Briz, M. W. Degner, and R. D. Lorenz, “Analysis and design of current regulators using complex vectors,” IEEE Trans. Ind. Appl., vol. 36, no. 3, pp. 817–825, 2000
[115] Sasaki, K., Athavale, A., Gagas, B., Fukushige, T. et al., "A Model Based Design Methodology for Variable Flux PMSMs to Obtain Desired Speed-Torque Characteristics," SAE Technical Paper 2016-01-1233, 2016
[116] S. Zhang and M. Wang, “Performance Evaluation and Design Consideration of Low Coercivity Magnets Used in Variable-Flux Permanent Magnet Synchronous Machine,” 2018 21st Int. Conf. Electr. Mach. Syst., pp. 449–453, 2018.